Unravelling Heating and Light Induced Degradation Mechanisms in Fullerene and Nonfullerene Acceptor Based Organic Solar Cells

By

Yissa Abdie Mohammed

A Dissertation Submitted to

the Department of Physics of Addis Ababa University

in Partial Fulfillment of the Requirements for the

Degree of Doctor of Philosophy in Physics (Polymer Physics)

Addis Ababa

Ethiopia

June 12, 2025

ADDIS ABABA UNIVERSITY

DEPARTMENT OF PHYSICS

The undersigned hereby certify that they have read and recommend to the College of Natural and Computational Sciences for acceptance a thesis entitled "**Unravelling Heating and Light Induced Degradation Mechanisms in Fullerene and Nonfullerene Acceptor Based Organic Solar Cells** " by **Yissa Abdie Mohammed** in partial fulfillment of the requirements for the degree of **Doctor of Philosophy**.

Dated: **June 12, 2025**

Approved by the Examination Committee

External Examiner

_____ Signature _____ Date _____

Internal Examiner

_____ Signature _____ Date _____

Advisors

Dr. Newayemedhin Aberra Signature _____ Date _____

Prof. Genene Tessema Signature _____ Date _____

Chairman

_____ Signature _____ Date _____

ADDIS ABABA UNIVERSITY

Date: **June 12, 2025**

Author: Yissa Abdie Mohammed

Title: **Unravelling Heating and Light Induced Degradation Mechanisms in Fullerene and Nonfullerene Acceptor Based Organic Solar Cells**

Department: **Physics**

Degree: **Ph.D.** Convocation: **April** Year: **2025**

Permission is herewith granted to Addis Ababa University to circulate and to have copied for non-commercial purposes, at its discretion, the above title upon the request of individuals or institutions.

_____

Signature of Author

THE AUTHOR RESERVES OTHER PUBLICATION RIGHTS, AND NEITHER THE THESIS NOR EXTENSIVE EXTRACTS FROM IT MAY BE PRINTED OR OTHERWISE REPRODUCED WITHOUT THE AUTHOR'S WRITTEN PERMISSION. THE AUTHOR ATTESTS THAT PERMISSION HAS BEEN OBTAINED FOR THE USE OF ANY COPYRIGHTED MATERIAL APPEARING IN THIS THESIS (OTHER THAN BRIEF EXCERPTS REQUIRING ONLY PROPER ACKNOWLEDGEMENT IN SCHOLARLY WRITING) AND THAT ALL SUCH USE IS CLEARLY ACKNOWLEDGED.

Dedication

This dissertation is dedicated to:

My Mother W/ro Fatim Mussa , My brother sheikh Ibrahim Abdie and My father Ato Abdie Mohammed who,unfortunately,is no longer with us.

Contents

Dedication iv

Table of Contents iv

List of Figures vii

List of Tables x

Acknowledgements xii

List of Symbols and Abbreviations xiii

Abstract xvi

1 Introduction 1

1.1 Background 1

1.2 Problem statement 6

1.3 Objectives of the study 7

1.3.1 General Objective 7

1.3.2 Specific Objectives 7

1.4 Thesis outline 8

2 Organic solar cells (OSC) 9

2.1 Organic Semiconductors: A Revolution in Materials Science 9

2.1.1 The role of carbon in organic small molecules and conjugated polymers. 11

2.2 Historical background of Organic Solar Cells 13

2.2.1 Single layer organic solar cells 14

2.2.2 Bilayer organic solar cells . . . 14
2.2.3 Bulk-heterojunction organic solar cells . . . 16
2.3 Working principle of OSC . . . 18
2.3.1 Energy Conversion Processes . . . 18
2.4 Current -voltage characteristics of OSC . . . 19
2.4.1 Short-circuit current density . . . 20
2.4.2 Open-circuit voltage . . . 21
2.4.3 Fill factor . . . 22
2.4.4 Power conversion efficiency (PCE) . . . 22
2.5 Charge Carrier Transport and Recombination in OSCs . . . 23
2.5.1 Charge carrier transport . . . 23
2.5.2 Recombination of organic solar cells . . . 25
2.6 Device structure . . . 28
2.7 Photo and thermal induced degradation of organic solar cells . . . 30
2.7.1 Photo-induced degradation of OSCs . . . 31
2.7.2 Thermally-induced degradation of organic solar cells . . . 38

3 Materials and methods **45**
3.1 Materials and solvents . . . 45
3.2 Methods . . . 46
3.2.1 Substrate preparation . . . 46
3.2.2 Organic solar cells fabrication . . . 47
3.3 Characterizations . . . 48
3.3.1 Structural and Morphological Characterizations . . . 48
3.3.2 Optical characterization . . . 50
3.3.3 Chemical Analysis . . . 52
3.3.4 Density Functional Theory calculations . . . 54
3.3.5 Electrical Characterization . . . 55

4 The Roles of Acceptors in the Thermal-degradation of P3HT-Based Organic Solar Cells **56**
4.1 Introduction . . . 56

4.2 Results and Discussion . . . 57
4.2.1 Photovoltaic performance . . . 57
4.2.2 Device degradation . . . 59
4.2.3 Evolution of the morphology P3HT-based OSCs with thermal degradation . . . 62
4.2.4 Thermogravimetric analysis . . . 65
4.2.5 FTIR . . . 66

5 Non-electron withdrawing unit copolymerization to enhance photo-stability of thiophene-based organic solar cells 69

5.1 Introduction . . . 69
5.2 Results and Discussion . . . 70
5.2.1 Optical and Electrochemical Properties . . . 70
5.2.2 Photovoltaic performance . . . 73
5.2.3 Charge generation and transfer kinetics . . . 74
5.2.4 Recombination Kinetics and Charge Transport Properties in OSCs . . . 77
5.2.5 Device degradation . . . 79

6 Summary and Outlook 85

6.1 Summary . . . 85
6.2 Future Outlook . . . 86

List of Figures

2.1 Illastrated examples of conjugated polymers 10

2.2 The process of sp^2p_z hybridization and the three hybridized orbital together with the perpendicular unhybridized 2p orbital. 12

2.3 Schematic diagram of the formation of σ- and π- bonding of Ethene (left). The energy diagram for the optical band gap(Eg) from π-bond to π*-bond (right)for ethene polymer carbon atoms forming σ-bonds and non-hybridized pz-orbitals overlapping and forming π-bonds 13

2.4 (a) A schematic single layer OSC structure and (b) energy band diagram 15

2.5 (a) A schematic bilayer OSC structure and (b) HOMO and LUMO energy levels of donor and acceptor. 16

2.6 (a) A schematic representation of a bulk heterojunction OSC structure and (b) its corresponding energy band diagram. 17

2.7 Energy conversion processes in OSCs. 20

2.8 (a) Equivalent circuit of OSC. (b) I-V curve for OSC in the dark (blue) and under illumination (red) 20

2.9 Schematic cross-sectional view of an OSC. 29

2.10 Schematic cross-sectional views of OSCs with (a) conventional and (b) inverted configuration. 30

2.11 Photooxidation mechanism of MDMO-PPV 33

2.12 Oxidation mechanism of the sulfur atom of the thiophene ring 37

2.13 Variation of PCE for OSCs with the active layer prepared at different temperatures from 130 to 190 °C 41

3.1 The structure of donor polymers used in this work 46

3.2 The chemical structure of fullerene and non fullerene acceptors used in this work 47

4.1 a)J-V b)J_{ph}-V_{eff} curves of the fullerene and Non- fullerene acceptor based device. . . . 58
4.2 Time evolution of (a) Normalized PCE, (b) Normalized J_{SC}, (c) Normalized V_{OC}, and (d) Normalized FF with thermal ageing in P3HT:PC_{60}BM, P3HT:PC_{70}BM, and P3HT:ITIC devices. 60
4.3 Selected absorption spectra of a) P3HT b) P3HT:PC_{60}BM c) P3HT:PC_{70}BM and d)P3HT: ITIC taken at different time intervals of thermal degradation. 61
4.4 Surface topography images of P3HT:PC_{60}BM,P3HT:PC_{70}BM, and P3HT:ITIC during thermal ageing 62
4.5 XRD traces of fresh and degraded a) P3HT b) P3HT:PC_{60}BM, c)P3HT:PC_{70}BM, and d) P3HT:ITIC films 63
4.6 Photoluminescence spectra of a) P3HT b)P3HT:PC_{60}BM c)P3HT:PC_{70}BM and d)P3HT:ITIC during thermal degradation 64
4.7 TGA and Derivative-TGA (DTG) curve of a)P3HT, b) $PC_{60}BM$, c) $PC_{70}BM$, and d) ITIC recorded in nitrogen atmosphere. 65
4.8 FTIR spectra of P3HT during thermal degradation. 66

5.1 a)Absorption spectra of P3HT (black) and PBDD4T(red) thin films b)TD-DFT simulated absorbance of P3HT(black) and PBDD4T(red) in gas using B3LYP-CAM level of theory at 6-31G(d,P) basis set. 71
5.2 Electron cloud distribution in Frontier molecular orbital of P3HT(left) and PBDD4T(right) 72
5.3 Average ESP values at each atom in the backbone of P3HT(top) and PBDD4T(bottom) 72
5.4 a) *J-V* curves b) Blend Abs of the PBDD4T and P3HT based device. 74
5.5 J-V characteristics under dark condition of the PBDD4T and P3HT based device. . . . 75
5.6 J_{ph} against the effective voltage V_{eff} of the PBDD4T and P3HT based device. 76
5.7 PL spectra of pristine and their blends of PBDD4T and P3HT. 77
5.8 Light intensity dependence of (a) V_{OC} (b)J_{sc} in PBDD4T and P3HT based OSCs with their corresponding light fitting Equations (1) and (2), respectively and (c)charge mobility of PBDD4T and P3HT based OSCs fitted with Equation 5.2.3 79
5.9 Time evolution of (a) Normalized V_{OC}, (b) Normalized J_{sc}, (c) Normalized FF, and (d) Normalized PCE with photo aging in PBDD4T:PC_{71}BM and P3HT:PC_{71}BM devices. . 80

5.10 Light intensity dependence of $\ln J_{sc}$ a) PBDD4T:PC_{71}BM b) P3HT:PC_{71}BM films . . . 81
5.11 Light intensity dependence of a) PBDD4T:PC_{71}BM and b)P3HT:PC_{71}BM films 81
5.12 The absorption loss due to photodegradation in a) PBDD4T:PC_{71}BM b) P3HT:PC_{71}BM films 81
5.13 Surface topography images of BDD4T:PC_{71}BM (a, c) and P3HT:PC_{71}BM (b, d) where a and c for 0 h and b and d for 7h. 83

List of Tables

5.1 Electrochemical and optical properties of PBDD4T and P3HT polymers. 71

5.2 Summary of the first excited state transition energy, oscillator strength (f) and molecular orbital (MO) contributions 73

5.3 Photovoltaic Parameter of $PC_{71}BM$ based OSCs fabricated 74

5.4 Charge generation and collection parameters of the PBDD4T and P3HT-based device. . 75

Acknowledgements

First and foremost, I extend my deepest gratitude to Allah, the Most Gracious and Most Merciful, for granting me the strength and perseverance to complete this PhD journey despite the many challenges along the way.

I would like to express my heartfelt appreciation to my supervisor, Dr. Newayemedhin Aberra, for her unwavering support, invaluable guidance, and insightful feedback throughout the course of this research. Her dedication to scientific excellence and mentorship has been truly inspiring. I am deeply grateful for her patience, encouragement, and commitment, which have played a pivotal role in shaping my academic growth.

I also extend my sincere gratitude to Professor Genene Tesema, who served as my supervisor. His constructive feedback and guidance have been instrumental in the success of this study.

My appreciation goes to Addis Ababa University (AAU) for providing me with the opportunity to pursue my PhD. In particular, I would like to thank Professor Fikadu Gashaw, Head of the Physics Department, for his valuable comments, feedback, and the support he provided in facilitating the completion of my research. I am also grateful to Dr. Bizuneh G/Michael for the courses and seminars that greatly contributed to my academic development. Additionally, I extend my thanks to Debre Berhan University (DBU) for sponsoring my PhD studies.

I am thankful to the Material Physics and Polymer Physics Research Group members in the Department of Physics at AAU. The discussions and collaborations I had with them significantly enriched this dissertation.

A special note of gratitude goes to my dear friends, Dr. Edris Mohammed and Dr. Nika Bekri, whose support, encouragement, and invaluable advice have made my academic and personal journey more fulfilling.

Finally, my deepest appreciation is reserved for my beloved wife, Habiba Birhan, and my children for their unconditional love, patience, and support. I am also profoundly grateful to my mother, W/ro Fatim Mossa, as well as my brothers and sisters, especially sheikh Ibrahim Abdie, Seid Abdie and Hawa Abdie, for their constant encouragement and moral support.

To each and every one of you, I extend my heartfelt thanks for your invaluable contributions to this journey.

List of Symbols and Abbreviations

E_g	Energy bandgap
I_{sc}	Short circuit current
V_{OC}	Open-circuit voltage
T_g	glass transition temperature
OSCs	Organic solar cells
Y6	2,2-((2Z,2Z)-((12,13-bis(2-butyloctyl)-3,9-diundecyl-12,13-dihydro-[1,2,5] thiadiazolo[3,4-e]thieno[2,3:4,5] thieno[2,3:4,5]pyrrolo[3,2-g]thieno[2,3:4,5] thieno[3,2-b]indole-2,10-diyl)bis(methanylylidene))bis(5,6-difluoro-3 -oxo- 2,3-dihydro-1H-indene-2,1-diylidene))dimalononitrile
PCE	Power conversion efficiency
NIR	Near infrared
PL	Photoluminescence
ICT	Intramolecular charge transfer
P3HT	Poly(3-hexylthiophene)
PBDD4T	Benzodithiophene-4,8-dione (BDD) unit copolymerized with α-quater thiophene(4 T) unit
PT	Polythiophene
BDT	Benzodithiophene
D-A	Donor-acceptor
$PC_{60}BM$	[6,6]-phenyl-C60-butyric acid methyl ester
$PC_{71}BM$	[6,6]-phenyl-C71-butyric acid methyl ester
HOMO	Highest occupied molecular orbital

LUMO	Lowest unoccupied molecular orbital
FRET	Förster resonance energy transfer
PTIN	Polyisothianaphthene
DTBT	Dithienylbenzothiadiazole
TT	Thieno[3,4-b]thiophene
ISOS	International Summit on Organic Photovoltaic Stability
ASTM	Americans Society of Testing Materials
ISC	Intersystem crossing
PPV	polyphenylene vinylene
EPR	Electron paramagnetic resonance
MDMO-PPV	Poly(2-methoxy-5-(3',7'-dimethyloctyloxy)-1,4- phenylenevinylene)
DPP	Diketopyrrolopyrrole
o-DCB	1, 2-dichlorobenzene
CF	Chloroform
Chex	Cyclohexane
Eox	Oxidation potential
Ered	Reduction potential
MPP	maximum power point
SEM	scanning electron microscopy
AFM	Atomic force microscopy
TGA	thermogravimetric analysis
DTG	Differential thermogravimetric
UV-Vis/NIR	Ultraviolet-Visible/Near infrared

XRD	X-ray Diffraction
SWV	Squarewave Voltammetry
XPS	X-ray photoelectron spectroscopy
DFT	Density Functional Theory
TD-DFT	Time-Dependent Density Functional Theory

Abstract

Organic solar cells (OSCs) have emerged as a promising alternative to expensive silicon-based solar cells. Over the past few years, these devices have achieved remarkable advancements, with power conversion efficiencies (PCE) surpassing 20 %, comparable to commercially available thin-film solar cells. However, under continuous illumination, OSCs are susceptible to thermal and photo-induced degradation. Addressing the challenges of thermal and photostability is essential for their industrial application. To enable widespread commercialization, a comprehensive understanding of the degradation mechanisms caused by exposure to light, heat, or humidity is crucial. This thesis examines how different acceptors influence the thermal degradation of thin-film OSCs under a controlled environmental condition. Poly(3-hexylthiophene) (P3HT), a commonly utilized donor polymer, was used to fabricate the bulk-heterojunction (BHJ) organic solar absorber. Changes in the optical and structural characteristics of the polymer film provided clear signs of degradation. Additionally, data collected from various characterization techniques demonstrated that the extent of degradation is heavily influenced by the type of acceptor molecules present in the polymer matrix. Notably, solar absorber films blended with PC_{60}BM acceptors exhibited greater stability compared to those based on 3,9-bis(2-methylene-(3-(1,1-dicyanomethylene)-indanone))-5,5,11,11-tetrakis(4-hexylphenyl)-dithieno[2,3-d:2',3'-d']-s-indaceno[1,2-b:5,6-b']dithiophene (ITIC). This difference was reflected in the measured device parameters, such as short-circuit current density (J_{sc}) and open circut voltage (V_{OC}), which showed poorer performance in P3HT:ITIC-based devices. Furthermore, a 50% drop in open-circuit voltage was observed in ITIC-based solar cells within one hour of thermal degradation. Additionally, impact of non-electron-withdrawing unit copolymerization on the photostability of fullerene-based OSCs was examined using two donor polymers: benzodithiophene-4,8-dione (BDD) copolymerized with α-quaterthiophene-thiophene (4T) (PBDD4T) and P3HT. Optical and electrochemical characterizations revealed that PBDD4T had a deeper highest occupied molecular orbital (HOMO) and broader absorption compared to P3HT, attributed to BDD copolymerization. This enhanced its power conversion efficiency (PCE), as evidenced by higher V_{oc} and J_{sc} values. The photostability study showed that PBDD4T-based devices retained 86% of their initial PCE after seven hours of irradiation, whereas P3HT-based devices experienced a 48% reduction. Further analysis of the differences in photostability suggested that BDD copolymerization suppressed photo-oxidation and recombination induced by irradiation in PBDD4T-based devices, leading to improved stability. Conversely, P3HT:PC_{71}BM-based solar absorbers exhibited bimolecular recombination due to photo-aging, which adversely affected their stability. This reduction in device stability was evi-

dent in the diminished photogenerated current, attributed to decreased charge mobility and increased surface roughness.

Chapter 1

Introduction

1.1 Background

Organic solar cells (OSCs) is one of the new generation of thin film solar cell technologies that offers several advantages over the high-cost silicon-based solar cell. Their key benefits include mechanical flexibility, lightweight design, and impressive power conversion efficiency (PCE) [1, 2, 3]. Additionally, the adjustable optoelectronic properties of organic semiconductors enable ongoing advancements in this field. Intensive efforts on the synthesis of new materials and device optimization have brought the PCE to a record level of as high as 20 % in single junction OSCs [4]. These PCE values are comparable to those achieved by commercialized thin-film solar cell technologies [5]. One of the main obstacles to the commercialization of OSCs is their environmental stability, which continues to be a significant limitation.

At present, significant research is being conducted to overcome the issue of environmental stability in OSCs. The number of publication on stability of OSCs increase from 143 in 2011 to over 700 in 2018 (data from Scopus). The tremendous attention on the issue has brought forth numerous structures with improved stability to several hours [6].Through continuous efforts, we have gained a much clearer understanding of the degradation processes in OSCs. Different protective structures have been developed to prevent degradation, leading to substantial enhancements in the lifespan of unencapsulated organic solar cells, which can now endure for thousands of hours. Moreover, the operational lifespan of encapsulated organic solar cells under prolonged exposure

to light has also seen considerable enhancement. These efforts have made organic solar cells increasingly attractive [7]. According to an economic assessment done comparing silicon based solar cells with OSCs, the OSCs technology can be commercially competitive with the matured Si based solar cell if a PCE of 7 % in large area with at least 5 years of efficiency is reached [8]. Degradation of organic solar cell can be either intrinsic or extrinsic. The intrinsic degradation is mainly due to the metastable morphology of the photoactive film that is thermodynamically unstable. This includes the formation excessive aggregate of donor/acceptor molecules in the solar absorber layer, which obstructs the charge transport process in the medium. Additionally, the diffusion of metal electrodes into the active layer leads to oxidation, creating an undesired potential barrier that hampers charge transport and extraction. On the other hand, the extrinsic factors are environmentally induced that includes humidity, oxygen, UV-irradiation and temperature exposure. Krebs et al. compiled a review on the correlation between the extrinsic degradation and the structure of the polymers/active layer materials. Thumb rules in synthesis of stable polymers can be found in his review [9].

OSCs are multi-layered devices constructed from various materials, making their degradation a complex process. This degradation can take place within specific layers or at their interfaces. For instance, when exposed to the surrounding environment, the materials in the active layer are susceptible to oxidation. Moreover, photo-oxidation can result in alterations to the optical and electrical characteristics of these materials. Under operating conditions, prolonged solar cell irradiation raises their temperature beyond that of the surroundings, making thermal degradation a critical challenge to address. In this study, we aim to investigate the effects of heating and irradiation on the stability of OSCs. Our approach focuses on systematically examining potential degradation pathways step by step to better understand the underlying mechanisms.

Significant efforts have been made to enhance the power conversion efficiency (PCE) of organic solar cells (OSCs), achieving values exceeding 18 %. These efforts include the design of electron donor and acceptor organic semiconductors, as well as the optimization of device architecture." [10, 11]. The highest PCE achieved by OSCs is now comparable to that of commercially available thin-film solar cells [11]. The widespread adoption of the technology faces numerous challenges, with device stability being a key concern. A cost analysis comparing OSCs to Silicon solar cells

indicated that OSCs could become economically viable against Silicon-based cells, provided their Power Conversion Efficiency (PCE) reaches 7% over large areas and they maintain a lifespan of at least 5 years. [8].

The stability of OSCs is affected by both external and internal factors. External factors mainly involve environmental conditions, such as oxygen and moisture exposure, radiation, temperature variations, and mechanical stress.Conversely, internal factors relate to the intrinsic properties of the materials, such as their metastable morphology and the migration of electrode and buffer layer components. Oxygen significantly influences the stability of organic solar cells (OSCs) by oxidizing low work function electrodes, which can result in the development of an insulating layer at the interface between the electrodes and the buffer layer. This, in turn, creates obstacles to charge collection. Furthermore, oxidation of the active layer components (donor and/or acceptor materials) can alter their chemical structure, impacting charge transport and light absorption. Oxygen doping, resulting from reactions with the active layer materials, can also occur, further compromising performance. The trapping of electrons by oxygen increases the hole concentration, which causes an imbalance in charge transport and ultimately leads to a reduction in both FF and open-circuit voltage V_{OC} [12, 13]. Water ingression in an organic solar cell can lead to the oxidation of low work-function electrodes and create pinholes, which allow further water penetration. Additionally, water ingress can disrupt the morphology of the active layer by causing excessive aggregation of $PC_{60}BM$, which in turn limits exciton dissociation in the active layer. Since solar cells operate under sunlight, maintaining stability under irradiation is crucial for their long-term performance.The main degradation mechanism caused by irradiation is the photo-oxidation of materials in the active layer [14] and photo-physical degradation of electrodes and buffer layers. The active layer material's absorption is impaired by photo-oxidation, which lowers exciton generation. The oxidized active layer materials can also have an increased sub-band gap states that increases recombination [15, 16].Accumulation of photo-generated charges within the active layer can lead to photophysical degradation, which modifies the device's energy landscape and reduces the open-circuit voltage. Continuous exposure to sunlight can increase the temperature of the solar cell, raising it above the ambient temperature, making heating an important extrinsic factor for degradation. While many conjugated polymers have a high glass

transition temperature (some examples PCDTBT and PCPDTBT), which prevents decomposition at typical operating temperatures, heating can still lead to physical degradation. This includes a loss of mobility in the active layer materials, particularly when the temperature exceeds their glass transition temperature. Thermal effects can alter the morphology of the active layer, causing fullerenes to aggregate and crystallize, which in turn leads to a decline in power output. The nucleation of fullerenes within the active layer promotes the formation of large domains, thereby decreasing the donor–acceptor interfacial area and reducing exciton dissociation efficiency. [17]. Besides the active layer, heat-induced degradation can also take place at the interfaces between the active layer, electrodes, and buffer layers [18].

Mechanical stability is crucial for organic solar cells, especially since their production relies on roll-to-roll techniques. Mechanical stress can lead to fractures in the active layer, electrodes, and buffer layers, as well as cause de-cohesion in the active layer, which may allow water ingression. Another factor that contributes to the degradation of OSCs is metastable morphology. Instability in the morphology of an OSC can arise due to the movement of different phases (donor, acceptor, or a third component) within the active layer. Additionally, electrode mobility can negatively impact charge photogeneration and collection. One specific cause of morphological instability is the diffusion of ITO into the PEDOT:PSS and active layers [19]. Moreover, the PEDOT:PSS layer itself can diffuse into the active layer, further reducing the overall stability of the device.

Significant efforts are being made to improve the stability of organic solar cells. This section will discuss some effective mechanisms that have been identified. One key approach is the rational design of donor material molecular structures, which plays a crucial role in enhancing the stability of active layer materials. Substitution of oxidizable units of the donor materials by chemically stable units is one of the design rules for stable materials [20]. These include avoiding the excoyclic double bonds and readily cleavable bonds and quaternary carbon atoms and including aromatic polycyclic units in the backbone of the donor material are recommended by Krebs et. al [21]. Another factor that can be adjusted to improve the photochemical stability of donor polymers is their crystallinity. In crystalline polymers, electrons and holes are spatially separated, reducing trap-assisted recombination compared to amorphous polymers. McGhee et.al reported a PCE loss of 16 % in the amorphous PCDTBT based device while the loss in the

crystalline KP115 was only 5 % after 60 h of aging [22]. Conversely, polymers exhibit greater mechanical stability when they are strong and amorphous in nature. Increasing the degree of polymerization could eliminate trap-assisted recombination in PCDTBT/PCBM70 based solar cells [23]. In addition, the glass transition temperature, Tg, of the material can be increased with increasing degree of polymerization[24]. The degree of polymerization can be utilized to regulate the photochemical properties and thermal stability of donor polymers. Tailoring side chains is another key synthesis parameter for controlling donor stability. While side chains enhance the solubility of donor materials, they become redundant after film deposition and can contribute to degradation. To address this issue, cleavable side chains are employed to enhance donor stability.

Similarly, the acceptor materials in the active layer of OSCs play a role in their degradation. Fullerene-based acceptors, including C_{60}, C_{70}, $PC_{60}BM$, $PC_{70}BM$, and ICBA, are widely recognized for their strong nanoscale interactions with donor materials and excellent electron mobility. However, exposure to irradiation can cause these acceptors to undergo dimerization, while heating can lead to the formation of large aggregates, both of which negatively impact charge photogeneration in OSCs. Adjusting the side chains of fullerene-based acceptors—such as increasing their size—helps break the high symmetry of $PC_{60}BM$ and minimizes crystallization, ultimately enhancing the stability of OSCs.

The role of acceptors in the thermal degradation of P3HT-based OSCs is a critical area of study, as it highlights how different acceptor materials affect the thermal stability and overall durability of these devices. This study is crucial for enhancing the efficiency and durability of OSCs under operational conditions. By comparing $PC_{60}BM$ and ITIC as acceptors, the study offers valuable insights into material selection for more stable solar cells. The findings reveal that $PC_{60}BM$-based blends exhibit greater thermal stability than those with ITIC, providing practical guidance for future material choices in OSC design. Detailed analyses of degradation mechanisms, including changes in optical and morphological properties and their correlation with device performance, contribute to understanding how to create more resilient solar cells. Notably, the study quantifies a 50 % reduction in V_{oc} in ITIC-based devices within just one hour of thermal degradation, establishing benchmarks for enhancing OSC durability. Furthermore, the identification of oxidation-induced -OH groups causing trap states that impair conductivity

is a significant discovery, shedding light on the chemical processes behind thermal degradation and their impact on device efficiency.

This study is also significant as it addresses the critical challenge of photostability in OSCs, a key factor for their commercial viability. By exploring non-electron-withdrawing unit copolymerization, the research paves the way for improving the durability of OSC materials. The introduction of the polymer PBDD4T, which incorporates the BDD unit, marks a notable advancement due to its superior optical and electrochemical properties compared to the conventional P3HT. PBDD4T features a deeper HOMO level and broader absorption spectrum, both of which are essential for enhancing solar cell efficiency. Devices utilizing PBDD4T demonstrate higher power conversion efficiency (PCE) than those with P3HT, primarily due to improved V_OC and J_SC metrics, which are critical for solar cell performance. A key achievement of this work is the significant improvement in photostability, as PBDD4T-based devices retain 86 % of their initial PCE after 7 hours of light exposure, in contrast to a 48 % loss observed in P3HT-based devices. This highlights the effectiveness of BDD copolymerization in reducing photooxidation and recombination processes, common contributors to OSC instability. The results provide important insights into the degradation processes of OSCs and serve as a basis for designing more durable and efficient materials in the future.

1.2 Problem statement

The problem of thermal and photo degradation in OSCs is a major barrier to their long-term stability and commercial viability. Despite significant advancements in their power conversion efficiency, OSCs often suffer from rapid performance deterioration under thermal stress and prolonged exposure to light. Thermal degradation leads to morphological changes, phase separation, and chemical instability within the active layer, adversely impacting charge transport and device efficiency. Similarly, photo degradation, driven by prolonged irradiation, induces photooxidation and the formation of trap states, which further reduce conductivity and efficiency. These degradation mechanisms are particularly pronounced in certain donor-acceptor material systems, such as those based on P3HT, which exhibit limited stability under operational conditions. Understand-

ing the specific factors that contribute to these instabilities, including molecular interactions, oxidation pathways, and structural changes, is crucial for designing OSCs with improved durability. Addressing this challenge requires identifying materials and processes that can mitigate degradation, ensuring stable performance, and extending the operational lifespan of OSC devices. A promising approach to enhancing photostability of organic solar cells is the copolymerization of non-electron-withdrawn units in thiophene-based organic solar cells. Furthermore, the field of organic solar cells can benefit from a detailed analysis of how acceptor materials influence the thermal degradation of P3HT-based organic solar cells. Such insights can guide future material selection and design strategies, ultimately leading to more durable and effective solar energy solutions.

1.3 Objectives of the study

This doctoral thesis has a general objective and specific objectives that will be addressed within the study period.

1.3.1 General Objective

The general objective of the study is to investigate the stability mechanisms in fullerene- and Nonfullerene Acceptor-based OSCs and recommend improvements.

1.3.2 Specific Objectives

A specific objective of this work is to enhance the stability of OSCs by addressing different degradation mechanisms within the device structure. Specifically, the study focuses on examining the role of acceptors in the thermal degradation of OSCs using P3HT as donor material. This includes a comparison of fullerene and Nonfullerene Acceptor-based acceptors within the device architecture of ITO/ZnO/active layer/MoO3/Ag. Lastly, to improve the photostability of thiophene-based OSCs, nonelectron-withdrawing unit copolymerization is employed. This approach utilizes P3HT and PBDD4T as donor materials and $PC_{71}BM$ as acceptor in an inverted device configuration.

1.4 Thesis outline

This research thesis is structured into six chapters, outlined as follows: Chapter One provides an introduction to the study, encompassing the background, problem statement, research objectives, and an overview of the organization of the thesis. Chapter Two reviews relevant literature associated with the study. Chapter Three describes the experimental procedures, materials, and methods used to analyze various conjugated polymers. Chapters Four and Five focus on presenting the research findings. Finally, Chapter Six concludes the thesis with a summary and recommendations for future research.

Chapter 2

Organic solar cells (OSC)

2.1 Organic Semiconductors: A Revolution in Materials Science

Organic semiconductors are solid materials primarily composed of hydrocarbons but may also include heteroatoms such as oxygen, sulfur, and nitrogen. These materials conduct electricity due to the presence of a conjugated -π electron system formed by sp^2-hybridized carbon atoms with overlapping pz orbitals. Organic semiconductors are typically divided into two primary subcategories: conjugated small molecules and conjugated polymers. Polymers are large macromolecules composed of repeating structural units, known as monomers, which are chemically linked ((via covalent bonds) in a continuous sequence. These repeating units form a structure large enough to exhibit consistent physical and chemical properties, even when additional monomers are added. Polymers are broadly classified into two categories based on the number of monomer units: oligomers, which contain 20 to 100 monomer units, and polymers, which have more than 100 monomer units. While oligomers' physical properties can vary significantly with the addition or removal of a few monomer units, polymers exhibit stable properties regardless of such changes.

Historically, polymers were considered excellent electrical insulators, leading to their widespread use in applications such as protective packaging, insulation around copper wires, and structural components of electrical appliances to ensure user safety [25, 26]. In the late 1970s, Shirakawa

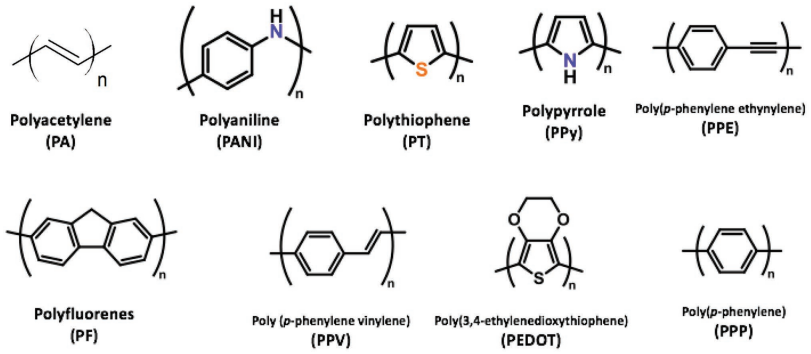


Figure 2.1: Illastrated examples of conjugated polymers [29]

and colleagues found that treating polyacetylene with iodine significantly enhanced its electrical conductivity, increasing it by a factor of 10^7[27]. Shirakawa and his team were awarded the Nobel Prize in Chemistry in 2000 for their groundbreaking work. Their discovery opened up a new field of research into π-conjugated polymers, which had earlier been considered electrical insulators.

Conjugated polymers are macromolecules characterized by a backbone composed of alternating double or triple bonds. This unique structural feature enables the delocalization of π-electrons along the polymer chain, giving rise to their semiconducting properties[28]. Conjugated polymer in The repeating backbone units, composed of conjugated chains, significantly influence the polymer's HOMO (highest occupied molecular orbital) and LUMO (lowest unoccupied molecular orbital) energy levels, as well as its band gap. Modifications to the side chains can alter the polymer's solubility, processability, and interaction with other materials, while introducing new substituents enables fine-tuning of the material's properties to enhance its performance in specific applications.

Small adjustments to the side chains and the polymer backbone structure can change in the polymer's properties. For instance, altering substituents can optimize the material's band gap, adjust molecular orbital energy levels, and enhance compatibility for use in OSCs devices. Conjugated polymers offer a unique combination of properties that make them highly versatile materials as shown in the figure 2.1. These materials retain the excellent mechanical properties of traditional plastics while exhibiting semiconducting behavior and desirable optical characteristics. Their synthesis allows for a high degree of structural and electronic tuning, making them ideal candidates for applications in advanced technologies such as OSCs, light-emitting diodes (OLEDs), and organic field-effect transistors (OFETs).

Conjugated polymers represent a novel and promising class of materials that bridge the gap between traditional plastics and conventional semiconductors. Their unique combination of mechanical, optical, and electronic properties, along with their unparalleled flexibility in synthesis, makes them attractive candidates for a wide range of applications in organic electronics. The groundbreaking discovery of conductive polymers has not only expanded our understanding of materials science but also paved the way for innovative technologies in energy and electronics.

2.1.1 The role of carbon in organic small molecules and conjugated polymers.

Carbon (C) plays a central role in the structure and functionality of polymeric materials, particularly organic semiconductors. The electronic properties of a polymer are fundamentally determined by the types of bonds formed between adjacent carbon atoms within its backbone. Polymers are categorized as either saturated or unsaturated on the basis of the nature of the carbon-carbon bonding and the involvement of carbon's valence electrons in forming chemical bonds with neighboring atoms[30].

In saturated polymers, all four valence electrons of each carbon atom participate in covalent bonds, resulting in a backbone where only single bonds exist between adjacent carbon atoms. Because all of the valence electrons are tightly bound in covalent bonds, saturated polymers are electrically insulating because there are no free or delocalized electrons available for charge transport. In contrast, unsaturated polymers contain double or triple bonds between carbon atoms, leaving some valence electrons less tightly bound. These unsaturated bonds provide the basis for unique electronic properties, particularly in conjugated polymers, which are essential for organic semiconductors.

Conjugated polymers are characterized by a repeating sequence of alternating single and double bonds along their backbone. This alternation creates a system of π-conjugation, where the π-electrons are delocalized across the polymer chain. The delocalization arises from the overlap of molecular orbitals formed by the unhybridized p-orbitals of adjacent carbon atoms. This phenomenon is a key contributor to the semiconducting behavior of conjugated polymers, as it facilitates the movement of charge along the polymer backbone.

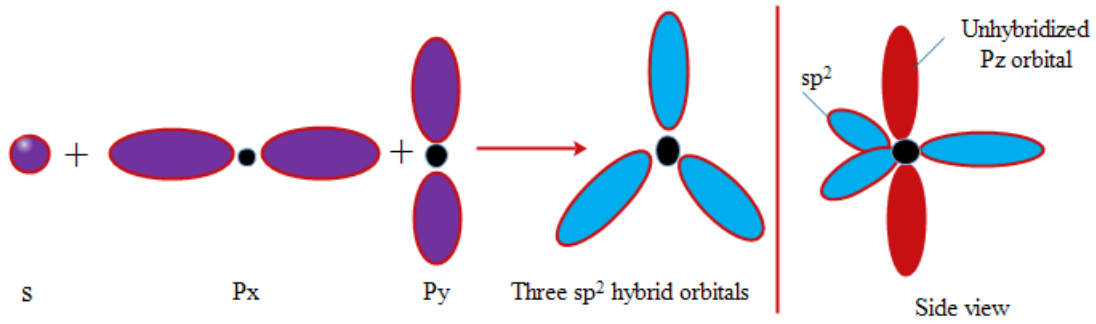


Figure 2.2: The process of sp^2p_z hybridization and the three hybridized orbital together with the perpendicular unhybridized 2p orbital.

The underlying mechanism of this delocalization is rooted in the sp^2p_z hybridization of carbon atoms. Each carbon atom in a conjugated polymer forms three sp^2p_z hybridized orbitals, which are arranged in a planar trigonal geometry with bond angles of approximately 120°. Figure 2.2 illustrates the process of sp^2p_z hybridization. These sp^2p_z orbitals participate in forming strong covalent σ-bonds that define the structural stability of the polymer[31, 32]. In addition to the three sp^2 hybrid orbitals, each carbon atom has one unhybridized p_z orbital, which lies perpendicular to the plane of the sp^2 orbitals. The overlap of p_z orbitals between adjacent carbon atoms in a polymer chain creates π-bonds, resulting in delocalization of electrons along the chain

The electrons in σ-bonds are strongly localized and tightly bound, contributing primarily to the mechanical and structural stability of the polymer. On the other hand, the electrons in π-bonds are more loosely bound due to their lower energy and are capable of delocalization. This delocalization is essential for the dynamic electronic processes required in semiconducting applications. For example, in a simple polymer such as ethene, each double bond consists of one σ-bond (formed by the overlap of sp^2 orbitals) and one π-bond (formed by the side-by-side overlap of unhybridized p orbitals)(See figure 2.3).

The interaction of orbitals in conjugated systems leads to the formation of molecular orbitals that are split into bonding (π, σ) and anti-bonding (π^*, σ^*) orbitals as shown in the figure 2.3. The energy of bonding orbitals (π or σ) is lower than that of the corresponding hybridized or unbonded atomic orbitals, whereas anti-bonding orbitals (π^* or σ^*) have higher energy. In conjugated polymers, as more carbon atoms are linked and their p orbitals overlap, a system of delocalized molecular orbitals is formed, giving rise to a band structure similar to that of

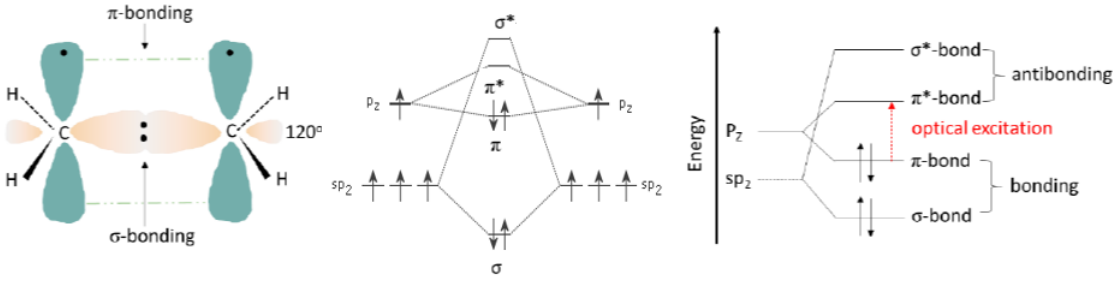


Figure 2.3: Schematic diagram of the formation of σ- and π- bonding of Ethene (left). The energy diagram for the optical band gap(Eg) from π-bond to π^*-bond (right)for ethene polymer carbon atoms forming σ-bonds and non-hybridized pz-orbitals overlapping and forming π-bonds [33].

inorganic semiconductors.

The semiconducting behavior of conjugated polymers arises from the energy difference between the HOMO and the lowest unoccupied molecular orbital (LUMO). This energy difference, known as the Energy gap (E_g), determines the electronic and optical properties of the polymer. When light is absorbed by the polymer, electrons are excited from the HOMO to the LUMO, creating excitons (electron-hole pairs) that can contribute to charge transport if properly separated. The size of the bandgap can be tuned by modifying the chemical structure of the polymer, enabling a wide range of applications in organic semiconductors.

2.2 Historical background of Organic Solar Cells

Organic solar cells (OSCs), also known as plastic solar cells, represent a photovoltaic cell technology utilizing organic semiconductors like polymers or small molecules for light absorption and charge transport. These materials act as the active layer in OSC devices, converting light into electricity. The journey of organic photovoltaics (OPV) started with the discovery of photoconductivity in anthracene by Pochettino in 1906 [34, 35]. In 1958, Kearns and Calvin developed solar cells using magnesium phthalocyanines, achieving a photovoltage of 200 mV [**?**]. During the 1980s, researchers explored polymer-based solar cells, which initially showed low power conversion efficiencies (PCEs) around 0.1 % [36, 37]. These early devices typically had a single active layer made of a dye or a polymer. However, in 1986, Tang significantly enhanced device efficiency to about 1 % by creating a donor-acceptor heterojunction (HJ) structure [38].Although

this efficiency was approximately 10^4 times greater than that of traditional single-layer OSCs, it remained relatively low. The early advancements in organic solar cells are outlined below.

2.2.1 Single layer organic solar cells

In 1982, Weinberger et al. introduced the first single-layer OSC, which served as the foundation for the development of OSC architecture [36]. A single-layer organic solar cell (OSC) comprises an organic semiconductor layer sandwiched between an anode and a cathode, as shown in Figure 2.4(a). The HOMO andLUMO levels are illustrated in Figure 2.4(b). Light enters the cell through the transparent anode, which is usually made of indium tin oxide (ITO), while the cathode consists of a metal electrode such as aluminum (Al) or silver (Ag). When photons with energy $E \geq E_g$ strike the OSC—where E_g denotes the energy gap of the organic material ($E_g = E_{\text{HOMO}} - E_{\text{LUMO}}$)—they are absorbed, causing electrons to transition from the HOMO to the LUMO, leaving behind holes in the HOMO.

Due to the low dielectric constant of organic materials, the generated electron-hole pairs experience strong Coulombic attraction, forming bound states known as Frenkel excitons [39]. These excitons possess a binding energy in the range of a few hundred millielectron volts (meV), which is considerably higher than that observed in inorganic semiconductors.

The excitons generated by light absorption are electrically neutral, meaning they cannot be directed or separated by the electric field arising from the difference in work functions of the two electrodes [40]. For current to be produced, these excitons must first be dissociated into free electrons and holes, which can then be transported to their respective electrodes under the influence of the electric field created by the work function disparity. Due to the lack of efficient exciton dissociation, single-layer organic solar cells exhibited extremely low PCE, typically an order of magnitude below 0.1% [41, 42, 43]

2.2.2 Bilayer organic solar cells

The concept of a bilayer OSC was invented by Tang [38], where two layers of organic semiconductor materials were sandwiched between the two electrodes; one layer consisted of a donor and the

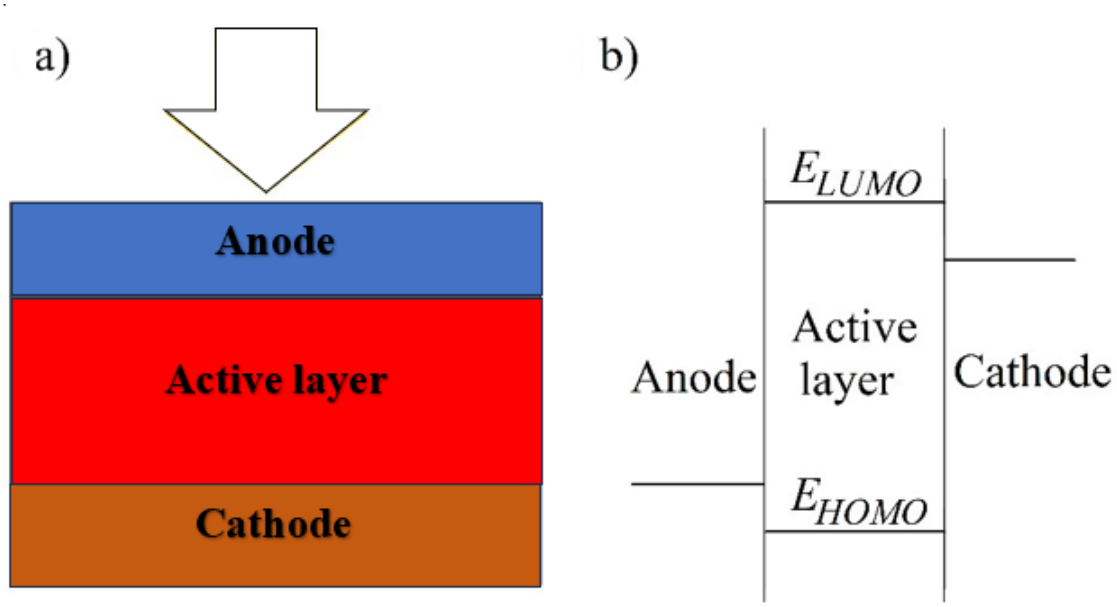


Figure 2.4: (a) A schematic single layer OSC structure and (b) energy band diagram

other of an acceptor material [44]. A bilayer OSC is schematically shown in Figure 2.5(a)which shows the structure and the right part shows the locations of HOMO and LUMO energy levels of donor and acceptor [45, 46] A donor material has lower ionization potential and acceptor has higher electron affinity. Typically, a donor exhibits higher energy levels in both the HOMO and LUMO compared to the acceptor, as illustrated in Figure 2.5(b). The region where the donor and acceptor meet is known as the donor-acceptor interface (D-A interface). At this junction, the energy levels of the donor's HOMO and LUMO are elevated relative to those of the acceptor. In this scenario, light first strikes the donor layer, and if the incident photons possess energy satisfying

$$E \geq E_g = \left(E^D_{\text{HOMO}} - E^D_{\text{LUMO}}\right)$$

, an electron transitions from the donor's HOMO to its LUMO, leaving behind a hole in the HOMO and generating a Frenkel exciton. Since excitons are electrically neutral, they diffuse randomly rather than moving in a specific direction. Upon reaching the donor-acceptor interface, the electron is transferred from the donor's LUMO to the acceptor's LUMO, which is at a lower energy level. This process results in the formation of a charge transfer (CT) exciton, with the excess energy dissipated into molecular vibrations. If this energy surpasses or equals the binding energy of the CT exciton and interacts with it again, the exciton can dissociate into a free electron

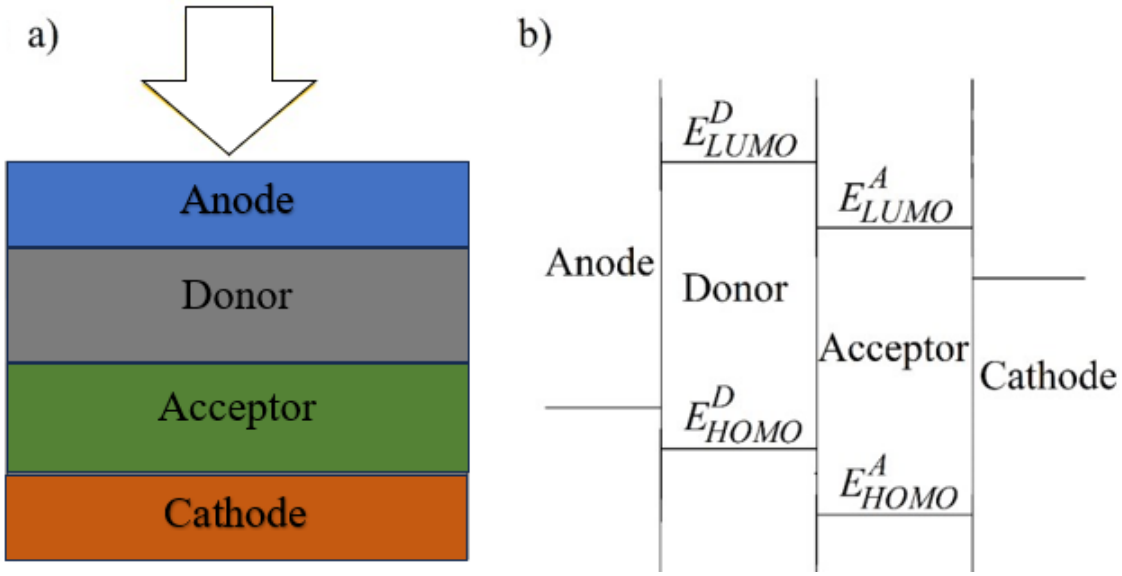


Figure 2.5: (a) A schematic bilayer OSC structure and (b) HOMO and LUMO energy levels of donor and acceptor.

and hole [47]. Once dissociation occurs, the free electrons move toward the cathode, while the free holes migrate toward the anode, driven by the electric field created by the difference in work functions between the two electrodes. However, as there is only one D-A interface at the end of the donor layer and excitons have a diffusion length of less than 10 nm [48, 49, 50, 51, 52, 53] in organic materials, many excitons may recombine before reaching the D-A interface. Even in bilayer structures, most NFAs have exciton diffusion lengths greater than 10 nm, which is not long enough to fully overcome the limitations of planar heterojunctions[54, 55] . This is why bulk heterojunctions remain essential for efficient charge generation in OSCs, even with modern NFAs. Due to the planar nature of the junction between the donor and acceptor materials, the layer thickness is restricted by the exciton relaxation time. Therefore, although a bilayer structure introduces a mechanism of dissociation of excitons resulting in a higher PCE than that of single layer, it is still very poor [41, 46, 56] , which has led to the invention of the bulk heterojunction (BHJ)0 structure as described below.

2.2.3 Bulk-heterojunction organic solar cells

The BHJorganic solar cell (OSC) structure and its energy band diagram are illustrated in Figure 2.6. In a BHJ arrangement, the donor and acceptor materials are intimately blended, cre-

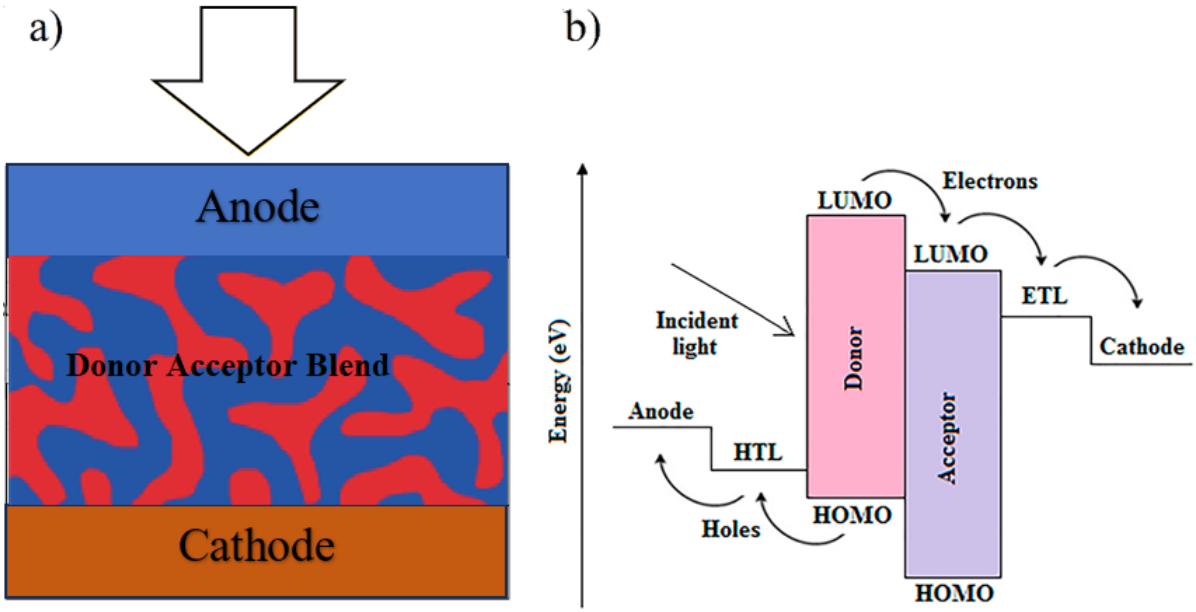


Figure 2.6: (a) A schematic representation of a bulk heterojunction OSC structure and (b) its corresponding energy band diagram.

ating a nanoscale interpenetrating network with numerous donor–acceptor (D–A) interfaces. This morphology ensures that most photo-generated excitons—quasi-particles with limited lifetimes—can reach a D–A interface within their diffusion length before recombining. While traditional fullerene-based materials typically exhibit exciton diffusion lengths of around 10 nm, non-fullerene acceptors (NFAs), such as ITIC and Y6 derivatives, have demonstrated longer diffusion lengths, ranging from approximately 10 to 20 nm or more in optimized systems. This enhancement is attributed to improved molecular ordering and stronger π-π stacking in NFAs, which facilitate more efficient exciton transport. Consequently, BHJ systems employing NFAs may support slightly coarser phase separation while still maintaining effective exciton dissociation, offering more design flexibility and potentially improved device performance[57, 55]. When light is absorbed by the organic active layer, both the donor and acceptor materials can be excited at the same time, depending on the the energy of the incoming photons. Figure 2.6(a) presents the schematic structure of a BHJ OSC, while Figure 2.6(b) depicts the corresponding energy band diagram.

Although the detailed working principle of BHJOSCs is discussed later, it is important to note here that the BHJ architecture significantly enhances light absorption and, consequently, the generation of photogenerated charge carriers. This improvement has contributed to PCEs exceeding 18% [58].

2.3 Working principle of OSC

2.3.1 Energy Conversion Processes

The following sections explore the key energy conversion processes in OSCs, including light absorption, exciton generation, exciton dissociation, charge transport, and charge extraction. Figure 2.7 shows a schematic energy diagram of an OSC, highlighting the key components, including the anode, donor, acceptor, and cathode.

1. **Light absorption and exciton generation** When photons with energy exceeding the band gap (E_g) of the active material—determined by the energy between LUMO) and HOMO—are absorbed, excitons are created. In organic semiconductors, the photo-generated excitons do not immediately produce free charge carriers because of the strong Coulombic attraction between the positively and negatively charged centers, or electrically neutral.

   Typically the binding energy of excitons in organic materials is in the range of 200 to 500 meV, which is much higher than the thermal energy of silicon semiconductors at room temperature (25 meV). This is because organic semiconductors have a low dielectric constant, leading to weak charge screening and intense Coulombic interactions between electron-hole pairs. Efficiency losses in OSCs mainly result from factors such as the disparity between the absorption spectrum of the active material and incoming photons, reflection losses across various layers, and exciton recombination within the active layer.

2. **Exciton diffusion** In a BHJsolar cell, photo-excited charge carriers are generated when excitons dissociate at the donor-acceptor (D/A) interface. To achieve efficient OSCs, excitons must be effectively dissociated within their diffusion length. To optimize performance, loss mechanisms such as exciton quenching and recombination through radiative and non-

radiative decay pathways must be minimized. Excitons need to diffuse and arrive the donor-acceptor (D/A) interface within their lifetime.

3. **Charge separation** The process of charge separation is illustrated in Figure 2.7 , depicting the events that occur after excitons reach the donor-acceptor (D/A) interface. When an exciton is generated within the donor material, it migrates to the D/A interface, where it transitions into charge transfer states (CTs). At this point, electrons move from the donor'sLUMO to the acceptor's LUMO, while the associated holes stay in the donor's HOMO. The separation of these charge transfer states leads to the formation of free electrons and holes.

   Charge recombination significantly impacts the efficiency of charge separation and is a primary cause of energy loss in photovoltaic conversion. Minimizing this process is essential. To achieve optimal performance, it is important to improve charge transfer and separation rates while effectively suppressing charge recombination.

4. **Charge transport** For effective charge collection, photo-generated electrons and holes must rapidly move along the internal electric field toward their respective electrodes. The quicker these charge carriers diffuse, the more efficiently they can be separated. In a BHJ structure, an internal electric field forms due to the potential difference between the anode and cathode. This field drives holes toward the anode and electrons toward the cathode. Efficient charge carrier collection at the electrodes is enabled by the energy alignment between the anode and the donor's HOMO, as well as the ohmic contact between the cathode and the acceptor'sLUMO. However, energy losses in this process mainly arise from charge recombination at the electrode interface or limited charge carrier mobility.

2.4 Current -voltage characteristics of OSC

When exposed to light, an organic solar cell (OSC) generates a photocurrent, which is then plotted against the applied voltage. As illustrated in Figure 2.8(b), the current-voltage (I-V) curve provides essential characteristics of the device. This section discusses four key parameters

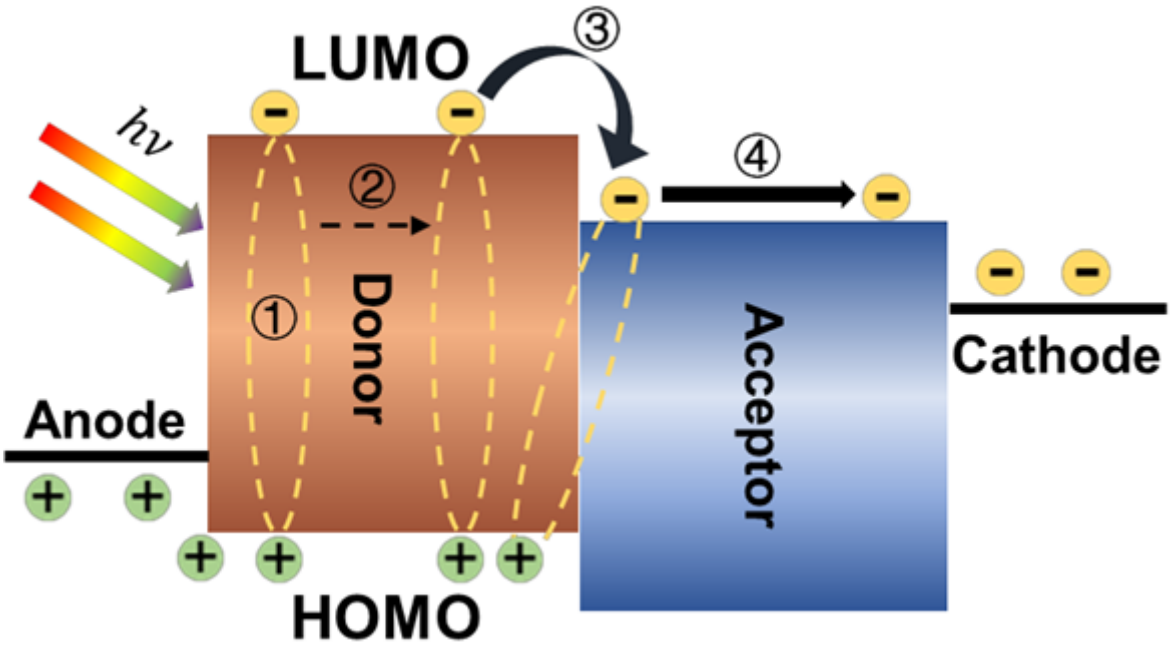


Figure 2.7: Energy conversion processes in OSCs.

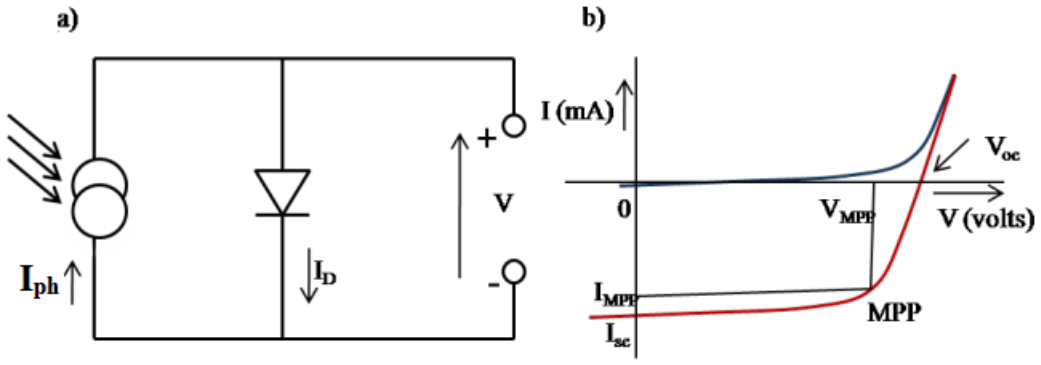


Figure 2.8: (a) Equivalent circuit of OSC. (b) I-V curve for OSC in the dark (blue) and under illumination (red) [59].

that can be derived from the I-V curve, which are crucial for evaluating the device's performance and comparing it with different polymer solar cells.

2.4.1 Short-circuit current density

The short-circuit current (I_{sc}) is the peak current a solar cell can generate under a given illumination power when there is no applied external voltage. Essentially, it signifies the maximum current that flows when the cell is in a short-circuit condition. The short-circuit current density (J_{sc}) is defined as the I_{sc} normalized by the cell's active area. Several factors can influence the

photocurrent extracted from the solar cell. For example, absorption of light, degree of interpenetration of donor acceptor network, non-geminate recombination at the interface and charge carrier mobility in the individual donor acceptor phases determines short-circuit current of OSCs [60]

2.4.2 Open-circuit voltage

Open-circuit voltage (V_{oc}) is the voltage at which the photocurrent generated is zero or in other words the voltage across the open terminals of OSC. The maximum value of open-circuit voltage of polymer solar cells is related to the difference between the HOMO of donor and the LUMO of acceptor [61]. Under illumination and at the open-circuit condition, the V_{oc} equals the difference between the quasi-Fermi levels within the polymer and fullerene phase separated domains [62, 63]:

$$V_{oc} = \frac{1}{q}\left(E_{\mathrm{LUMO}}^{\mathrm{fullerene}} - E_{\mathrm{HOMO}}^{\mathrm{polymer}} - \Delta\right) - \frac{kT}{q}\ln\left(\frac{n_e n_h}{N_c N_v}\right) \tag{2.4.1}$$

where $E_{\mathrm{LUMO}}^{\mathrm{fullerene}}$ is the LUMO energy level of fullerene derivatives; $E_{\mathrm{HOMO}}^{\mathrm{polymer}}$ is the HOMO energy level of donor polymers; N_c, N_v are the density of conduction states at the band edges HOMO of the polymer and LUMO of fullerene respectively, k is the Boltzmann constant, Δ is the energy shift originating from disorder within the solution cast and phase separation, T is the absolute temperature. The open-circuit voltage (V_{oc}) can be influenced by different factors, as outlined in Equation 2.4.1. From Equation 2.4.1, it is clear that V_{oc} decreases in both of the following scenarios.

The first occurs in polymer–fullerene BHJ solar cells, the molecular ordering of the polymer donor significantly influences the electronic properties of the active layer. Enhanced crystallinity, resulting from tighter polymer chain packing, facilitates stronger π–π stacking interactions. This increased order leads to a delocalization of the π-electron system, effectively narrowing the bandgap of the polymer. A reduced bandgap allows the material to absorb a broader spectrum of sunlight, particularly extending into the near-infrared region, thereby enhancing the photocurrent and overall power conversion efficiency (PCE) of the device[64]. This, in turn, leads to an increase in the number of states in both the HOMO and LUMO bands. Depending

on the processing condition, the crystallinity of the polymer changes and those changes results in the change in bandgap [65, 66, 67].

The second case occurs when additional shunt pathways enable charge carriers to reach the opposite electrodes. If a photogenerated charge carrier finds a low-resistance route that circumvents the bulk heterojunction, it reduces the separation between the quasi-Fermi levels. This occurs due to a decline in charge carrier density within the HOMO and LUMO bands, ultimately lowering V_{oc}.

2.4.3 Fill factor

The fill factor (FF) is the ratio of the maximum achievable power to the product of J_{sc} and V_{oc}. It measures the squareness of the J-V curve of the solar cell is when exposed to light. It is indicator of the quality of the J-V characteristic of the solar cell [68]. Fill factor of a device is calculated as [60]:

$$FF = \frac{V_{\mathrm{MPP}}}{V_{\mathrm{oc}}} \times \frac{J_{\mathrm{MPP}}}{J_{\mathrm{sc}}} \tag{2.4.2}$$

FF is a very important parameter affecting the power conversion efficiency and it is affected by several factors such as shunt and series resistances, mismatching in charge carrier mobility (hole and electron) and charge carrier collection due to interface state recombination etc [69]. High charge carrier mobilities result in high fill factor (FF) values, whereas an imbalance in charge carrier mobility reduces FF. This occurs because a decrease in the mobility of one type of charge carrier causes charge accumulation in either the fullerene or polymer domain, which lowers the built-in potential and hinders charge collection. Inefficient charge carrier collection, and consequently a reduction in FF, is caused by both mobility mismatch and trap-assisted recombination.

2.4.4 Power conversion efficiency (PCE)

The power conversion efficiency (PCE), denoted as η, refers to the proportion of maximum output power (P_{max}) to the incident light power (P_{in}) that falls on the active area of the device. The

PCE of a solar cell can be expressed as follows [60]:

$$\eta = \frac{P_{\text{max}}}{P_{\text{in}}} = \frac{FF \cdot J_{\text{sc}} \cdot V_{\text{oc}}}{P_{\text{in}}} \tag{2.4.3}$$

P_{in} is the incident power density, which is standardized at 1000 W/m^2 with a spectral intensity matching that of the sun on the earth's surface at an incident angle of 48.19° (AM 1.5) [70].

2.5 Charge Carrier Transport and Recombination in OSCs

2.5.1 Charge carrier transport

Various techniques exist for analyzing the charge transport properties of solar cell devices and extracting essential transport parameters, such as charge mobility (μ). These methods include time-of-flight, field-effect transistor, and space charge-limited current (SCLC) techniques. This discussion highlights the widely adopted SCLC method. The SCLC model is particularly useful for assessing the charge transport characteristics of organic semiconductors, such as free carrier density, trap density, and effective carrier mobility. When an external voltage is applied, charge carriers are injected into the device, leading to the formation of a space charge region. This region limits current flow due to the inherently low charge carrier mobility in organic materials. The current described by the Mott-Gurney law equation 5.2.3 is therefore referred to as SCLC [71, 72].

Now, let's derive the Mott-Gurney law equation for SCLC. Consider a crystal of thickness L through which a current J flows. Let $E(x)$ represent the electric field at a distance x from the surface. The core principle of SCLC theory is based on the Poisson equation, which establishes a relationship between the electric field (E) and the charge density ρ within the material. In one dimension, it is given by:

$$\frac{dE}{dx} = \frac{\rho}{\epsilon\epsilon_0} \tag{2.5.1}$$

where (ϵ) is the dielectric constant of the material and (ϵ_0) is the vacuum permittivity. The current density (J) is given by:

$$J = qn\mu E \tag{2.5.2}$$

where (q) is the charge of the carriers, (n) is the carrier density, and (μ) is the mobility of the carriers. The case of SCLC, the current is limited by the space charge, so the carrier density (n) is related to the charge density ρ by:

$$(\rho = qn) \tag{2.5.3}$$

Substitute $(\rho = qn)$ into Poisson's equation:

$$\frac{dE}{dx} = \frac{qn}{\epsilon\epsilon_0} \tag{2.5.4}$$

Substitute $(n = \frac{J}{q\mu E})$ into the above equation:

$$\frac{dE}{dx} = \frac{J}{\epsilon\epsilon_0\mu E} \tag{2.5.5}$$

Integrate with respect to (x) from 0 to (L) (thickness of the material):

$$\int_0^L \frac{dE}{E} = \frac{J}{\epsilon\epsilon_0\mu}\int_0^L dx \tag{2.5.6}$$

This simplifies to:

$$\ln\left(\frac{E(L)}{E(0)}\right) = \frac{JL}{\epsilon\epsilon_0\mu} \tag{2.5.7}$$

Boundary Conditions: At (x = 0), (E(0) = 0) and at (x = L),

$$(E(L) = \frac{V}{L}) : \ln\frac{V}{L} = \frac{JL}{\epsilon\epsilon_0\mu} \tag{2.5.8}$$

Therefore:

$$J = \frac{\epsilon\epsilon_0\mu V}{L^2} \tag{2.5.9}$$

Considering the quadratic dependence on voltage for SCLC, the final form of the Mott-Gurney law is:

$$J_{SCLC} = \frac{9}{8}\epsilon\epsilon_0\mu\frac{V^2}{L^3} \tag{2.5.10}$$

In this model, ϵ represents the permittivity of the organic material, while ϵ_0 denotes the permittivity of free space. The mobility of free carriers is indicated by μ, L corresponds to the device

thickness, and V signifies the applied voltage. To incorporate the effect of traps, a trap factor θ is introduced in Equation 5.2.3, which depends on the concentration of both free and trapped carriers. After integrating θ, the space-charge-limited current (SCLC) is expressed by Equation 2.5.11.

$$J_{SCLC} = \frac{9}{8}\epsilon\epsilon_0\mu\theta\frac{V^2}{L^3} \tag{2.5.11}$$

where the charge changes with the applied electric field E, μ is then given by

$$\mu = \mu_0 \exp(\gamma\sqrt{E}), \tag{2.5.12}$$

where μ_0 is the zero-field mobility, γ is the field-dependence effect factor, and $E{=}V/L$ is the applied electric field, then equation 5.2.3 can be rewritten as

$$J_{SCLC} = \frac{9}{8}\epsilon\epsilon_0\mu\frac{V^2}{L^3}\exp\left(\gamma * 0.86\sqrt{\frac{V}{L}}\right) \tag{2.5.13}$$

The constant value of 0.86 is utilized to align the model with experimental data. To determine the charge mobility (μ_0) and the field-dependence factor (γ) in practice, the Mott-Gurney equation 2.5.13 must be applied to the J-V experimental data obtained in dark conditions, where the relationship $J \propto V^2$ holds.

2.5.2 Recombination of organic solar cells

In OSCs, recombination plays a critical role in determining device efficiency and stability. The two primary recombination mechanisms, bimolecular recombination and trap-assisted recombination, can be understood more deeply by considering their influence on the current-voltage (J-V) characteristics. Bimolecular recombination is a key process in organic solar cells that can negatively impact their efficiency [73, 74]. It occurs when an electron and a hole, generated by the absorption of light, encounter each other and recombine before they can be collected at their respective electrodes. This recombination process follows second-order kinetics, meaning that the recombination rate depends on the concentration of both electrons and holes. When a photon is absorbed, an exciton is generated, and it needs to dissociate into free charge carriers (electrons

and holes) at the donor-acceptor interface. Ideally, these carriers should move to their respective electrodes and contribute to the photocurrent. However, in bimolecular recombination, some of the free electrons and holes recombine before they reach the electrodes, reducing the efficiency of the solar cell. In terms of the ideality factor, bimolecular recombination typically results in an ideality factor n close to 1, indicating minimal influence from external traps or defects. This is because it follows second-order kinetics, where the recombination rate depends on the product of electron and hole densities. In a solar cell dominated by bimolecular recombination, the current density J and voltage V are related by an ideal diode equation:

$$J \propto \exp\left(\frac{qV}{nkT}\right) \tag{2.5.14}$$

where J is the current density, q is the elementary charge, k is the Boltzmann constant, T is the temperature, V is the voltage and n is the ideality factor. Trap-assisted recombination (other types of recombination), also known as Shockley-Read-Hall (SRH) recombination, occurs when charge carriers are captured by localized defect states (traps) within the energy gap of the semiconductor[75]. These traps can be caused by impurities, molecular disorder, or fabrication defects in the organic material. An electron (or hole) first gets trapped at one of these defect sites, and then a hole (or electron) recombines with the trapped carrier. This process introduces additional pathways for recombination, which do not depend directly on the concentration of free carriers, but are instead limited by the density and energy levels of the traps.

In the presence of significant trap-assisted recombination, the ideality factor n increases beyond 1. Typically, ideality factors between 1 and 2 are observed, with values closer to 2 indicating a strong influence of trap-assisted recombination [76]. A higher ideality factor means that the recombination process is no longer purely bimolecular, but is significantly affected by trap states. The kinetics in this case are governed by the capture and release of carriers from trap states, which slow down charge transport and increase recombination losses. The relationship between the ideality factor and the dominant recombination mechanism can be summarized as $n \approx 1$, bimolecular recombination is dominant and the system behaves like an ideal diode. When $n > 1$ (often closer to 2): Trap-assisted recombination is significant, indicating the presence of deep-level defects or disorder in the material that facilitate recombination via traps. The ideality

factor provides insight into the dominant recombination processes affecting the performance of an OSC. A high ideality factor ($n \approx 2$) suggests that trap-assisted recombination is severe, which typically leads to poor device performance, as traps create energy barriers that hinder the extraction of charge carriers. Conversely, an ideality factor closer to 1 indicates that recombination is primarily bimolecular, and the OSC has better potential for high PCE, as free charge carriers are less likely to recombine before contributing to the photocurrent.

In conclusion, the ideality factor n serves as a useful diagnostic tool to understand the balance between bimolecular recombination and trap-assisted recombination in organic solar cells. Lower values of n suggest that recombination is primarily bimolecular, while higher values indicate significant trap-assisted recombination. Reducing the impact of traps through material optimization, defect passivation, and improved morphology can lead to lower recombination losses and higher efficiency in OSCs.

When discussing current density (J) in OSCs in relation to light intensity (I) and recombination, the power-law relationship between the photocurrent (J_{ph}) and light intensity can be written as:

$$J_{\text{ph}} \propto I^{\alpha} \tag{2.5.15}$$

Where: - J_{ph} is the photocurrent density, which is the current generated by the cell when illuminated, - I is the incident light intensity, - α is the power-law exponent.

The value of α provides important information about the dominant recombination mechanism in the OSC. Here's how the value of α, particularly when it is 1 or less than 1, relates to recombination: If the power law exponent α is equal to 1, this suggests that the photocurrent increases linearly with light intensity: In this case, recombination losses are minimal, and most of the photogenerated charge carriers (electrons and holes) are efficiently extracted before they can recombine. Recombination in the device is low or negligible. This scenario typically corresponds to ideal device performance in which bimolecular recombination is very weak or suppressed.

In an ideal organic solar cell , $\alpha = 1$ suggests that bimolecular recombination is not a dominant process. The charge carrier extraction is very efficient. The cell is operating in a regime in which the majority of photogenerated carriers contribute to the current, resulting in a good power conversion efficiency. When α is less than 1 (e.g. $\alpha \approx 0.9$ or less), the photocurrent does not increase

as fast as the light intensity. This indicates that as the light intensity increases, the fraction of charge carriers that recombine also increases, reducing the current extracted. A lower α signifies a higher rate of recombination. This situation typically occurs when trap-assisted recombination or other nonideal recombination mechanisms (such as space-charge-limited recombination) are significant. If traps (defects or impurities in the material) capture carriers, they are more likely to recombine, reducing the photocurrent. As the light intensity increases, these traps fill up, but the level of recombination remains higher than under ideal conditions. In some cases, high carrier densities can lead to the build-up of space charge in the active layer, which reduces the efficiency of charge extraction and enhances recombination. This is also reflected by $\alpha < 1$.

In generaral, $\alpha = 1$ the recombination is minimal, and the photocurrent increases linearly with light intensity. The solar cell is operating efficiently, and most photogenerated charge carriers contribute to the current and $\alpha < 1$, recombination is significant. The photocurrent increases less than proportionally with the light intensity, suggesting that a higher fraction of charge carriers recombine before they are extracted, especially at higher light intensities. Trap-assisted recombination and space-charge effects may dominate.

Understanding the value of α in experiments helps in diagnosing the recombination dynamics within organic solar cells and provides insights for improving device design to minimize recombination and maximize performance.

2.6 Device structure

The standard device structure is depicted in Figure 2.9, where a BHJlayer is positioned between a metal cathode and a transparent conducting oxide (TCO) anode. TCOs, used as front electrodes, exhibit over 80 % transparency to visible light and possess a conductivity greater than 10^3 S/cm. Currently, indium tin oxide (ITO) is considered the industry benchmark among TCOs due to its low resistivity of approximately 10^{-4} $\Omega \cdot$ cm and its high transparency to visible light, exceeding 80 %. ITO front electrodes, typically 100-200 nm thick, are commonly deposited on glass or flexible transparent substrates for use in OSCs. The application of other TCOs such as fluorine-doped tin oxide (FTO) or zinc oxide (FZO), aluminum-doped zinc oxide (AZO), and indium

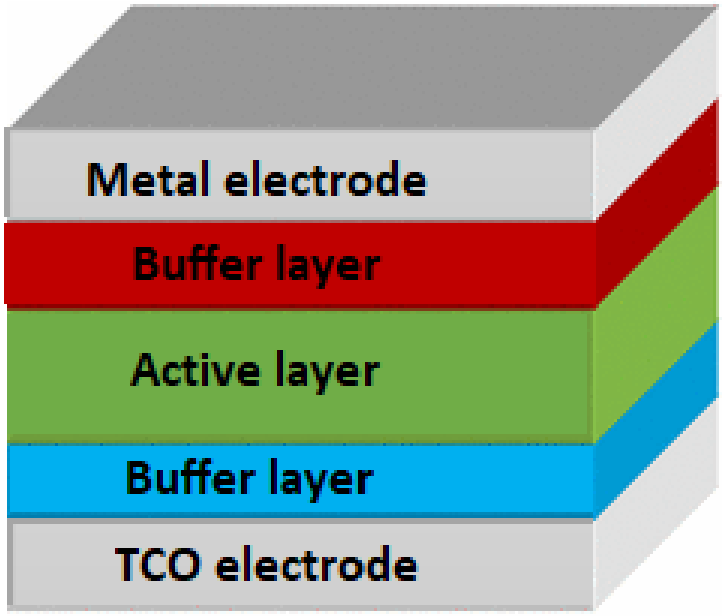


Figure 2.9: Schematic cross-sectional view of an OSC.

gallium zinc oxide (IGZO) have been also reported for use in OSCs [77, 78, 79]. Transparent conducting oxides (TCOs) possess a wide bandgap (E_g) with an energy value higher than that of visible light photons. As a result, photons with energy lower than E_g are not absorbed by these materials. This allows visible light to pass through the TCO electrode and be absorbed by the functional layers. To maximize the utilization of the solar spectrum, TCO electrodes with high transparency in the visible light wavelength range are preferred.

Metals with a low work function (WF), like aluminum (Al) and silver (Ag), are frequently utilized as rear electrodes in OSCs. Placing the active BHJ layer between the anode and cathode generates a potential difference within the BHJ, promoting the transport of photogenerated charges to their respective electrodes. Moreover, the inclusion of a hole extraction layer (HEL) and an electron extraction layer (EEL) enhances charge collection efficiency at the interfaces between the organic layer and the anode/cathode in OSCs.

OSCs are typically designed using either a conventional or an inverted device configuration, as illustrated in Figure 2.10. Indium tin oxide (ITO) remains one of the most widely used transparent conductive oxide (TCO) materials in OSCs. In conventional OSCs, it functions as the anode, while in inverted configurations, it can serve as the cathode. The TCO layer, whether acting as the anode in conventional OSCs or the cathode in inverted OSCs, is exposed to incoming light.

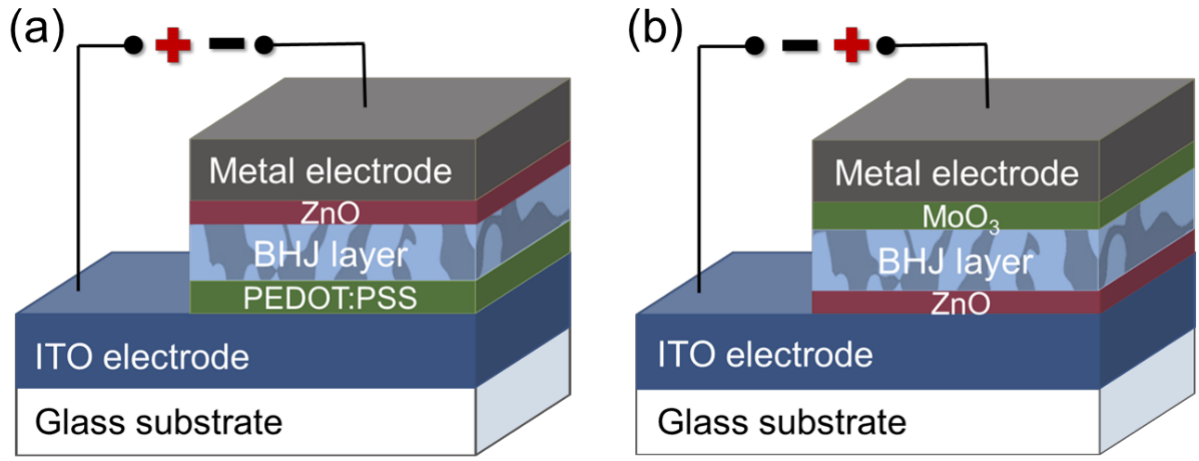


Figure 2.10: Schematic cross-sectional views of OSCs with (a) conventional and (b) inverted configuration.

To enhance charge collection efficiency at the anode/BHJor cathode/BHJ interfaces, the work function (WF) of ITO can be adjusted using various interlayers. In conventional OSCs, poly(3,4-ethylenedioxythiophene):polystyrene sulfonate (PEDOT:PSS) is the most commonly used hole extraction layer (HEL) and is typically applied onto the ITO surface via spin coating. However, PEDOT:PSS is acidic, which can lead to degradation of the ITO layer, negatively impacting the long-term stability of conventional OSCs. In contrast, inverted OSCs use a thermally evaporated molybdenum trioxide (MoO) layer ($\approx 2nm$) as the HEL instead of PEDOT:PSS, which helps extend the device's operational lifetime. Additionally, solution-processed zinc oxide (ZnO) is often employed as an electron extraction layer (EEL) in OSCs.

2.7 Photo and thermal induced degradation of organic solar cells

Although OSCs have achieved significant power conversion efficiency (PCE) improvements, surpassing 19% in some cases, their long-term stability remains a critical challenge, hindering their full commercialization. Despite the potential of OSCs in terms of flexibility, lightweight properties, and low-cost manufacturing, the devices often suffer from instability due to factors like environmental degradation from oxygen and water, thermal stress, humidity, the amount of sunlight outside and morphological changes in the active layers. This has been a key limitation in

transitioning OSCs to large-scale [80, 81, 82, 83]. Therefore, it is imperative to have a detailed understanding of the mechanisms of degradation and stability improvement. In order to address these issues, the International Summit on Organic Photovoltaic Stability (ISOS) conference held in 2010 established standard protocols for various testing conditions, including dark, outdoors, light soaking, thermal cycling, and others [84]. For example, standard protocols such as ISOS-D-2 and ISOS-L-3 proposed by the organic photovoltaic community require a test temperature of 85°C and a light intensity of 100 mW/cm^2 to study the thermal and photo stability of OSCs, respectively. However,each of the layers of OSCs and the interfaces are prone to test stresses like heat, light, and moisture, so it's crucial to control the aging conditions to show the degradation mechanism for only one layer. Degradation of the OSC that form the active layer is one of the main problems. Accordingly, this section focuses on the photo and thermally-induced degradation mechanisms and perspectives of OSC. Some attempts and strategies of researchers to improve the stability of OSC are also mentioned.

2.7.1 Photo-induced degradation of OSCs

The active layer in OSCs is usually composed of acceptor molecule and conjugated polymer with extensively delocalized π-electrons. These electrons are crucial for the material's optical and electrical properties, enabling photon absorption and charge carrier transport necessary for the device's operation. The ability of these polymers to absorb light depends on the length of the π-conjugation and the arrangement of the polymer chains. Consequently, any photochemical oxidation that changes the extent of π-conjugation or disrupts the polymer chain arrangement can lead to a decrease in PCE of the solar cell[68, **?**]. When photoinduced degradation affects the π-conjugation in conjugated polymer materials, it impairs their ability to absorb light and transport charge. As a result, the performance of solar cells declines[85]. Therefore, this section will explore the mechanisms behind photoinduced degradation.

Photo-induced degradation mechanisms of OSCs

A solar cell device is expected to have an undisrupted working property when exposed to irradiation. Photo-induced degradation has to be minimized to enable the application of OSCs to the

real environment. In order to do so, it is important to understand the different photo-induced degradation mechanisms of the OSC active layer. Thus, in the following section, we will focus exclusively on photo-induced degradation processes that lead to polymer degradation.

Photo-Induced Degradation in the Presence and Absence of Oxygen

Photo-induced degradation refers to the chemical breakdown of materials when exposed to light, typically in the ultraviolet (UV) or visible spectrum. This process is influenced by various factors, with the presence or absence of oxygen playing a critical role. To understand how these environments affect degradation pathways, it is essential to consider molecular interactions, photophysical phenomena, and environmental factors.

a. Mechanisms in the Presence of Oxygen

In the presence of oxygen, photo-induced degradation is predominantly driven by oxidative processes that significantly accelerate material breakdown. The interaction of light, particularly in the UV or visible spectrum, with oxygen initiates a series of chemical reactions known as photo-oxidation [86, 87]. In the figure 2.11, explain the photo-oxidation reaction process. The oxidation of the ether substituent followed by the oxidation of the double bonds is summarized in this figure. This mechanism involves the absorption of photons by the material, which excites electrons to higher energy states. In organic polymers, this excitation leads to the formation of excited singlet or triplet states. These excited states can then interact with molecular oxygen (O_2), transferring energy to oxygen molecules and converting them into reactive oxygen species (ROS)[88]. These ROS, which include singlet oxygen ($^1O_2$), superoxide anions (O_2^-), and hydroxyl radicals (OH), are highly reactive and capable of attacking the polymer chains at various sites.

The first step in this oxidative degradation process is the formation of hydro-peroxides (ROOH)[89]. Hydro-peroxides are unstable and, under the influence of heat or UV radiation, decompose into free radicals such as alkoxy (RO•) and hydroxyl radicals (OH•). These free radicals can then initiate a chain reaction that leads to the breaking of chemical bonds in the polymer backbone, a process known as chain scission. Chain scission reduces the molecular weight of the polymer, leading to loss of mechanical properties such as tensile strength, flexibility, and toughness [90]. The material becomes brittle, prone to cracking, and eventually disintegrates. This is a common occurrence in materials like polyethylene (PE), where prolonged exposure to

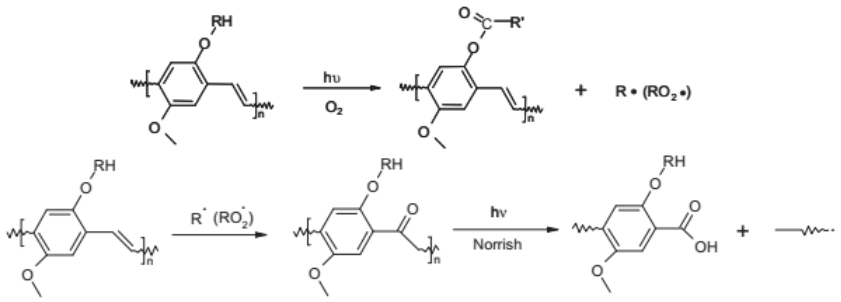


Figure 2.11: Photooxidation mechanism of MDMO-PPV [93].

sunlight in the presence of oxygen results in extensive oxidative degradation [91, 92].

Moreover, photo-oxidation leads to the formation of various oxidized functional groups, such as carbonyl groups (C=O), carboxyl groups (-COOH), and hydroxyl groups (-OH), on the polymer chains[87]. The incorporation of these oxygen-containing groups not only weakens the material's structural integrity but also alters its physical and chemical properties. The introduction of carbonyl groups, for example, is often responsible for yellowing or discoloration in materials like polyvinyl chloride (PVC) or polystyrene. The carbonyl index, which measures the concentration of these groups, is frequently used as an indicator of the extent of degradation in polymers.

The generation of ROS in the presence of oxygen can also trigger crosslinking reactions in certain polymers[94]. Crosslinking involves the formation of covalent bonds between polymer chains, resulting in a more rigid, less flexible material. Although crosslinking might initially increase the strength of the material, it ultimately leads to embrittlement because the polymer is less able to dissipate mechanical stress.

In addition to chain scission and crosslinking, oxygen promotes photo-fragmentation, where large polymer chains are broken down into smaller fragments. These fragments often possess low molecular weight and may migrate to the surface of the material, where they can volatilize or further oxidize. This process is particularly detrimental in outdoor applications, where polymers are exposed to both oxygen and sunlight, such as agricultural films, outdoor furniture, or plastic packaging.

The presence of heat and humidity can further exacerbate the rate of photo-oxidation. Heat accelerates the decomposition of hydroperoxides, while moisture can enhance the mobility of oxygen within the material, facilitating deeper oxidative damage[95, 96]. This combination of light, oxygen, heat, and moisture leads to a synergistic degradation pathway known as thermo-

photo-oxidation, which is particularly aggressive in polymers used in outdoor environments.

An example of this can be seen in polypropylene (PP), a polymer widely used in packaging and textiles. Under UV exposure in the presence of oxygen, polypropylene undergoes rapid oxidation, resulting in the formation of peroxide radicals [97]. These radicals initiate a self-sustaining chain reaction that leads to the degradation of the material, making it brittle and prone to cracking. To mitigate such degradation, stabilizers such as UV absorbers and antioxidants are often added to polymers to quench excited states and neutralize ROS before they can initiate damage. However, over time, even these stabilizers can degrade, leaving the material vulnerable to photo-oxidation.

In general, the presence of oxygen plays a crucial role in accelerating the photo-induced degradation of materials. Through the formation of reactive oxygen species, oxygen promotes oxidative reactions that cause chain scission, crosslinking, and the formation of oxidized functional groups, ultimately leading to deterioration of both the physical and chemical properties of the material[98]. These processes are influenced by environmental factors, such as heat and humidity, making oxygen-rich environments particularly challenging for the longevity of materials exposed to light.

b. Mechanisms in the Absence of Oxygen

In the absence of oxygen, the mechanisms of photo-induced degradation are significantly different, as oxidative reactions driven by ROS do not occur. Without molecular oxygen to participate in the degradation process, the breakdown of materials exposed to light proceeds primarily through direct photolysis and radical-driven processes. These mechanisms are typically slower and less severe compared to degradation in oxygen-rich environments, but can still cause notable changes in the material's structure and properties.

The absence of oxygen prevents the formation of ROS, meaning that the degradation process is limited to the energy absorbed directly from the light by the material. When a polymer absorbs UV or visible light, its electrons are excited to higher energy states. In an oxygen-free environment, these excited electrons can cause photo-dissociation, where chemical bonds within the polymer break due to the energy provided by the absorbed photons. This bond cleavage often leads to the formation of free radicals within the polymer chain, such as alkyl or aryl radicals[99]. Because there is no oxygen to react with these radicals and propagate oxidative chain reactions,

the radicals remain localized within the polymer structure.

One of the key outcomes of photo-induced degradation in an oxygen-free environment is photo-fragmentation. The energy from UV light can break the polymer chains into smaller segments, though the absence of ROS means that this process occurs at a slower rate than in oxidative environments. The resulting fragments may not volatilize or escape the polymer matrix as they do in the presence of oxygen, instead leading to internal rearrangements of the polymer structure. [100]

Moreover, in the absence of oxygen, free radicals generated by light exposure tend to recombine, leading to crosslinking reactions[101]. Crosslinking involves the formation of covalent bonds between different polymer chains, resulting in a more rigid and less flexible material. This is especially common in materials like rubber or elastomers, where crosslinking under UV light can cause hardening and loss of elasticity. Although crosslinking can initially enhance the strength of the material, it typically leads to embrittlement over time, as the material becomes stiffer and less capable of withstanding mechanical stress.

Another common effect of photo-induced degradation in oxygen-free environments is the formation of color centers, also known as chromophores. These color centers are created when light energy rearranges the electronic structure of the material, leading to selective absorption of certain wavelengths of light. This can cause photo-yellowing or other color changes in materials, even in the absence of significant structural damage. This phenomenon is particularly prevalent in natural polymers such as cellulose (found in paper and textiles), where prolonged exposure to light, even under anaerobic conditions, results in yellowing or browning of the material.

In addition to color changes, photo-induced degradation in the absence of oxygen can lead to surface-level modifications. Since the degradation process is not driven by deep oxidative reactions, the effects are often more localized to the surface of the material. For example, in materials like polycarbonate or PVC, surface-level photo-dissociation can occur, resulting in slight roughening or etching of the material surface. Although most of the material remains relatively intact, these surface changes can alter its appearance and may affect its interaction with the environment, such as increased susceptibility to moisture or pollutants.

It is important to note that while oxygen-free environments slow the degradation process,

materials can still degrade over time because of the accumulation of small defects caused by repeated light exposure. Over time, these defects can compromise the structural integrity of the material. However, the absence of oxygen allows for a longer material lifespan compared to oxygen-rich conditions, especially in applications where light exposure cannot be avoided [102, 103].

In some specialized applications, materials are deliberately kept in inert or oxygen-free environments to reduce the rate of degradation. This is common in museum displays, archives, or art conservation, where sensitive materials like ancient manuscripts, textiles, or paintings are exposed to light but protected from oxygen to minimize both oxidative and photo-induced degradation[104]. Inert gases like nitrogen or argon are often used in these cases to displace oxygen and create a stable environment that reduces the reactivity of free radicals generated by light exposure.

Furthermore, many advanced polymer systems incorporate photostabilizers specifically designed to quench the excited states or free radicals generated during photo-induced degradation, even in the absence of oxygen. These stabilizers act by absorbing excess energy from ultraviolet light or by capturing free radicals before they can cause further damage, thereby extending the useful life of the material in light-exposed applications.

In summary, photo-induced degradation in the absence of oxygen is primarily governed by direct photochemical processes such as bond cleavage, free radical generation, and crosslinking. These mechanisms lead to structural changes like hardening, photo-yellowing, and surface modifications. While the rate of degradation is slower compared to oxidative environments, the absence of oxygen does not completely halt the degradation process. Materials can still degrade over time through these non-oxidative pathways, especially when exposed to high-intensity light or UV radiation.

Morphological Instability by Photo-Degradation of Organic Solar Cells

Morphological instability due to photo-degradation is one of the most critical issues that affect the long-term performance of OSCs [105, 106, 107]. Unlike thermal or mechanical degradation, photo-degradation is induced by prolonged exposure of the organic materials to sunlight. The active layer in OSCs, which typically consists of a donor polymer and an acceptor material (often

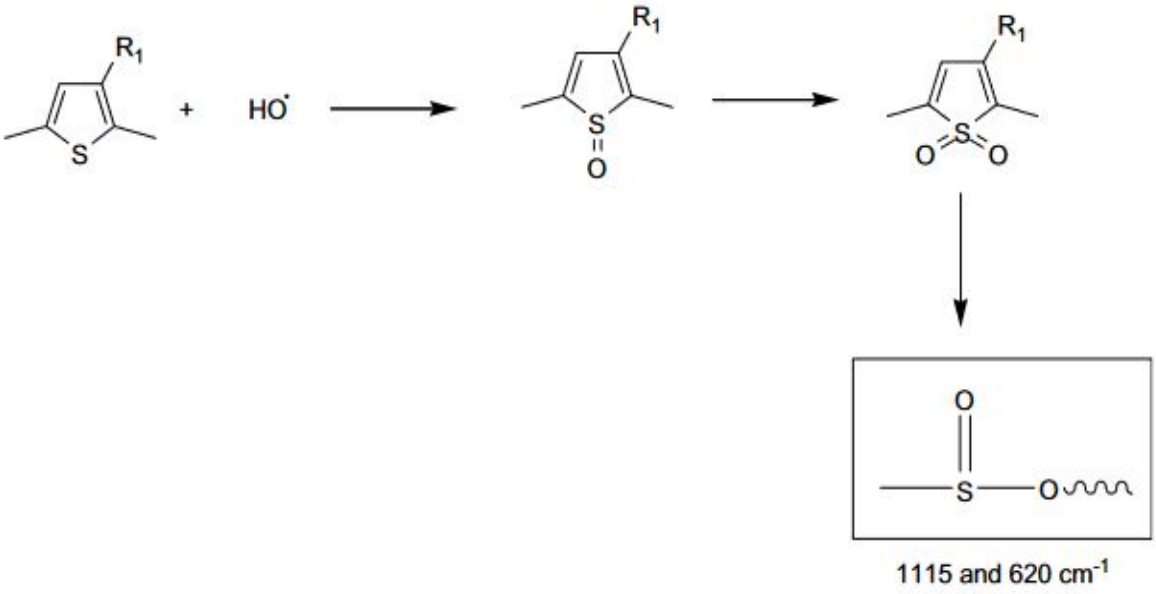


Figure 2.12: Oxidation mechanism of the sulfur atom of the thiophene ring [111].

fullerene or non-fullerene small molecule acceptor), absorbs photons from sunlight to generate excitons. However, continuous exposure to high-energy photons leads to chemical and structural changes in the materials, triggering morphological instability and, ultimately, a loss of device efficiency [108]. The degradation mechanisms are multifaceted, involving photochemical reactions, bond cleavage, and molecular rearrangements, all of which contribute to phase separation, phase segregation, and crystallization within the active layer.

One of the primary causes of photo-degradation in OSCs is the breakdown of chemical bonds in the organic materials under exposure to UV and visible light. High-energy photons can break the bonds in polymer chains, leading to the formation of free radicals and molecular fragments that disrupt the donor-acceptor interface. For example, in the widely used polymer donor poly (3-hexylthiophene) (P3HT), exposure to sunlight causes the breaking of C–S bonds in the thiophene ring, resulting in the formation of sulfur-containing radicals [109, 110, 111], as shown in figure 2.12. These radicals can initiate secondary reactions that degrade the polymer's electronic properties. Studies have shown that such photochemical reactions can lead to a significant reduction in charge carrier mobility, further contributing to the loss of device performance [112, 113, 114].

In fullerene-based OSCs, photo-degradation often involves the dimerization of fullerene molecules. Fullerenes, such as PCBM (phenyl-C_{61}-butyric acid methyl ester), tend to form dimers when

exposed to light. Dimerization changes the molecular structure of the fullerene, reducing its electron-accepting ability and altering its solubility [115]. This process also drives phase separation between the fullerene and the donor polymer, leading to a coarser morphology and larger domains that are detrimental to efficient charge transport [116, 117, 118]. Although non fullerene acceptors (NFAs) have been developed to improve the efficiency and stability of OSCs, they are not immune to photodegradation. NFAs typically have more complex molecular structures that are prone to photo-induced molecular rearrangements. For instance, in Y6-based OSCs, which have shown record-breaking efficiencies, photo-degradation can lead to the formation of photoproducts that are less soluble and tend to crystallize over time[119, **?**]. This crystallization causes morphological changes, such as the formation of large acceptor domains, which impair charge transport pathways [120]. Another major pathway for morphological instability in OSCs is photo-oxidation. Oxygen molecules, which can diffuse into the active layer through imperfections in the encapsulation or the thin-film structure, react with excited states in the organic materials under illumination. This leads to the formation of ROS, such as singlet oxygen and superoxide radicals. These species can initiate oxidation reactions in both the donor and acceptor materials, breaking chemical bonds and altering the molecular structure. For example, the oxidation of P3HT can lead to the formation of carbonyl groups, which disrupt the polymer's conjugated backbone, decreasing its ability to transport charges. Similarly, oxidation of fullerene derivatives reduces their electron affinity, leading to poorer electron transport. Studies have shown that photo-oxidation can cause significant phase segregation [121, 13, 122], as oxidized materials have different solubilities and intermolecular interactions compared to their unoxidized counterparts. This results in a more unstable morphology and reduced device performance over time.

2.7.2 Thermally-induced degradation of organic solar cells

OSCs are highly sensitive to temperature fluctuations, and thermally-induced degradation is one of the most critical challenges facing their stability and commercial viability. Unlike traditional inorganic solar cells, which are generally more thermally stable, the organic semiconductors used in OSCs, including polymer donors and fullerene/non-fullerene acceptors, are prone to morphological and chemical changes under thermal stress[123]. Elevated temperatures, whether

from the fabrication process or long-term exposure to sunlight, accelerate various degradation pathways, such as phase separation, crystallization, and molecular rearrangement, which impair the performance of OSCs over time. Understanding the mechanisms behind thermal degradation and developing strategies to mitigate its impact is essential to improve the operational stability of OSCs.

Phase Separation and Domain Coarsening Under Thermal Stress

Thermal stress significantly impacts the stability and performance of OSCs, particularly through phase separation and domain coarsening within the active layer [124, 125, 126, 127]. The active layer of OSCs is typically designed as a BHJstructure, consisting of nanoscale intermixed domains of donor and acceptor materials. This finely tuned morphology maximizes the interfacial area between the two phases, which is critical for efficient exciton dissociation and charge transport. However, under thermal stress, the increased thermal energy enhances the molecular mobility of the donor and acceptor materials, leading to their segregation into larger, more distinct domains [128, 129]. This process, known as domain coarsening, reduces the donor-acceptor interfacial area, limiting exciton dissociation and increasing recombination rates. As a result, fewer free charge carriers are generated, leading to a decline in the PCE of the device.

Furthermore, domain coarsening disrupts the continuous percolation pathways required for effective charge transport within the active layer. The finely intermixed donor and acceptor domains in an optimized BHJ structure ensure efficient charge extraction by providing uninterrupted pathways for holes and electrons to travel to their respective electrodes. However, as phase separation progresses under thermal stress, the formation of larger domains leads to charge trapping, increased resistance, and reduced charge extraction efficiency[130]. These morphological changes severely impact the overall device performance. The extent of phase separation and domain coarsening depends on factors such as the glass transition temperature (T_g) of the materials, their miscibility, and the processing conditions used to fabricate the active layer. Materials with low T_g or poor donor-acceptor compatibility are particularly prone to thermal degradation.

Thermal-Induced Crystallization of Fullerene and Non-Fullerene Acceptor

Thermal stress can also lead to crystallization within the active layer of OSCs, particularly for fullerene acceptors like PCBM and certain NFAs. While a degree of molecular ordering can

enhance charge transport in some cases, excessive crystallization leads to the formation of large, highly ordered domains that disrupt the delicate donor-acceptor morphology. This reduces the efficiency of charge separation and creates regions within the active layer where charges are more likely to recombine before reaching the electrodes.

For instance, Xianzhen et al [131] demonstrated that PCBM crystallization occurs at temperatures at or above 130 ^0C, forming micron-sized aggregates in the active layer. In their study, they showed scanning electron microscopy (SEM) images of the active layer after thermal aging at 130 ^0C for 6 hours, revealing large PCBM crystals that significantly disrupt the donor-acceptor network. This morphological change is accompanied by a dramatic reduction in PCE, from 3.2 % in the fresh device to 0.2 % after aging, illustrating the detrimental impact of thermal-induced crystallization on device performance .

NFAs, such as ITIC, also exhibit thermal instability, though their degradation mechanisms differ from fullerenes. NFAs tend to have more flexible molecular backbones, making them susceptible to thermally-induced molecular rearrangements that lead to phase separation or crystallization. studies showed that after thermal aging, ITIC-based OSCs exhibited significant phase segregation, as observed through atomic force microscopy (AFM) images [132, 133]. Phase-separated morphology resulted in a decrease in device efficiency, demonstrating that NFAs offer higher initial efficiencies, their thermal stability still requires significant improvement.

Thermal Annealing and Its Dual Effects

Thermal annealing is a common processing step used to optimize the morphology of the active layer in OSCs. Controlled annealing at moderate temperatures can improve the molecular ordering and crystallinity of the donor and acceptor materials, enhancing charge transport and PCE. However, excessive thermal annealing can have the opposite effect, driving phase separation, crystallization, and degradation of the active layer.

For example, a study by Shaban et al. [134] explored the effects of thermal annealing on P3HT:PCBM OSCs. When devices were annealed at 160°C for 5 minutes, the PCE improved due to enhanced molecular ordering and better donor-acceptor interfacial contact. However, when the annealing temperature was extended to 160 ^0C , significant phase separation occurred. This excessive annealing led to a decline in performance, illustrating the delicate balance between

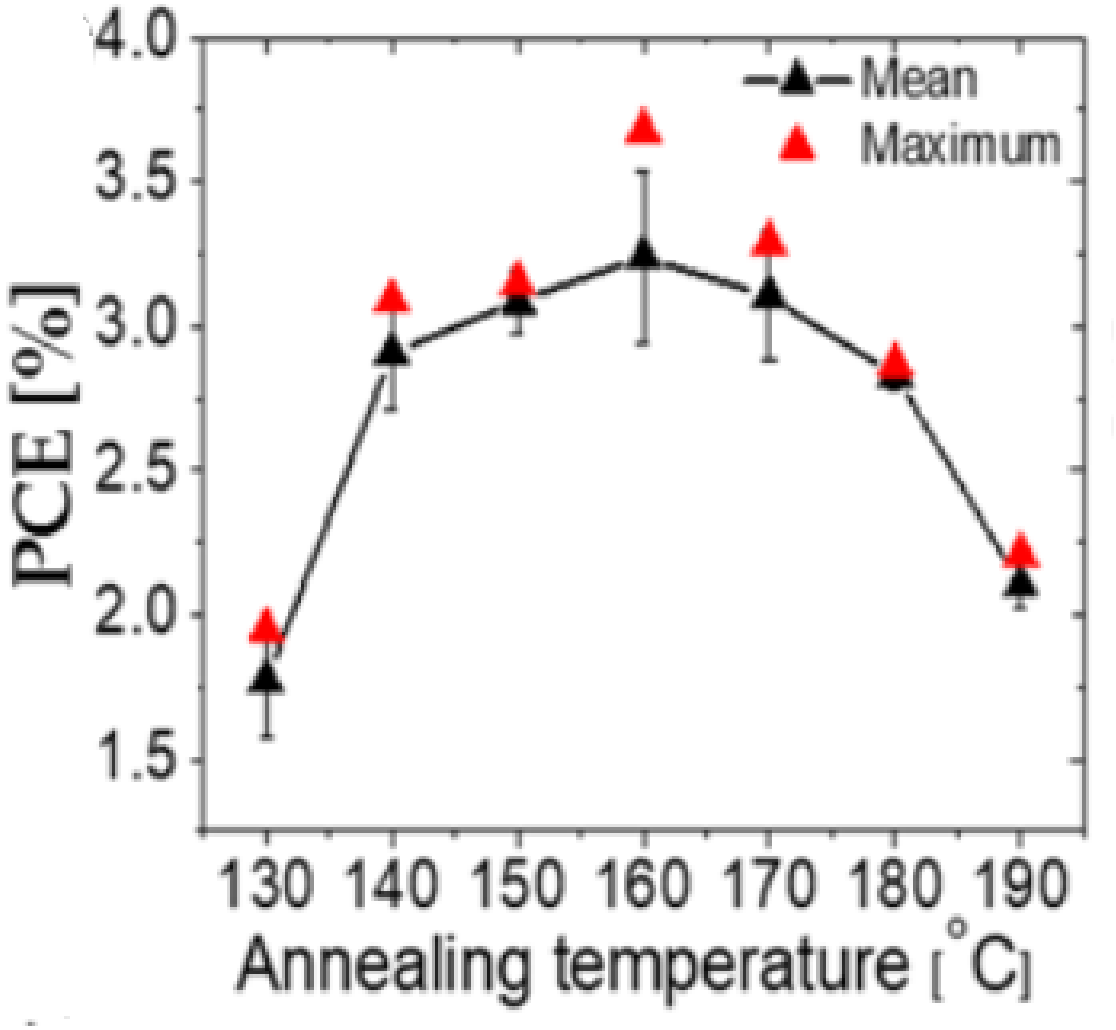


Figure 2.13: Variation of PCE for OSCs with the active layer prepared at different temperatures from 130 to 190 °C [134].

optimizing morphology and avoiding thermal-induced degradation.

Thermal Stress and Electrode Interfacial Degradation in Organic Solar Cells

The performance and stability of OSCs are not only influenced by the active layer but also significantly affected by the interfaces between the active layer and the electrodes. These interfacial regions are particularly vulnerable to thermal stress, which can lead to material degradation and adversely impact device functionality. At elevated temperatures, thermal stress can induce the diffusion of materials from the electrodes into the active layer, initiating chemical reactions or physical changes that degrade the device's efficiency and operational stability[135, 136].

One common example of this phenomenon occurs with indium tin oxide (ITO), a widely used transparent electrode in OSCs due to its excellent conductivity and optical transparency.

However, ITO is thermally unstable under prolonged exposure to heat. Elevated temperatures can cause the indium and tin components of ITO to diffuse into the adjacent active layer or interfacial buffer layers. This diffusion can lead to unwanted chemical reactions that alter the electronic properties of the active layer, such as reducing the efficiency of charge extraction or increasing recombination rates. Additionally, the diffusion of ITO can result in the formation of insulating or resistive compounds at the interface, leading to increased series resistance in the device and a subsequent decline in its overall performance.

Another critical factor in thermal degradation is the mechanical mismatch between layers, which can exacerbate stress at the interfaces during temperature fluctuations[137]. Organic materials, being more flexible than inorganic electrodes, expand and contract differently when subjected to heat cycles. This mismatch can create microcracks or delamination at the electrode-active layer interface, further deteriorating charge transport pathways and reducing device efficiency[138]. Over time, these mechanical defects can propagate, leading to irreversible damage and device failure.

In addition to ITO, metallic electrodes such as aluminum (Al) or silver (Ag), often used as cathodes, can also degrade under thermal stress. These metals may oxidize or diffuse into the underlying layers, disrupting the finely tuned energy alignment at the interface and increasing charge transport barriers[136]. Furthermore, the incorporation of buffer layers, such as poly(3,4-ethylenedioxythiophene):polystyrene sulfonate (PEDOT:PSS) or electron transport layers like zinc oxide (ZnO), can help mitigate some of these effects but may also degrade themselves under high temperatures. For instance, PEDOT:PSS has been shown to be hygroscopic and can degrade through thermal and humidity-induced changes, which, in turn, affect the stability of the interface[139].

To address these challenges, researchers have explored several strategies to improve interfacial stability under thermal stress. One approach involves the use of thermally stable electrode materials or protective interfacial layers that act as diffusion barriers[140, 141]. For example, incorporating thin layers of transition metal oxides, such as molybdenum oxide (MoO_3) or nickel oxide (NiO), between the active layer and the electrode can help suppress the diffusion of electrode materials while maintaining good charge transport properties. Another strategy is the

development of low-temperature processing methods and materials with higher glass transition temperatures (Tg), which are less prone to structural changes under heat[142].

To sum up, thermal stress and electrode interfacial degradation are critical challenges in the long-term stability of OSCs[136]. Elevated temperatures can cause material diffusion, chemical reactions, and mechanical defects that degrade device performance. Efforts to mitigate these effects through advanced material design, improved interfacial engineering, and protective barriers (as some examples Al_2O_3, ZnO, TiO_2) [143, 144]are essential for the development of thermally robust OSCs with extended operational lifetimes [81]. As the demand for reliable and durable organic solar cells continues to grow, addressing interfacial thermal degradation remains a key focus in the field.

Strategies to Mitigate Photo- and Thermally-Induced Degradation in Materials

Photo- and thermally-induced degradation significantly affect the long-term performance of materials, particularly in areas like photovoltaics, polymers, and coatings [145]. Several strategies have been employed to mitigate these effects, with notable advancements in the stabilization of organic solar cells [119]. One such method is the incorporation of UV stabilizers or absorbers, which prevent photodegradation by absorbing harmful ultraviolet radiation and converting it into harmless heat [146, 147]. These stabilizers, like benzophenones and hindered amine light stabilizers (HALS), are widely used in outdoor plastics and coatings to prevent surface cracking, discoloration, and mechanical failure. For thermally-induced degradation, heat stabilizers such as calcium/zinc compounds in PVC (polyvinyl chloride) help prevent breakdown by neutralizing free radicals that form under high temperatures [147, 148].

A promising advancement OSC technology is the use of non-electron withdrawing unit (non-EWU) copolymerization to enhance photo-stability. This approach is particularly effective in thiophene-based organic solar cells, which are known for their high efficiency but are prone to photodegradation. Thiophene units in the polymer backbone are typically vulnerable to oxidative degradation under UV exposure, which accelerates the breakdown of the material. By introducing non-electron withdrawing units, such as alkyl or aryl groups, into the polymer chain through copolymerization, the electronic environment of the polymer is modified to enhance stability. These non-EWU units reduce electron deficiency along the polymer backbone, making it less

susceptible to UV-induced oxidation and improving the material's photo-stability [149, 150].

For example, in thiophene-based organic solar cells, co-polymerizing thiophene units with non-electron withdrawing moieties like cyclopentadithiophene or benzodithiophene has been shown to stabilize the polymer against photodegradation [151]. The result is a material that maintains higher efficiency over time, with less degradation of the active layer in the presence of sunlight. This approach improves the durability of organic solar cells, making them more viable for long-term outdoor applications.

In addition to non-EWU copolymerization, the incorporation of nanoparticles like titanium dioxide (TiO_2) or zinc oxide (ZnO) into the polymer matrix can further improve UV resistance [152, 153]. These nanoparticles scatter and absorb UV light, reducing photodegradation. Encapsulation techniques, such as the use of ethylene-vinyl acetate (EVA) in photovoltaic cells, also play a crucial role in protecting the active layers from environmental stresses such as UV radiation and thermal cycling. When combined with antioxidants to mitigate thermally-induced degradation, these strategies enable longer-lasting and more stable organic solar cells.

By using a combination of non-EWU copolymerization, UV stabilizers, and encapsulation techniques, thiophene-based organic solar cells can achieve enhanced photo-stability and thermal resilience, leading to improved performance and longevity in real-world applications [154, 155, 156].

Chapter 3

Materials and methods

This chapter describes the experimental procedures carried out to accomplish research objectives, including their molecular structures. It also depicts the experimental methods and characterization techniques used in the research.

3.1 Materials and solvents

Regioregular poly(3-hexylthiophene) (P3HT) and PBDD4T are low bandgap donor polymers widely used in organic solar cells. These materials, utilized in this study, were purchased from Ossila. The electron acceptor materials used in the experiments include $PC_{60}BM$, $PC_{71}BM$, and ITIC, all of which were also purchased from Ossila.

The chemical structures of the donor polymers, P3HT and PBDD4T, are shown in Figure 3.1, while Figure 3.2 presents the chemical structures of the fullerene-based acceptors, $PC_{60}BM$ and $PC_{71}BM$, as well as the NFA, ITIC.

To prepare solutions for thin-film fabrication , solvent such as 1,2-dichlorobenzene (o-DCB), was employed. Additionally, cleaning solvents, including acetone, isopropanol, and deionized water, were used during the study to ensure proper sample preparation and substrate cleaning.

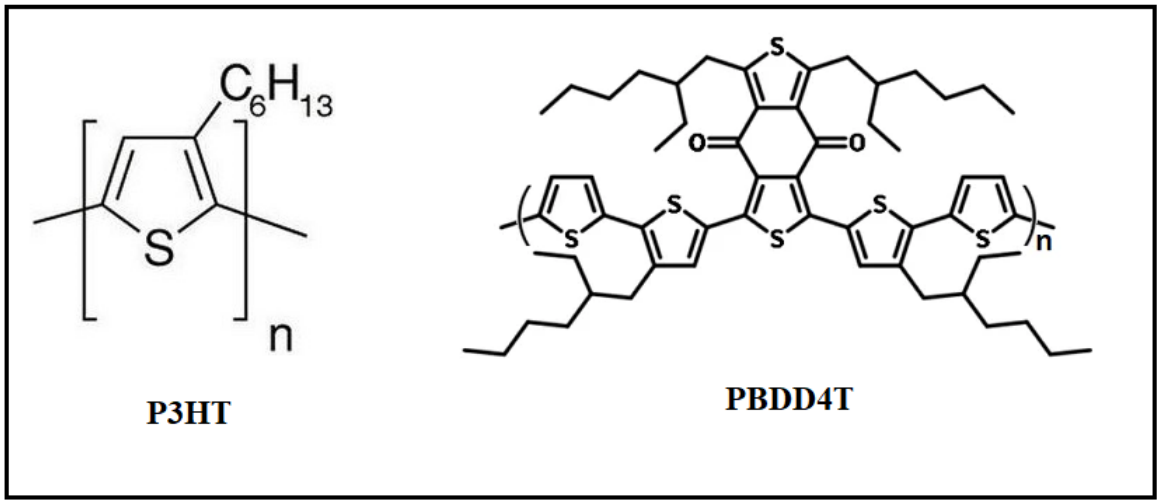


Figure 3.1: The structure of donor polymers used in this work

3.2 Methods

3.2.1 Substrate preparation

The substrates used in this research consisted of plain glass and glass coated with indium tin oxide (ITO), were also purchased from Ossila. Ltd. Initially, the plain glass substrate was utilized for characterization and optimization, while the ITO-coated glass substrate was employed for the fabrication of the final organic solar cell. The ITO substrates used in the study had a sheet resistance of approximately 15 Ω/square, and the plain glass substrates were sourced from a local scientific supplies vendor. Prior to each experiment or sample deposition, thorough cleaning of the substrates was conducted to ensure accuracy and reliability, as contaminants on the surface could adversely affect the quality of the deposition. Although the cleaning procedures for plain glass and ITO-coated glass were largely similar, the ITO-coated glass required an additional etching step before the cleaning process. The cleaning process involved several steps to ensure the substrates were free of contaminants. First, a cleaning solution was prepared by mixing deionized water with soapy water in a 2:1 ratio, and the substrates were immersed in this solution and sonicated for 15 minutes. Afterward, they were thoroughly rinsed with deionized water to remove any visible soap residue. This was followed by sonication in acetone and isopropanol for 10 minutes each, which helped remove residual contaminants. The substrates were then rinsed again with deionized water and dried in an oven at 120°C for 30 minutes. Finally, the cleaned

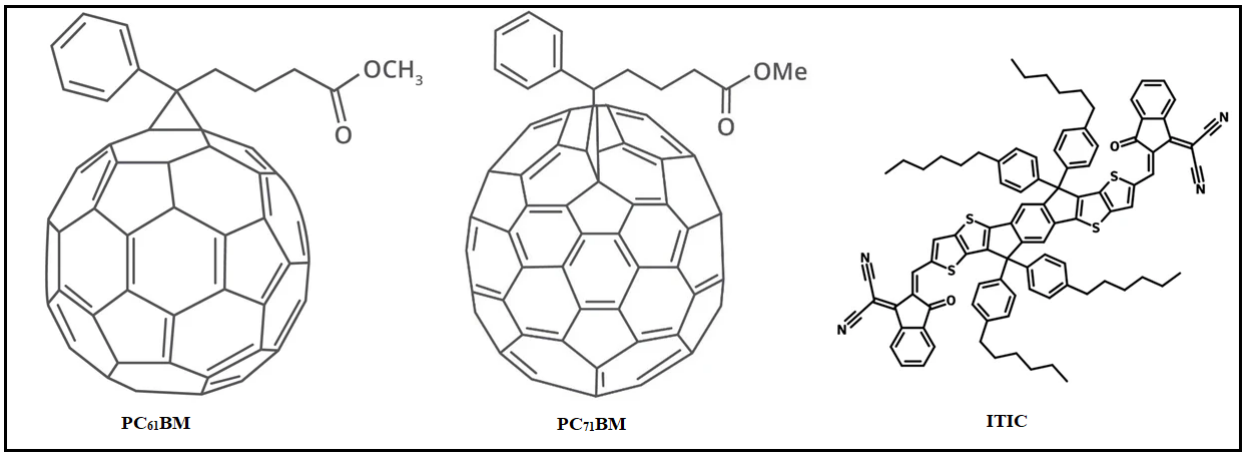


Figure 3.2: The chemical structure of fullerene and non fullerene acceptors used in this work

substrates underwent ozone treatment for 30 minutes to prepare them for spin coating. For ITO-coated glass substrates, the process included an additional step of partial etching with an acid solution before the standard cleaning procedure. This extra step ensured the surface of the ITO layer was optimally prepared for deposition. The electron transport layer (ETL) was prepared from 219.5 mg ZnAc.H_2O mixed with 60.4 μl ethanol amine, and 2 ml of 2-methoxyethanol solution that was stirred for 12 h at room temperature in air. The mixture was spin coated on the precleaned ITO-substrate and annealed at 150 °C for 30 minutes followed by slow cooling to room temperature to produce a 40 nm-thick ZnO layer.

3.2.2 Organic solar cells fabrication

The electron transport layer (ETL) was synthesized by dissolving 219.5 mg of zinc acetate dihydrate (ZnAc·H_2O) in 2 mL of 2-methoxyethanol, followed by the addition of 60.4 μL of ethanolamine. The solution was continuously stirred at room temperature in an air environment for 12 hours to ensure uniform mixing. This prepared solution was then applied onto pre-cleaned indium tin oxide (ITO)-coated glass substrates via spin-coating. Subsequently, the coated substrates were subjected to annealing at 150 °C for 30 minutes to develop a uniform ZnO layer of approximately 40 nm in thickness. After annealing, the substrates were gradually cooled to room temperature to minimize thermal stress.

To fabricate inverted OSCs incorporating the ZnO ETL buffer layer, a device structure of ITO/ZnO/active layer/molybdenum Oxide (MoO_3)/aluminum (Al) was employed. The active

layer was deposited onto the pre-cleaned ITO/ZnO substrates through spin-coating a ZnO solution at 3000 rpm for 40 seconds. This was followed by thermal annealing at 150°C for 30 minutes, and the substrates were then allowed to cool slowly to room temperature. The active layer solution comprised a 1:1 ratio of donor and acceptor materials, dissolved in *o*-dichlorobenzene (*o*-DCB) at a concentration of 20 mg/mL. After deposition, the active layer underwent thermal annealing at 120°C for 10 minutes to remove residual solvents.

The hole transport layer (HTL), an 8 nm-thick molybdenum oxide (MoO_3) layer, and the anode, an 80 nm-thick aluminum (Al) layer, were sequentially deposited using thermal evaporation under low pressure. An evaporation mask was utilized to precisely define the device area, yielding an active area of 0.04 cm^2. The performance of the fabricated OSC devices was assessed through current density–voltage (J–V) measurements using a Keithley 2400 source meter, a Japanese-made SS-50AA solar simulator system was used which had been calibrated using a KG5 silicon photodiode, under simulated solar illumination at an intensity of 100 mW/cm^2 (1-sun conditions). The J-V characteristic data was analyzed using Origin software, version 2019b.

3.3 Characterizations

3.3.1 Structural and Morphological Characterizations

XRD Measurement

The X-ray diffraction (XRD) measurements were performed to study the structural characteristics and ordering changes in a films of pristine polymers and their BHJ blends under thermal induced conditions. The analysis was carried out using the Shimadzu Scientific Instruments X-ray diffractometer 7000S, which was calibrated to record diffraction patterns over a 2θ range of 2° to 40°. This range is ideal for capturing key diffraction peaks indicative of molecular and crystalline structures. The diffractometer utilized Cu-Kα radiation, generated from a copper target, with an electron gun operating at a power setting of 40 kV and 40 mA. These parameters ensured high-quality and consistent X-ray generation suitable for precise diffraction measurements.

The structural information obtained from XRD patterns allowed for the calculation of inter-layer spacing (d) between atomic planes using Bragg's Law [157]:

$$n\lambda = 2d\sin\theta \tag{3.3.1}$$

In this equation, n represents the diffraction order (typically 1 for primary reflections), λ is the wavelength of the Cu-Kα radiation (0.154 nm), and θ is the angle of diffraction. This calculation provided critical insights into the degree of crystallinity, the molecular arrangement, and the structural changes induced by thermal treatment.

The XRD analysis was particularly significant for evaluating the impact of blending and processing on the structural order of the materials. Comparing the diffraction patterns of the pristine polymers with those of the BHJ blends revealed changes in crystallinity and phase separation, essential for understanding material performance in applications like organic photovoltaics or electronics. Moreover, the ability to monitor thermally induced structural changes provided valuable information on the stability and adaptability of materials under varying environmental conditions. In this work we were taken the XRD patterns of the fresh and degraded samples spin coated on glass substrate to identify the effect of heating on the lamellae stacking in the polymer backbone. The XRD of each polymer both fresh and degraded would be measured using X-ray differactometer XRD-7000S using target copper. The result obtained would be fitted with Gaussian to calculate the D-value using equation shown in equation 3.3.2.

$$D = \frac{k\lambda}{\beta\cos\theta} \tag{3.3.2}$$

Where K is dimensionless constant and has a value of 0.89 for heterogeneous sample. β is the FWHM expressed in radian λ is the wavelength that indicate X-ray which is around 0.154 nm because of our target copper(Cu). θ is half of the diffraction angle. Finally the result obtained for fresh and degraded samples would be compared to study the difference.

Atomic force microscopy (AFM)

Atomic Force Microscopy (AFM) is a critical analytical tool for studying and improving organic solar cells. This advanced imaging technique works by scanning a sharp tip across the sample surface to produce high-resolution, three-dimensional topographic maps at the nanometer scale. AFM is particularly valuable for research on organic solar cells because it provides detailed insights into surface morphology, phase separation, and the nanostructural features of active layers, which are essential for optimizing device performance.

AFM is widely used to analyze the surface morphology of the active layer, a blend of donor polymers and acceptor materials that plays a vital role in device efficiency. By capturing precise height images, AFM reveals details about uniformity, roughness, and domain distribution within the blend. These characteristics directly affect charge generation, transport, and collection. Moreover, AFM's phase imaging mode helps researchers study the nanoscale phase separation between donor and acceptor materials, a critical factor for efficient exciton dissociation and charge transport.

AFM can be used to manipulate materials at the nanoscale, applying localized pressure to modify the morphology or structure of the active layer, which is valuable for experimental performance enhancements. In this study, the films were prepared in the same condition as the devices on a clean glass substrate. The surface topography of the active layer films were recorded using the AFM model NT-MDT-NTE-GRA in tapping mode. Both height and peak force errors are collected and analyzed using Gwyddion software.This analysis provided valuable insights into the efficiency and behavior of the active layer materials in the context of their optical and electronic properties.

3.3.2 Optical characterization

UV-Visible absorption spectroscopy

UV-Visible absorption spectroscopy is a fundamental analytical technique in the study of OSCs, providing crucial insights into the optical properties of active layer materials. This method measures the absorption of ultraviolet (UV) and visible light across a range of wavelengths,

enabling the determination of critical parameters such as absorption onset, bandgap energy, and light-harvesting efficiency. UV-Visible spectroscopy is particularly valuable for characterizing the donor and acceptor materials used in the active layer, as well as their blends. It reveals changes in absorption profiles due to molecular interactions and morphological effects [158]. Additionally, the technique aids in optimizing device performance by identifying materials with broad and intense absorption in the visible range, enhancing photon harvesting. It also monitors the structural and thermal stability of materials, detecting degradation or phase transitions under different conditions. By analyzing spectral features, researchers can fine-tune the donor-acceptor ratios and layer thickness to maximize light absorption and energy conversion. Thus, UV-Visible absorption spectroscopy plays a vital role in advancing OSC technology, facilitating the design of efficient and stable photovoltaic materials. The absorption spectra of spin-coated films of polymers P3HT, PBDD4T as well as blends of these donor were recorded using Perkin Elmer Lambda 19 UV–Vis /NIR and DS5 UV-Vis spectrophotometers.

Photoluminescence Spectroscopy

Photoluminescence spectroscopy is a technique that examines the emission of light, or photons, from a material after it has absorbed energy from an external light source. This non-contact and non-destructive method is widely used for material testing. When light interacts with a sample, the absorbed energy causes the material to undergo photoexcitation, elevating it to a higher electronic state. As the material relaxes and returns to a lower energy state, it emits photons, a phenomenon known as BHJ. Photoluminescence occurs as a result of this energy emission and is crucial for understanding various material properties. When an acceptor material like PCBM is introduced into the mixture, photoluminescence quenching occurs because some excitons are dissociated at the interface, reducing radiative recombination. Complete quenching signifies that all excited pairs have been effectively separated into free charge carriers. In this study, the PL spectra of thin films were analyzed using the HORIBA FLUOROMAX-4 spectrofluorometer to assess the quenching efficiency of the active layer material. The quenching efficiency (QE) was

calculated using the formula:

$$QE = 1 - \frac{PL_{blend}}{PL_{pristine}} \times 100\% \tag{3.3.3}$$

Where Q_E is quenching efficiency, PL_{blend} and PL_{pristine} are PL of the blend and pristine films, respectively.

3.3.3 Chemical Analysis

Degradation changes the chemical structure of the active layer materials. The mechanism of the degradation can be unraveled by systematically following the chemical structure evolution due to degradation. The following chemical analysis spectroscopes will be used.

Fourier transform infrared spectroscopy (FTIR)

Fourier Transform Infrared Spectroscopy is a powerful analytical technique widely used to investigate the structural and chemical properties of materials, including organic solar cells. Organic solar cells, which rely on the interplay of organic semiconducting materials, benefit significantly from FTIR analysis to understand their molecular composition, functional groups, and interaction mechanisms [159].

FTIR spectroscopy works by measuring the absorption of infrared radiation by a material as a function of wavenumber or frequency. The resulting spectrum represents the molecular vibrations, including stretching, bending, and twisting, of bonds within the material. This provides detailed information about the chemical bonds and functional groups present in the organic components of solar cells, such as donor and acceptor materials, polymers, and small molecules.

In the context of organic solar cells, FTIR spectroscopy can be employed to study the functional groups and chemical interactions between the active layer components, such as the donor-acceptor blend. It is particularly useful for analyzing the incorporation of additives, processing aids, and interfacial layers. FTIR spectra can reveal characteristic peaks corresponding to specific molecular vibrations, such as C=C stretching in conjugated backbones, C=O stretching in

ester groups, or N–H and O–H stretching vibrations.

Additionally, FTIR is crucial for monitoring chemical stability and degradation mechanisms in organic solar cells. During operational conditions or environmental exposure, the organic materials can undergo chemical changes, such as oxidation or hydrolysis, leading to performance losses. FTIR spectroscopy can detect these changes by observing shifts in peak positions, changes in peak intensities, or the appearance of new peaks corresponding to degradation products.

Furthermore, FTIR spectroscopy is an essential tool in the development and optimization of organic solar cells. It provides valuable insights into material composition, chemical interactions, and degradation processes, contributing to the design of more efficient and stable devices. The FTIR of the fresh and degraded films would be taken to see the formation of any new chemical bond and change in peak intensities.

Thermogravimetric analyses (TGA) and differential thermal analyses (DTA)

Thermogravimetric Analysis (TGA) and Differential Thermal Analysis (DTA) are complementary thermal techniques used to study the thermal stability, composition, and phase transitions of materials. These methods are widely employed in material science, including in the evaluation of organic solar cells, polymers, composites, and other advanced materials.

TGA measures the change in mass of a sample as a function of temperature or time under a controlled atmosphere, such as air or inert gas. This technique is particularly useful for analyzing thermal stability, decomposition patterns, and the content of volatile components in a material. During a TGA test, a sample is heated at a defined rate, and any loss in weight, such as due to moisture evaporation, decomposition, or combustion, is recorded. TGA provides critical insights into the thermal behavior of materials, including the identification of degradation temperatures, residual mass after thermal treatment, and the presence of fillers or impurities. For example, in the case of organic solar cells, TGA can help evaluate the thermal stability of active layer components and encapsulation materials, which is crucial for device longevity.

DTA, on the other hand, measures the difference in temperature between a sample and a reference material as both are subjected to the same thermal conditions. This technique is used to identify endothermic and exothermic events, such as melting, crystallization, phase transitions,

and chemical reactions, by monitoring the energy changes associated with these processes. DTA is particularly effective in detecting subtle thermal events that might not result in a weight change, such as glass transitions or rearrangements in molecular structure. The resulting thermogram provides a clear picture of the thermal events occurring within the sample.

When combined, TGA and DTA offer a comprehensive understanding of the thermal properties of a material. For instance, in the analysis of organic solar cells, these techniques can help identify the thermal stability of the donor and acceptor materials, phase transitions in the active layer, and degradation mechanisms. Such information is essential for optimizing material formulations, improving device performance, and ensuring the durability of solar cells under operational conditions.

Thermogravimetric analyses (TGA) and differential thermal analyses (DTA) would be carried out on the materials using DTG-60H under nitrogen atmosphere to determine the thermal properties of the materials that will be used in this work. The bond breaking due to heating can be understood with the mass loss with temperature curve that would be obtained from the TGA together with the enthalpy change from DTA.

3.3.4 Density Functional Theory calculations

Density functional theory (DFT) calculations were performed using the Gaussian 16 package, with the input geometries built using GaussView 3. The DFT calculations employed the B3LYP hybrid functional and the 6-31G(d,p) basis set to optimize the geometries and calculate molecular energy levels. To reduce computational time, the side chains were replaced by a single methyl unit, as recommended in various reports[160, 161] . Additionally, time-dependent DFT (TD-DFT) was used to calculate absorption, employing the CAM-B3LYP level of theory with the 6-31G++(d,p) basis set.

3.3.5 Electrical Characterization

Current-voltage Characterization

A fundamental approach to evaluating device performance involves simple measurements of the solar cell's diode characteristics. This method requires a source meter, which applies voltage over a specific range while measuring the corresponding current to generate I-V curves. Key parameters such as V_{oc}, short-circuit current (I_{SC}), fill factor (FF), power conversion efficiency (PCE), shunt resistance (R_{sh}), and series resistance (R_s) can be extracted from these curves under illumination, as they are crucial in defining device performance. Additionally, dark I-V characteristics provide valuable insights into series resistance, shunt resistance, saturation currents, and ideality factors. When analyzing device degradation, it is essential to periodically measure diode characteristics, as photovoltaic parameters may vary depending on the material type and measurement conditions. A decline in device efficiency is often attributed to a decrease in photocurrent; however, in some cases, reductions in FF or even V_{OC} can also contribute to a drop in PCE. A Ketihely 2401 from textronics and illumination source of G2V optics will be used. The J-V curves will be followed by periodically taking them from the degradation (heating and Illumination) both in dark and under illumination.

Chapter 4

The Roles of Acceptors in the Thermal-degradation of P3HT-Based Organic Solar Cells

4.1 Introduction

For organic solar cell (OSC) technology to be viable for outdoor applications, its stability must be verified through standardized testing protocols. According to the American Standard Test Method (ASTM) [162], polymers must be tested at a temperature of 85°C to be certified as thermally stable. During operation, the surface temperature of solar cells increases due to irradiation. Therefore, ensuring thermal stability is crucial for OSC technology to function reliably as an energy source. Several studies have been conducted to investigate the photodegradation of OSCs in their actual working environments. Doumon et al., for instance, investigated the role of fullerene derivative (PC_{70}BM) and non-fullerene (ITIC) in the photostability of their respective solar cells with Poly[(2,6-(4,8-bis(5-(2-ethylhexyl)thiophen-2-yl)-benzo[1,2-b:4,5-b'] dithiophene))-alt-(5,5-(1',3'-di-2-thienyl-5',7'-bis(2-ethyl hexyl)benzo[1',2'-c:4',5'-c']dithiophene-4,8-dione)(PBDB-T)[163]. However, the role of these acceptors in the thermal degradation of P3HT-based OSCs is not yet known.

In this study, two fullerene (FA) and one non-fullerene (NFA) acceptor molecules were em-

ployed in the preparation of three different solar absorbers namely, P3HT:PC_{60}BM, P3HT:PC_{70}BM, and P3HT:ITIC. The molecules under investigation were chosen because of the availability of information on the chemical and physical properties of the polymers. The degradation mechanisms of the three OSC devices were investigated using UV-VIS absorbance, BHJ, current-voltage (I-V), FTIR, XRD, and AFM. The results confirm that the main cause of degradation in the FA-based devices is the crystallization that led to segregation in the active layer, while in the NFA-based devices it is the change in the energy levels leading to higher recombination.

4.2 Results and Discussion

4.2.1 Photovoltaic performance

OSCs were fabricated using P3HT as a donor and two fullerene acceptors (FAs), (PC_{60}BM and PC_{70}BM) and one NFA,ITIC, to determine the roles of acceptors on degradation(structures given in Figure 3.1 and Figure 3.2. The recorded PCE of the FA-based devices were around 1.5%, which is relatively low compared to those devices produced under controlled environment. However, the main purpose of the investigation is to understand the role of acceptors on the degradation mechanism of OSC. The efficiency of ITIC based solar cell is found to be much lower than FA-based devices because of the higher formation of molecular agglomeration in the photoactive medium [164]. The device performances that were obtained in these investigations are similar to those reported in litratures [165, 164]. When the photovoltaic parameters of the devices are closely examined, it is clear that the low J_{sc} (1.17 mA/cm^2) and V_{oc} (0.45 V) are the main reasons for the lower performance of the P3HT:ITIC-based device. The lower V_{oc} is mainly due to the low lying LUMO of ITIC (-3.83 eV) [166]. On the other hand, the J_{sc} is determined by each of the charge photo-generation processes.

To elucidate the low J_{sc} despite the broad absorption of P3HT:ITIC blend film, we studied the charge generation, exciton quenching, and charge collection efficiencies in the devices prepared. The photogenerated currents (J_{ph}) in the three devices were calculated from J_{ph}=J_L-J_D, where J_L and J_D are current densities recorded under illumination and dark, respectively, and plotted against the effective voltage V_{eff}, which is given as V_{eff} = V_0-V, where V_0 is the voltage

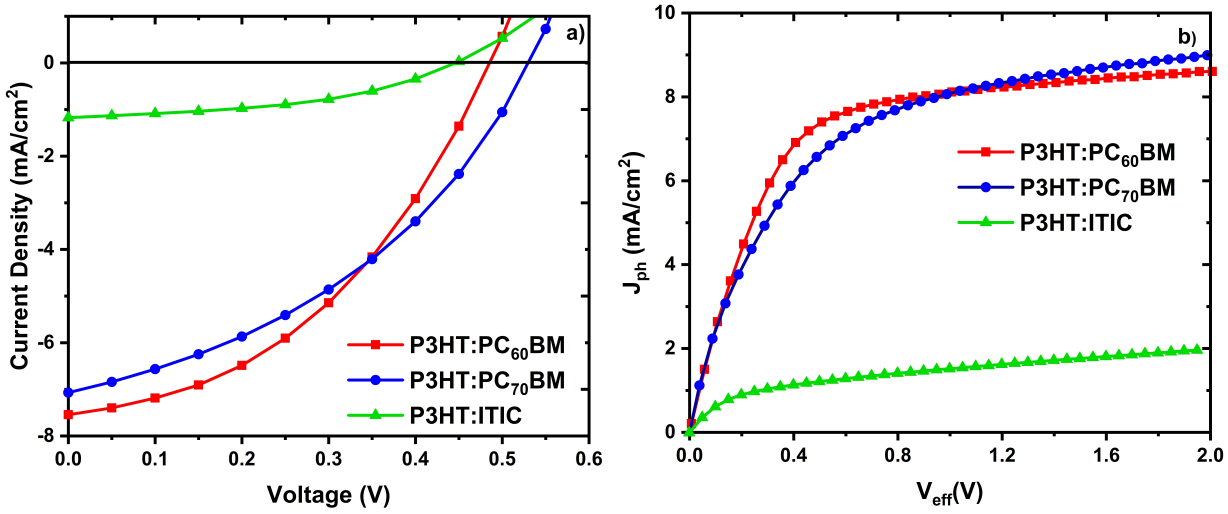


Figure 4.1: a)J-V b)J_{ph}-V_{eff} curves of the fullerene and Non- fullerene acceptor based device.

at $J_L = J_D$, and V is the applied voltage [167, 168, 169] as shown in Figure 4.1 (b). The graph of J_{Ph} versus V_{eff} shows a linearly increasing region at low V_{eff} that is primarily limited by charge carrier diffusion, followed by a saturation region (J_{sat}) at higher $V_{eff} \approx 2V$. The maximum charge generation rates (G_{max}) in the devices were calculated as J_{sat}/qL, where q is the elementary charge and L is the active layer thickness and were found to be 3×10^{27}, 3.52×10^{27}, and $5.9 \times 10^{26} m^{-3}s^{-1}$ in P3HT:PC_{60}BM, P3HT:PC_{70}BM, and P3HT:ITIC-based device, respectively, confirming an order of magnitude less charge in generation of P3HT:ITIC-based devices. The amount of free charges that can be collected is determined by the charge transfer at the donor/acceptor interface. In this regard, exciton quenching efficiencies (QE) of the devices were determined using the relation, $QE = (1 - \frac{PLblend}{PLpristine}) \times 100\%$ [170] where PL_{blend} and $PL_{pristine}$ are emission of the blend and pristine films, respectively, recorded at excitation of 520 nm . The QE of the devices were found to be 66, 80 and 55% in P3HT:PC_{60}BM, P3HT:PC_{70}BM, and P3HT:ITIC OSCs, respectively. It should be noted that PC_{70}BM followed by ITIC has a substantial absorption at the excitation wavelength, making our calculation highly inaccurate. Nevertheless, the QE provides qualitative evidence that charge transfer in P3HT:ITIC-based devices is highly impaired. Similarly, the charge collection efficiency ($P(E,T)_{coll}$) of P3HT:ITIC device is calculated using the equation

$P(E,T)_{coll} = J_{ph}^{MPP}/J_{sat}$, where J_{ph}^{MPP} is the photocurrent at the maximum power point, and was found to be the smallest. Hence, the current generated in P3HT:ITIC-based OSCs is limited

by the lower generation of charge carriers, exciton quenching, and finally, poor charge collection.

4.2.2 Device degradation

The main purpose of this study was to investigate the role of acceptors on the thermal stabilities of the commonly used thiophene-based OSC devices. The devices were fabricated in an inverted device structure which offers much longer shelf life time in ambient environment compared to the conventional one. Hence, the evolution of the photovoltaic parameters due to thermally-induced degradation were carefully studied for the duration of nearly 48 hours, as depicted in Figure 4.2. Despite the similar PCE of the FAs-based OSCs, the evolution of their photovoltaic parameters exhibited different degradation kinetics. The P3HT:$PC_{60}BM$ based OSC kept more than 50% of its initial PCE while the
P3HT:$PC_{70}BM$ and P3HT:ITIC based devices kept only 22 and 32 % of their initial PCE after 48 h of thermal ageing, respectively. To determine the origin of the causes for these differences in the thermal stability of the P3HT based devices, the time evolution the J_{sc}, and FF of the devices are plotted as shown in Figure 4.2.

The V_{oc} of the FAs ($PC_{60}BM$ and $PC_{70}BM$) based devices followed the same trend in the first hour, followed by a stable value of 76% and 71%, respectively, with respect to the initial value until the accelerated ageing. On the contrary, the ITIC-based OSC lost more than 50% its V_{oc} in 1 h and then stabilized. Since $\propto (E_{HOMO}^{Donor} - E_{LUMO}^{Acceptor})$ [171], its drastic change in ITIC based devices due to thermal degradation suggested the energy level of the NFA is affected leading to higher charge recombination thus loss of both and FF. Comparing the three devices, thermo-oxidation that caused a change in energy levels of the acceptors is suppressed more in FA. The oxidation of both donor and acceptors in the active layer induces an imbalance in charge transport due to oxygen doping that increases hole transport while the electron is trapped [172, 173].

Unlike , FF and J_{sc} of the devices revealed higher loss in $PC_{70}BM$-based device, followed by ITIC-based one. The $PC_{60}BM$ based device, on the other hand, retained 91% and 80% of its initial FF and J_{sc} respectively. The higher loss in FF of $PC_{70}BM$ and ITIC-based devices during the accelerated ageing period confirmed that thermal degradation in the devices causes a high recombination of charge carriers. Interestingly, these recombination mechanisms are reduced

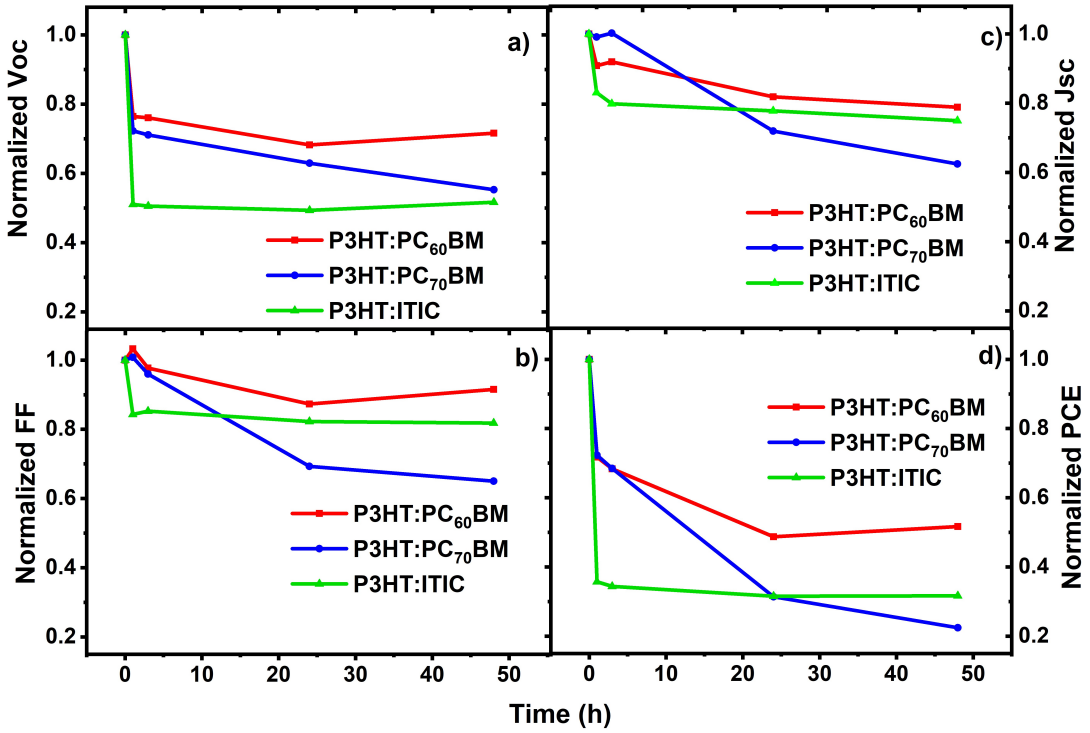


Figure 4.2: Time evolution of (a) Normalized PCE, (b) Normalized J_{SC}, (c) Normalized V_{OC}, and (d) Normalized FF with thermal ageing in P3HT:PC_{60}BM, P3HT:PC_{70}BM, and P3HT:ITIC devices.

significantly in $PC_{60}BM$-based devices. The free charge mobility is one of the parameters that determine FF in the devices. The total charge mobility in the devices during degradation was calculated using the Mott-Gurney space-charge limited-current (SCLC) law [174]. Mathematically, it is given as follows:

$$J_{SCLC} = (\frac{9}{8})(\frac{V^2}{L^3})\varepsilon_r\varepsilon_0\mu_0 exp(\Upsilon\sqrt{\frac{V}{L}}) \tag{4.2.1}$$

where ε_r and ε_0 are the relative dielectric constant of the active layer and the permittivity of free-space respectively, while μ_0, Υ, V and L represent the charge carrier mobility, the strength of the field-dependence, the applied voltage, and the thickness of the device,respectively. The total mobility (μ_0) of the fresh and degraded P3HT:PC_{60}BM, P3HT:PC_{70}BM, and P3HT:ITIC were calculated to be 2.92 and 2.44, 2.43 and 0.63 and 0.22 and 0.16 ($\times\ 10^{-4}\ cm^2V^{-1}s^{-1}$), respectively. The charge mobility in PC_{60}BM-based device is relatively higher and remained almost unchanged after 48 h of degradation while, drastically reduced,is ITIC followed by PC_{70}BM based devices, confirming a high recombination dynamics due to thermal degradation in the latter devices,

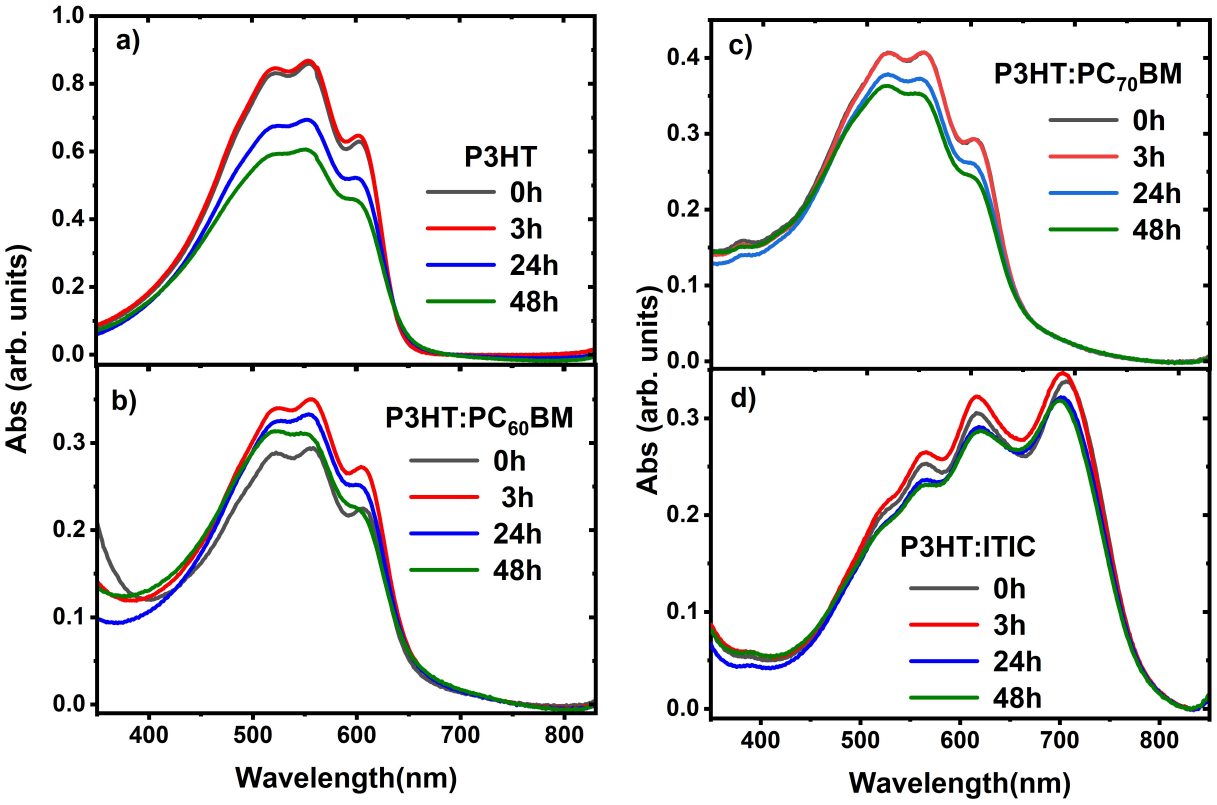


Figure 4.3: Selected absorption spectra of a) P3HT b) P3HT:PC_{60}BM c) P3HT:PC_{70}BM and d)P3HT: ITIC taken at different time intervals of thermal degradation.

consistent with their higher drop in FF.

On the other hand, the J_{sc} of the devices is determined by the absorption of photons in the active layer. The absorptions of P3HT:PC_{60}BM, P3HT:PC_{70}BM, and P3HT:ITIC thin films were recorded during thermal degradation at 85 °C as depicted in Figure 4.3. The absorptions of the blends in Figure 4.3(b-d) were more stable compared to the pristine P3HT film (figure 4.3a), confirming the acceptor's role in preventing polymer oxidation. Comparing the blend films with three acceptors, the absorption of P3HT:PC_{60}BM was found to increase during the degradation time, while the PC_{70}BM and ITIC-based films lost 14 and 8% of their initial absorbances, respectively. However, the 48 and 25% loss in J_{sc} of PC_{70}BM and ITIC based devices, respectively, can not be attributed solely to the less than 15% absorption loss. The absorption loss in the P3HT-based thin films can be attributed to the change in crystalline order of the donor as well as the disruption of π-conjugation due to oxidation [110]. The latter is accompanied by a blue shift in absorbance, which is clearly seen in PC_{70}BM and ITIC-based films. The large difference in these degradation properties between the PC_{60}BM and PC_{70}BM is an intriguing question that

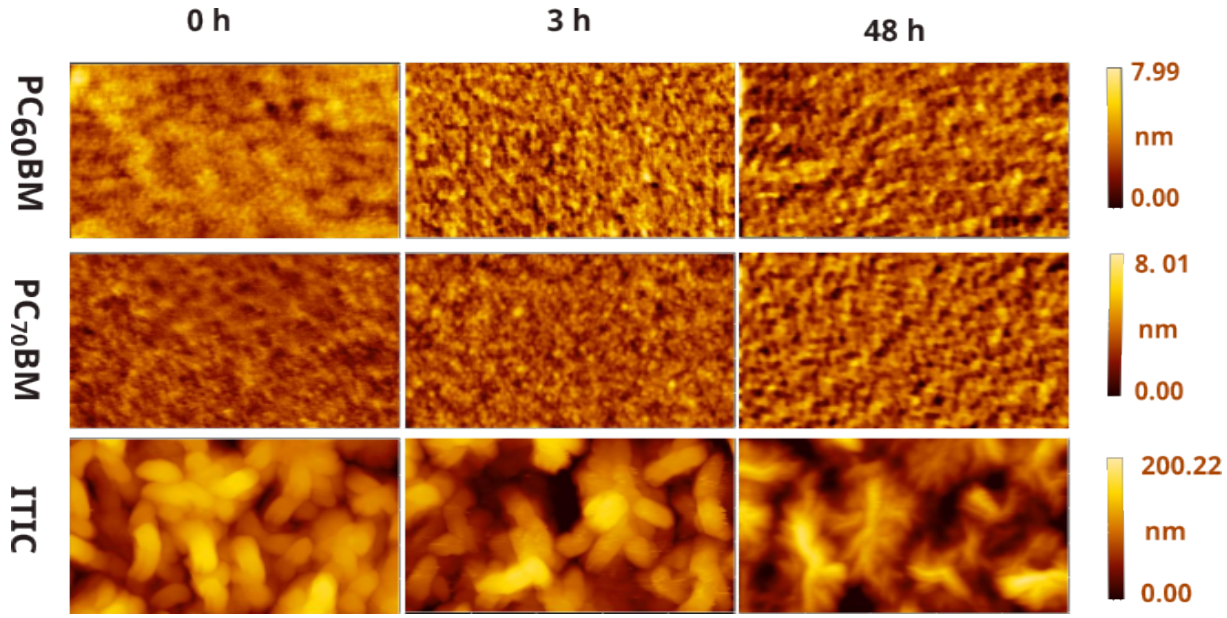


Figure 4.4: Surface topography images of P3HT:PC_{60}BM,P3HT:PC_{70}BM, and P3HT:ITIC during thermal ageing

needs further clarification. More importantly, the degradation kinetic of PC_{70}BM is closer to the non-fullerene small molecular acceptor ITIC, than the FA (PC_{60}BM). Recent reports revealed that the oxidation of blended films is highly influenced by the LUMO level of the acceptors [175]. The LUMO difference in the three acceptors might have played a significant role.

4.2.3 Evolution of the morphology P3HT-based OSCs with thermal degradation

The morphology of an OSC is generally a metastable state that readily evolves into a thermodynamically stable state, even at room temperature[176, 177]. The stability of morphology of an OSC is critical due to its determining role in charge photogeneration. The roles of PC_{60}BM, PC_{70}BM, and ITIC on the stability of the P3HT blended active layer were monitored using their AFM images taken during thermal stress, as shown in Figure 4.4. The fresh samples of the FA-based films displayed a much lower root mean square (RMS) roughness (less than 1 nm) compared to the P3HT:ITIC BHJ film (above 29 nm), consistent with its much lower J_{sc}. The roughness of active layers in all films increased with the highest increment in a P3HT:PC_{70}BM-based device. The roughness of the P3HT:PC_{70}BM active layer showed a negligible increase in the first 3 h, followed by a higher than doubled roughness value after 48 h. The evolution of the

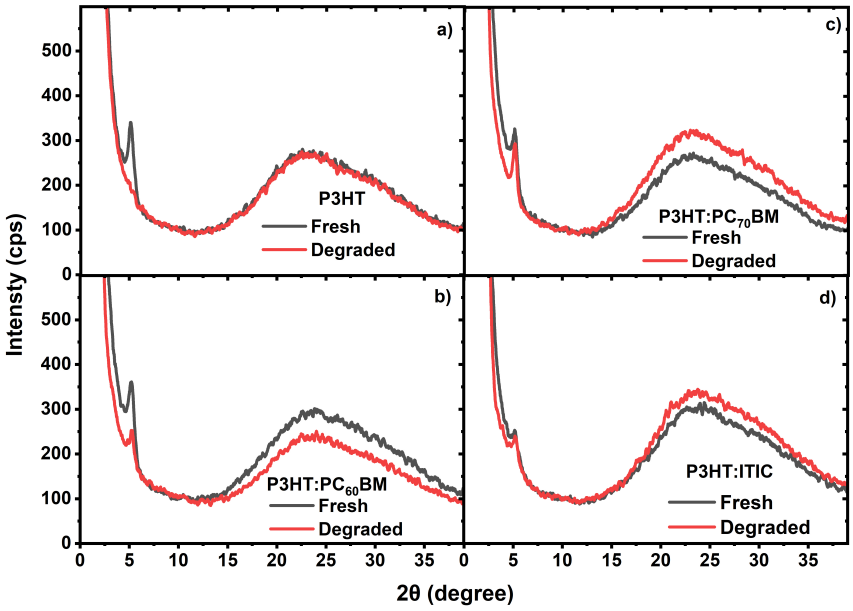


Figure 4.5: XRD traces of fresh and degraded a) P3HT b) P3HT:PC_{60}BM, c)P3HT:PC_{70}BM, and d) P3HT:ITIC films

current in this device follows the trend of the active layer morphology, confirming the crucial role it played in the device's stability. On the other hand, the roughness of the P3HT:PC_{60}BM film increased from 0.99 to 1.99 nm in the first three hours, followed by an improvement in roughness to a value of 1.62 nm. Interestingly, the J_{sc} trend in P3HT:PC_{60}BM-based devices with thermal degradation follows its morphological evolution; a significant decrease in J_{sc} until 3 h, followed by a stable value until the accelerated ageing time. This explains why the two FA-based devices' degradation kinetics differ despite their very similar molecular structures. The P3HT:ITIC-based active layer, on the other hand, remained rough throughout the measurement and did not follow the J_{sc} trend, suggesting that device morphology did not play a significant role in device degradation. The rough morphology of P3HT:ITIC-based device during the degradation time explains, the reason for its degradation being V_{oc} unlike the FAs, as shown in the Figure 4.2a.

Thermally-induced crystallization of donor and acceptor units in the active layer can create a large phase separation. To determine the cause of the evolution of the morphology of the P3HT-based active layers, we recorded the XRD traces of the fresh and 48 h degraded films as depicted on Figure 4.5. The XRD trace of fresh P3HT film shows a sharp peak around $2\theta = 5.28°$

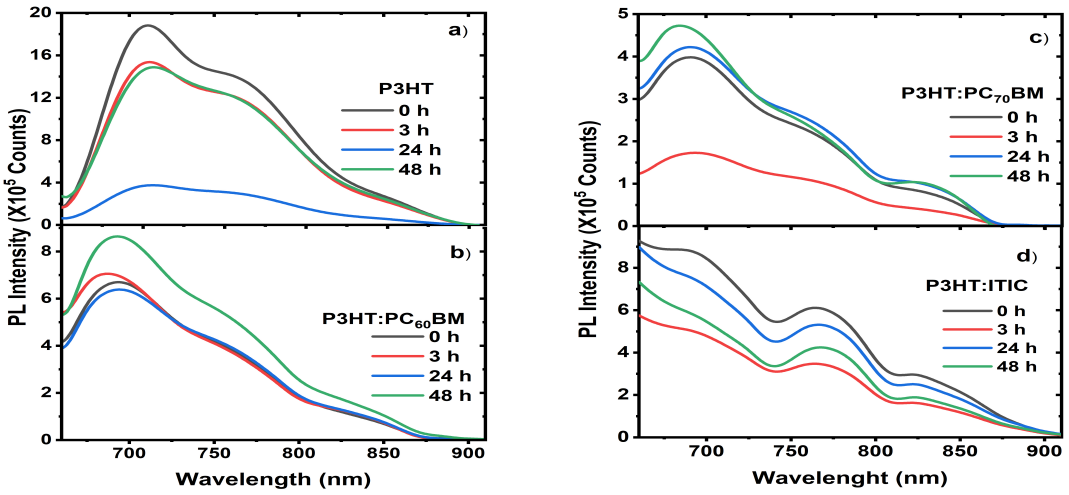


Figure 4.6: Photoluminescence spectra of a) P3HT b)P3HT:PC_{60}BM c)P3HT:PC_{70}BM and d)P3HT:ITIC during thermal degradation

which corresponds to self-organized lamellar structures oriented at (100) plane separated by an interplanar distance of 1.67 nm as calculated by using Bragg's law. The diffraction trace also revealed a broad halo around 2θ=23°, which corresponds to diffraction from the (010) planes. These peaks are maintained in the blended films, as shown in Figure 4.5b-d. However, the diffraction intensity of the (100) plane of P3HT is reduced due to the intercalation of the acceptors, with ITIC depicting the lowest value. However, upon degradation, the peak around 5.28° becomes sharper and its intensity increased in P3HT:PC_{70}BM and P3HT:ITIC-based films, while it decreased significantly in P3HT:PC_{60}BM film. The growth of the peak corresponding to the crystallinity of P3HT in PC_{70}BM and ITIC-based devices confirm a higher phase segregation of the polymer while it was suppressed in PC_{60}BM based OSC. These results further confirm that crystallization-induced degradation is suppressed in the PC_{60}BM device, making it more stable acceptor than PC_{70}BM and ITIC.

It is well known that, the morphology of the active layer directly affects charge transfer in the BHJ active layer. The charge transfer in these devices is investigated using PL spectroscopy, as shown in Figure 4.6, to further interrogate the evolution of the morphology during thermal ageing. Upon blending P3HT with an acceptor, its emission is expected to be quenched, provided that there is a good charge transfer in the BHJ film. The QE of the P3HT:PC_{60}BM device

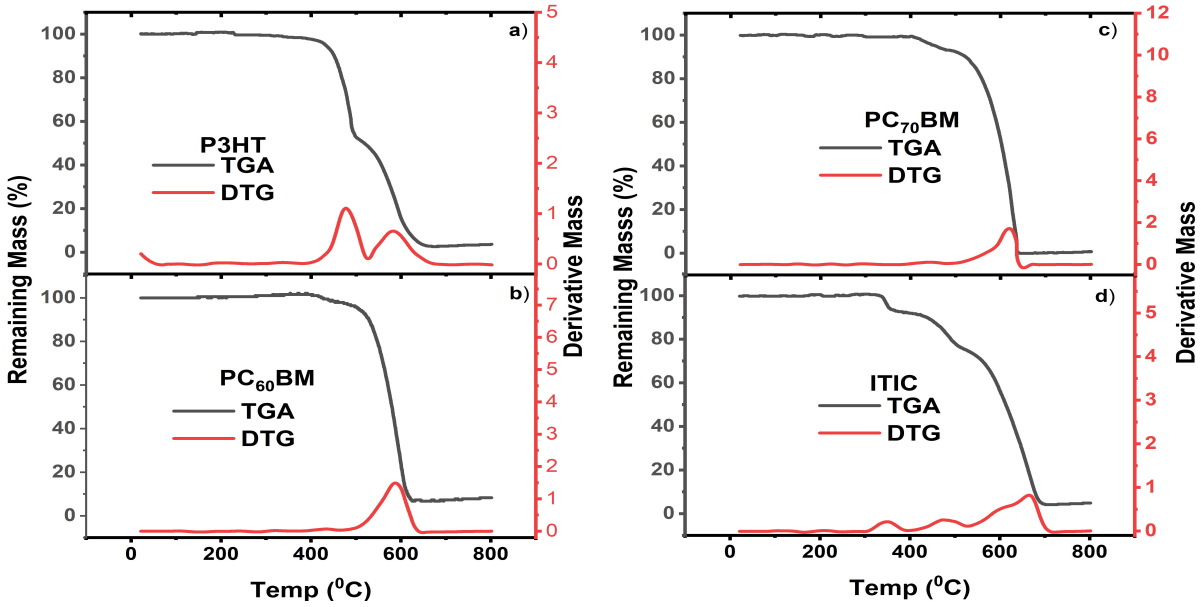


Figure 4.7: TGA and Derivative-TGA (DTG) curve of a)P3HT, b) $PC_{60}BM$, c) $PC_{70}BM$, and d) ITIC recorded in nitrogen atmosphere.

remained unchanged for 24 h, followed by a decrease of 16%, while in the P3HT:PC_{70}BM device it increased in the first 3 h, followed by a decrease to the initial value afterwards, confirming a stable donor/acceptor interface in P3HT:PC_{60}BM active layer. Unfortunately, the exciton QE of the P3HT:ITIC based device is difficult to determine as ITIC has a significant contribution in the emission region recorded. However, consistent with the XRD and AFM images, the demixing of donor and acceptor domains is suppressed in the P3HT:PC_{60}BM based device due to the freezing of the active layer morphology.

4.2.4 Thermogravimetric analysis

The thermal properties of three acceptors and P3HT were studied using thermogravimetric analysis as depicted in Figure 4.7 . The decomposition temperatures (T_D = 5% mass loss) of P3HT, PC_{60}BM, PC_{70}BM, and ITIC were found to be 397, 405, 400, and 325 °C, respectively, confirming the higher thermal stability of the fullerene-based acceptors. The derivative TGA (DTG) curves of P3HT shown in red (Figure 4.7a) exhibited a two-step degradation mechanism. The FA acceptors, on the other hand, depict a one-step degradation that peaks at temperatures above 450 °C indicating chain breaking in the isotropic bucky-ball structures is inhibited. On the contrary, the NFA revealed a more than three-step degradation mechanism attributed to

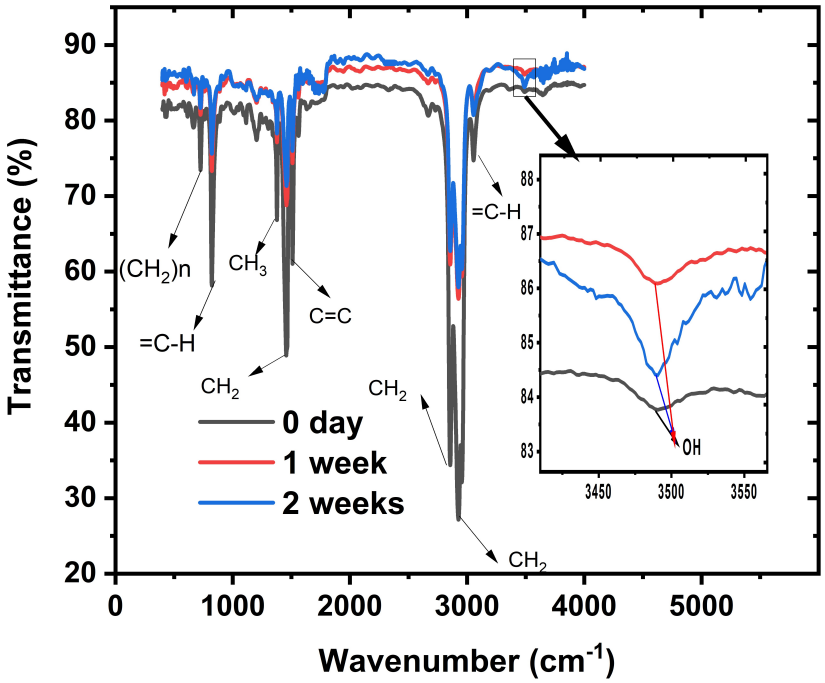


Figure 4.8: FTIR spectra of P3HT during thermal degradation.

chain breaking, intra-molecular bond breaking, and side chain breaking due to its long molecular structure [178]. The excellent thermal stability of PC_{60}BM has undoubtedly endowed a better lifetime OSC fabricated based on P3HT:PC_{60}BM, as shown in the device section.

4.2.5 FTIR

The FTIR spectra of P3HT were recorded during thermal degradation, as illustrated in Figure 4.8, to further elucidate the cause of the device degradation in the devices studied. The spectra revealed the most fundamental modes in P3HT, as labeled in Figure 4.8 ;including vibrational peaks at 3055, 2925 and 2856 cm^{-1} corresponding to for aromatic =C-H stretching, for CH asymmetric and symmetric stretching, respectively. The FTIR of P3HT spectra also displays the 1510 and 1456 cm^{-1} peaks that are due to thiophene rings stretching and 1377 $cm^{-}1$ peak due to methyl deformation. The peaks at 821 and 725 $cm^{-}1$ are due to CH-out-of plane bending vibration and methyl rocking [179, 180, 181]. The intensity of the vibrational modes attributed to the functional groups decreased in the first week of annealing, clearly confirming the breaking of the bonds in the P3HT backbone structure. In addition, after 1 week of thermal degradation, an -OH group evolved, as shown in the inset. This OH group is a well-known degradation initiator

that will aggressively attack the thiophene ring, leading to complete degradation or ring opening and subsequently killing the conductivity of the polymer. As a result, polymer degradation caused by thermal ageing occurs mainly through OH-mediated reactions

Conclusion

Experimental investigation of the role of acceptors on the stability of P3HT based inverted OSCs was done using three acceptors namely, $PC_{60}BM$, $PC_{70}BM$, and P3HT:ITIC. The results revealed that P3HT:$PC_{60}BM$ devices kept more than 50 % of its initial PCE while $PC_{70}BM$, and ITIC-based devices maintained only 22 and 32 % of their initial PCE, respectively. The PCE loss in P3HT:ITIC-based was mainly due to the drastic decrease in which indicated that the change in the energy level of ITIC by annealing as the main cause of degradation on the other hand the degradation of P3HT:$PC_{60}BM$ and P3HT:PC_{70} are due to J_{sc}. Further investigation confirmed that the morphology of FA-based device played a crucial role in their stability. The morphology of P3HT:$PC_{60}BM$ device was found to be stable that demixing of donor and acceptor phases was effectively suppressed. Further more, OH-production by thermal oxidation of the polymer was found to be an initiator of the degradation in the devices.

Chapter 5

Non-electron withdrawing unit copolymerization to enhance photo-stability of thiophene-based organic solar cells

5.1 Introduction

OSCs have garnered significant attention due to their low production costs and high PCEs, which have reached as high as 20 % from single-junction devices [4]. To enhance PCE, donor materials should possess deep HOMO energy levels which is one mechanism to achieve high open-circuit voltage (V_{OC}), a broad absorption spectrum in the visible light range, and high hole mobility [182]. Conversely, acceptor materials should have shallow LUMO energy levels for efficient charge transfer, high electron mobility, and a strong electron affinity to effectively accept electrons. Thiophene is one of the most widely used donor units in OSCs, which is highly studied and better understood in the process of solar energy conversion. However, the stability of P3HT is poor, which limits its wide application [183, 184]. Photo-degradation is the main cause of PCE loss in these polymer based devices. Reports have indicated that P3HT undergo photo-bleaching and photo-oxidation, leading to material degradation [110, 185]. The latter is

primarily mediated by singlet oxygen ($^1O_2$) formation through the transfer of holes from the HOMO of the polymer, as its HOMO level is close to the oxidation level of O_2 (-5.2 eV) [186].

Thiophene-based polymers typically exhibit a high HOMO level, resulting in a lower V_{OC} and increased photo-oxidation. This suggests that lowering the HOMO level could enhance both the photostability and the V_{OC} of these polymers. Recent work by Martynov et al[187] reported that donor polymers with deeper HOMO levels afford much better photostability, mainly due to suppressed photo-oxidation. Thus, deepening the HOMO level of donor materials can be a promising route to improve their photostability. Copolymerization with non-electron withdrawing units can downshift the HOMO level if there is good molecular orbital coupling.

In this study, we continued our investigation in the copolymerization of thiophene units with benzodithiophene-4,8-dione (BDD) to achieve a deeper HOMO level with aim of suppressing photooxidation and limiting oxygen diffusion. We utilized a copolymer, benzodithiophene-4,8-dione copolymerized with α-quaterthiophene (PBDD4T), which has highly delocalized electrons that push its HOMO level down to -5.30 eV. This was done to investigate the effect of HOMO stabilization in thiophene-based polymers, specifically through the incorporation of a non-electron-withdrawing unit (BDD), on the photostability of fullerene-based OSCs. The computational results confirmed that the BDD unit copolymerized with quarterthiophenes could effectively increase its electron-donating property, downshifting the HOMO level by approximately 0.25 eV. Interestingly, the BDD unit also broadened the absorption spectrum, resulting in a higher J_{sc} in the PBDD4T device compared to the P3HT device. Furthermore, the deeper HOMO level of PBDD4T resulted in a higher and significantly improved photostability.

5.2 Results and Discussion

5.2.1 Optical and Electrochemical Properties

The absorbance of P3HT and PBDD4T in films is depicted in Figure 5.1a. The onset of absorbance of PBDD4T was red-shifted by 50 nm, resulting in a lower band gap of 1.76 eV compared to P3HT (1.89 eV). Additionally, the benzodithiophene-4,8-dione (BDD) copolymerization with the thiophene units pushed the absorption maximum of the copolymer to 590 nm, which aligns

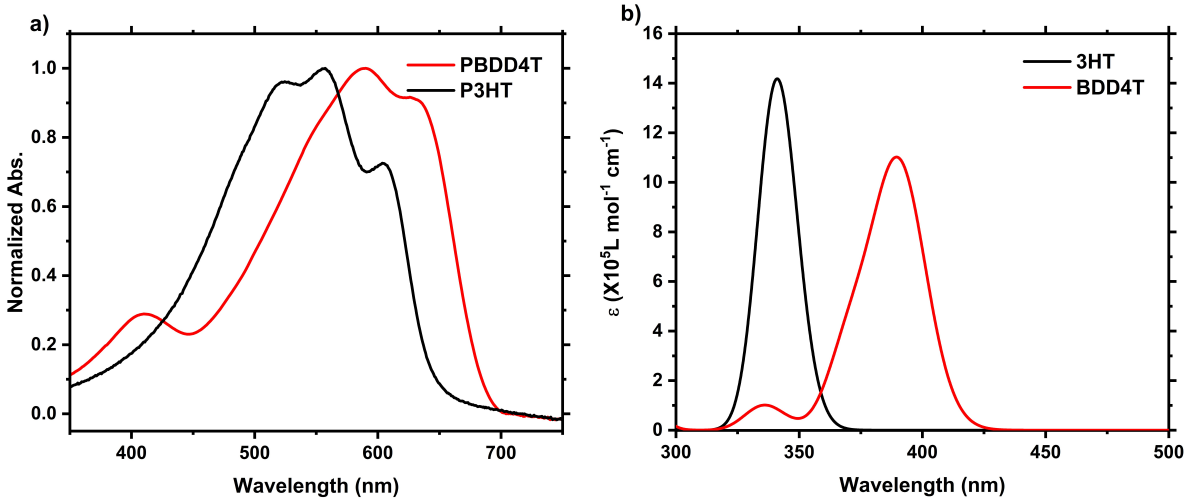


Figure 5.1: a)Absorption spectra of P3HT (black) and PBDD4T(red) thin films b)TD-DFT simulated absorbance of P3HT(black) and PBDD4T(red) in gas using B3LYP-CAM level of theory at 6-31G(d,P) basis set.

well with the high solar spectral flux region. Consequently, a higher J_{sc} is expected in PBDD4T-based OSCs.

Furthermore, the electron-donating BDD group in the copolymerization also lowered the HOMO level to -5.30 eV, compared to P3HT's HOMO level of -5.20 eV as shown in Table 5.1. A stabilized HOMO level is crucial for attaining a high open-circuit voltage [171]. Moreover, the polymer is expected to be resistant to oxidation [188, 187]. The electrochemical and optical properties of the polymers are summarized in Table 5.1

Table 5.1: Electrochemical and optical properties of PBDD4T and P3HT polymers.

Polymer	**Electrochemical**				**Optical**			
	HOMO (eV)	LUMO (eV)	HOMO (eV)[a]	LUMO (eV)[a]	E_g^{elec} (eV)	λ_{max} (nm)	λ_{onset} (nm)	E_g^{opt} (eV)
P3HT	-5.20	-3.20	-5.14	-1.94	2.00	555	654	1.89
PBDD4T	-5.30	-3.53	-5.39	-2.50	1.77	590	704	1.76

[a] DFT calculated

To clarify the effect of BDD-unit copolymerization on the optical and electrochemical properties of the polymer, DFT and TD-DFT calculations were employed. The frontier molecular orbitals of the two copolymers were calculated, as depicted in Figure 5.2, and their values are summarized in Table 5.1. Both the HOMO and LUMO of P3HT were delocalized along its backbone, while a less delocalized HOMO was observed in PBDD4T. The HOMO level of PBDD4T was found to be downshifted by 0.25 eV compared to P3HT consistent with the experimentally obtained results.

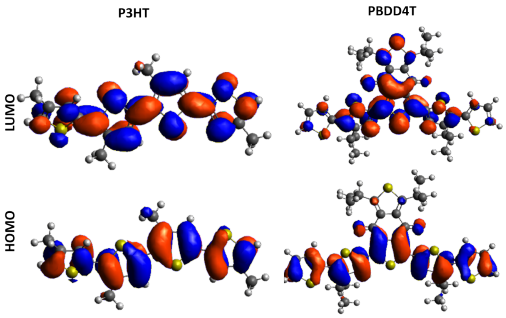


Figure 5.2: Electron cloud distribution in Frontier molecular orbital of P3HT(left) and PBDD4T(right)

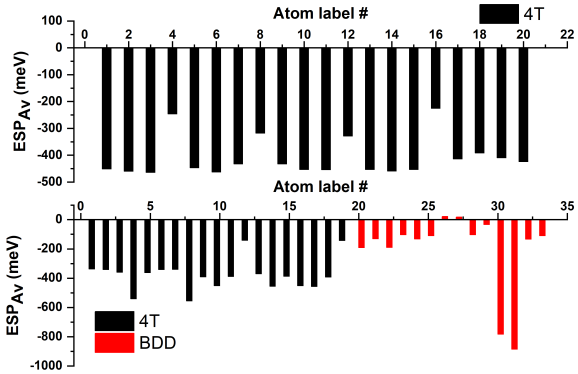


Figure 5.3: Average ESP values at each atom in the backbone of P3HT(top) and PBDD4T(bottom)

Since the molecular energy levels are dictated by the charge distribution in the backbone of the polymer , the electrostatic potential (ESP) of the copolymers along their backbones was calculated as shown in Figure 5.3. The ESP of both polymers mainly revealed a negative potential along their backbones, confirming that all the units involved in the polymers' backbone have electron-donating properties. The sum of ESP on the P3HT and PBDD4T backbones was found to be -8.19 eV and -10.17 eV, respectively, confirming the higher electron-donating properties of the latter due to the BDD electron-donating unit copolymerization. This explains the deeper HOMO level of PBDD4T. Notably, the two oxygen atoms in the BDD units contributed significantly to the total ESP in PBDD4T, highlighting the importance of strongly electro-negative materials in deepening the HOMO level of a polymer.

Furthermore, the absorption of the polymers was simulated in gas phase using time dependent DFT(TD-DFT) in CAM-B3LYP/6-31G++(d.p) level of theory/basis set, as shown in Figure

Table 5.2: Summary of the first excited state transition energy, oscillator strength (f) and molecular orbital (MO) contributions

Polymer	Transition	Energy (eV)	λ_{st} (nm)	f	Main MO Contribution
P3HT	$S_0 \longrightarrow S_1$	3.64	341.08	1.05	H $\longrightarrow$ L (92.0%)
PBDD4T	$S_0 \longrightarrow S_1$	3.17	390.92	0.77	H $\longrightarrow$ L (86.5%)

5.1a, revealing a significant red shift of approximately 50 nm in the first excitation of PBDD4T compared to P3HT. Note that a termer unit was used for P3HT to make the comparison more reliable. The important excitation parameters from the TD-DFT calculations are summarized in Table 5.2. The oscillator strength of the transition to the first excited state in P3HT was higher than in PBDD4T, confirming its higher absorption coefficient despite its blue-shifted absorption.

5.2.2 Photovoltaic performance

The photovoltaic performances of the polymers were determined utilizing $PC_{71}BM$ as an acceptor in a device architecture of Glass/ITO/ZnO/active-layer/Mo_2O_3/Al. Figure 5.4a depicts the J–V curves of the fabricated devices, and Table 5.3 summarizes the corresponding PV parameters. The BDD unit copolymerization was found to increase both the J_{sc} and V_{OC} of PBDD4T compared to P3HT. The increases in J_{sc} of the copolymer compared to P3HT is attributed to its broader and red-shifted absorption as depicted in Figure 5.4b. The BDD-copolymerization was also found to downshift its HOMO level as shown in Figure 5.4b inset, resulting in a higher V_{OC} according to the empirical relation $V_{oc} = (1/e)(E^{Donor}_{HOMO} - E^{Acceptor}_{LUMO}) - 0.3V$ [171]. Consequently, the PCEs of PBDD4T and P3HT OSCs were found to be 4.68 and 2.44% respectively, confirming a nearly two-fold increase in PCE by BDD copolymerization.

On the other hand, a slight increase in the FF is also found in PBDD4T, resulting in PCE enhancement due to BDD-copolymerization. The PCE of the PBDD4T-based and P3HT-device is equivalent to the reported values [189] but could go higher than 6% in PBDD4T-based devices when the solvent additive, 1,8-diiodooctane (DIO) is used [190, 189]. DIO is typically employed to enhance device performance; however, its omission in this case was intentional, as DIO has been found to accelerate photodegradation due to hydrogen iodide (HI) formation upon irradiation [191, 14]. Furthermore, the dark J-V curves of the devices were recorded, and their semi-logarithmic plot is shown in Figure 5.5. The curve reveals three distinct regions, and the second

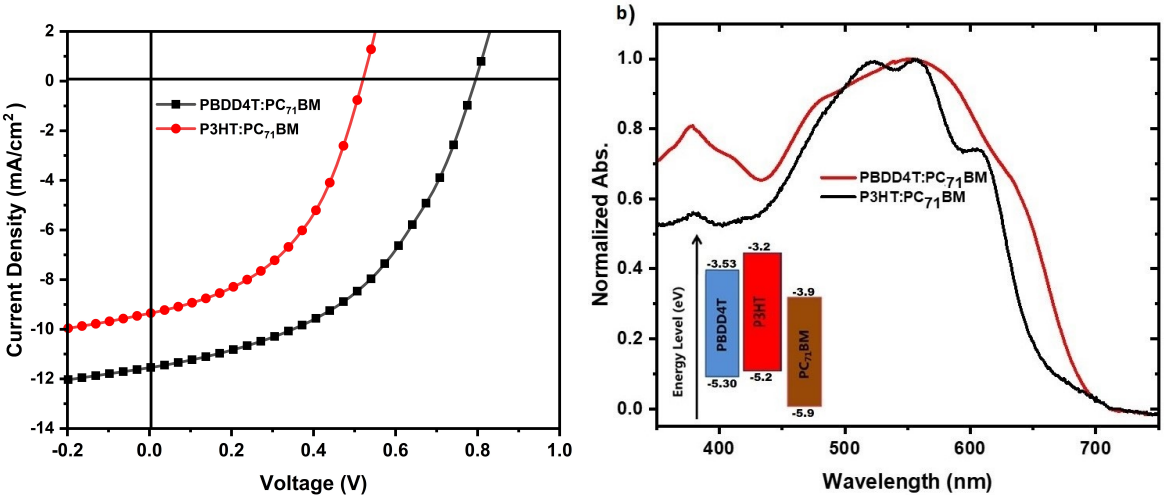


Figure 5.4: a) J-V curves b) Blend Abs of the PBDD4T and P3HT based device.

Table 5.3: Photovoltaic Parameter of $PC_{71}BM$ based OSCs fabricated

Donor Name	$\mathbf{J}_{SC}$ (mA/cm^{-2})	(V)	**FF** (%)	**PCEmax**(*) (%)
PBDD4T	12.23	0.79	48.43	4.68 (4.57±0.07)*
*P3HT	10.02	0.52	46.92	2.44 (2.42±0.01)*

*averaged for four devices

region (II) is predominantly dictated by the leakage current. In this region, it is evident that the P3HT:$PC_{70}BM$ device exhibits a higher leakage current than the PBDD4T:$PC_{71}BM$-based device, which contributes to its lower fill factor (FF) due to the increased leakage.[192]

5.2.3 Charge generation and transfer kinetics

Although the increase in PBDD4T is directly related to its deeper level of HOMO, the improvement in J_{sc} and FF is the result of multiple processes. Hence, charge generation and recombination in the devices were studied. The photocurrent (J_{ph}), defined as J_{ph} = J_L - J_d, where J_L and J_d stand for the current densities under illumination and in the dark, respectively, was recorded against the effective voltage (V_{eff}), defined as V_o - V, where V_o is the voltage at which J_L = J_d. The J_{ph}-V_{eff} curves of PBDD4T and P3HT-based devices are given in Figure 5.6. The graph shows a linearly increasing J_{ph} with V_{eff} up to approximately 0.5 V, followed by a saturated region where J_{ph} = J_{sat} (saturation photocurrent density).

At high voltage, the electric field is strong enough to sweep out all the generated carriers, so

Table 5.4: Charge generation and collection parameters of the PBDD4T and P3HT-based device.

Device Name	**QE** (%)	$\mathbf{J}_{Sat}$ (mA/cm^{-2})	$\mathbf{G}_{max}$ (s^{-3} m^{-3}x10^{27})	**P (E,T)** (%)
PBDD4T:PC$_{71}$BM	94	12.91	5.04	94.6
P3HT:PC$_{71}$BM	88	11.04	3.81	90.78

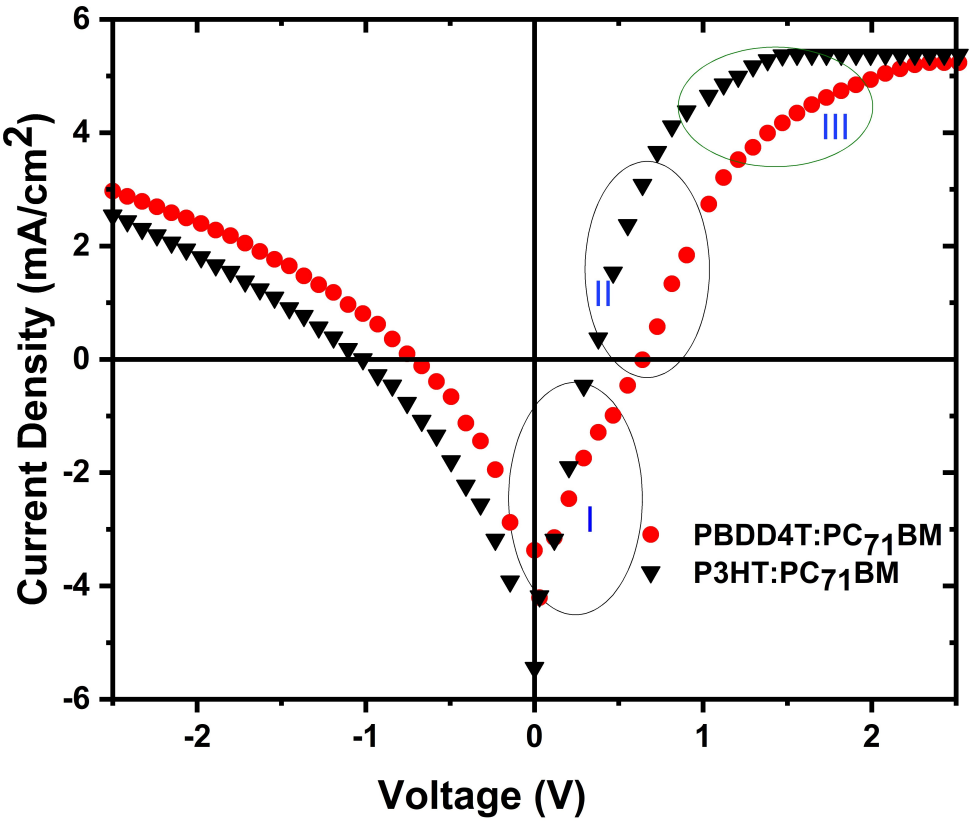


Figure 5.5: J-V characteristics under dark condition of the PBDD4T and P3HT based device.

no further increase in J_{ph} is expected: i.e., $J_{sat} = qLG_{max}$, with q, L, and G_{max} being elementary charge, thickness of the active layer, and maximum exciton generation rate. The G_{max} and the probability of charge dissociation and collection (P(E,T)) = J_{ph}/J_{sat}, at short circuit, are calculated and summarized in Table 5.4.

The exciton generation rate in PBDD4T and P3HT-based devices was found to be 5.04 $\times 10^{27}$ and 3.81 $\times 10^{27} m^{-3} s^{-1}$, respectively, consistent with the higher absorption width of the BDD-copolymerized polymer. Additionally, the P(E,T) of PBDD4T and P3HT-based devices was found to be 94.6 and 90.78%, respectively, confirming a higher charge dissociation and collection probability could be attained by BDD-copolymerization, confirming recombination is highly suppressed in the device. The reduced recombination led to the increase in both J_{sc} and

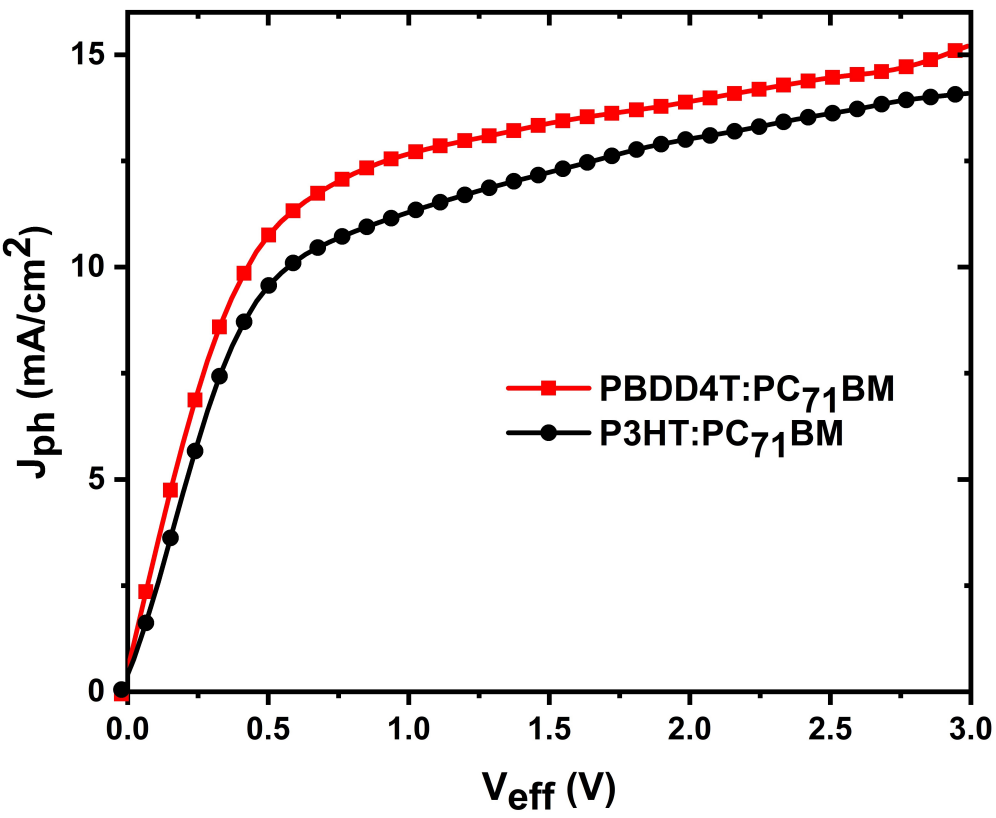


Figure 5.6: J_{ph} against the effective voltage V_{eff} of the PBDD4T and P3HT based device.

FF in the devices upon BDD-copolymerization.

Moreover, after the generation of excitons in the polymers, the fraction of these excitons dissociating into free charges determines the preceding charge generation process. In this regard, we employed steady-state PL spectroscopy to record the emission of the pristine ($PL_{Pristine}$) and the polymer blend (PL_{Blend}) as shown in Figure 5.7 to calculate exciton quenching efficiency (QE) according to the relation $QE = (1 - \frac{PL_{Blend}}{PL_{Pristine}}) \times 100\%$ as given in Table 5.4. The higher QE in PBDD4T-based device (94%) compared to P3HT-based device (88%) indicates a better charge transfer at the donor-acceptor interface in the BDD-copolymerized polymer. Recent studies have demonstrated that the intermolecular electric field force (IEF) between the electron-donating and electron-accepting units within the active layer materials plays a crucial role in dictating charge transfer from the donor to the acceptor. [193, 194] Consequently, this charge transfer process is governed by the electrostatic potential (ESP) of the donor units, as a consistent acceptor is used throughout the study.

The stronger negative ESP in the backbone of PBDD4T is thus expected to lead to higher

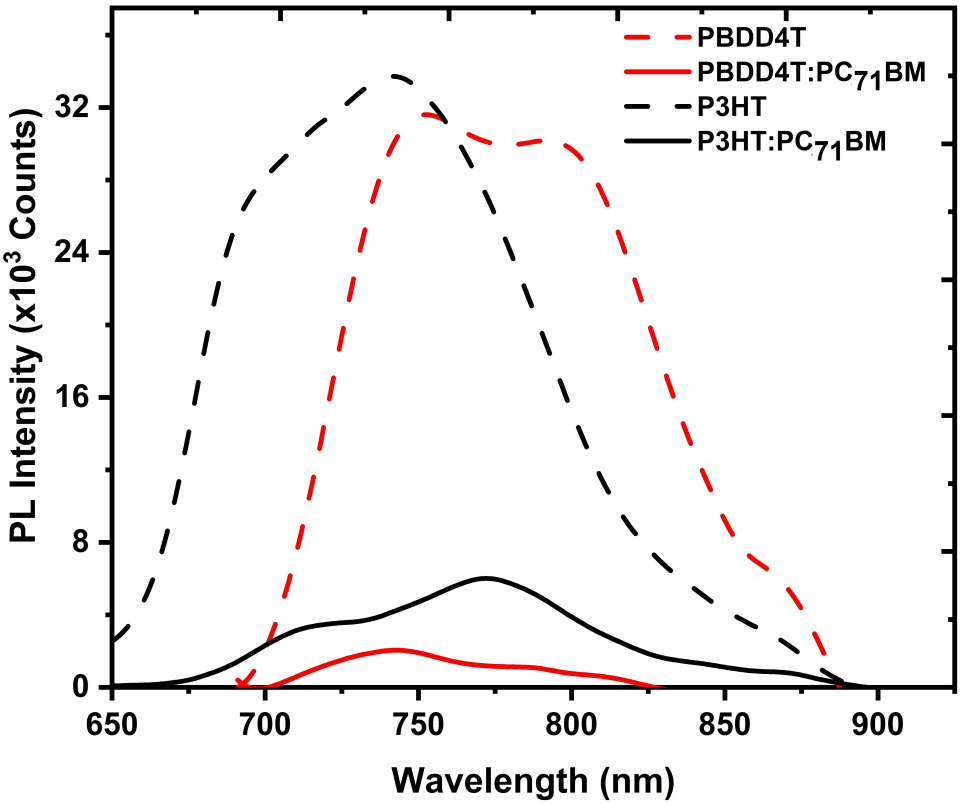


Figure 5.7: PL spectra of pristine and their blends of PBDD4T and P3HT.

charge transfer probability, leading to higher QE. In summary, BDD-copolymerization can lead to better charge generation and transfer kinetics owing to its higher electron-donating property that broadened its absorption and increased the IEF in the device.

5.2.4 Recombination Kinetics and Charge Transport Properties in OSCs

Further investigation into the increment in J_{sc} involved light intensity-dependent J-V measurements on the fabricated devices to elucidate the recombination mechanism. As the highest and lowest recombination in a solar cell device occur at open and short-circuit conditions, respectively, the corresponding values of and J_{sc} were plotted at different light intensities, as shown in Figure 5.8a and b. The V_{OC} and J_{sc} vs Intensity plots were fitted using Equation 5.2.1 and 5.2.2, respectively. [195].

$$V_{oc} \propto n\frac{kT}{q}ln(I) \tag{5.2.1}$$

In this context, the factor nkT/q, where n, k, T, and q correspond to the ideality factor, Boltzmann constant, temperature, and elementary charge, respectively, represents the slope of the fitted line in the plot of V_{OC} versus ln(I). When n is approximately 1, bimolecular recombination is the dominant process, whereas as n nears 2, trap-assisted recombination becomes the primary mechanism. The fitting of V_{OC} versus ln(I), illustrated in Figure 5.8a, using Equation 5.2.1, resulted in slope values of 1.13kT/q and 1.21kT/q for devices based on PBDD4T and P3HT, respectively. This suggests that trap-assisted recombination plays a less significant role in PBDD4T-based devices, which contributes to their enhanced J_{sc} and FF.

Furthermore, the recombination kinetics of these devices can be better understood by analyzing the dependence of J_{sc} on light intensity. The power-law relationship between J_{sc} and light intensity (I) is described by Equation 5.2.2:

$$J_{\mathrm{sc}} \propto I^{\alpha} \tag{5.2.2}$$

,where an α value deviating from 1 indicates bimolecular recombination under short-circuit conditions. The α values in PBDD4T- and P3HT-based devices, calculated using Equation 5.2.2 from the fit of J_{sc} versus I, as depicted in Figure 5.8b, were found to be 0.96 and 0.95, respectively, indicating slightly lower bimolecular recombination in the BDD-copolymerized polymer.

Charge mobility in the active layer determines the recombination dynamics in the devices. The space-charge-limited current density (J_{SCLC}) of the fabricated devices recorded in the dark was fitted with the Mott-Gurney law given by Equation 5.2.3 to determine the charge mobilities (μ_o) in PBDD4T- and P3HT-based devices. The J_{SCLC} – V_{bi} curves with the Mott-Gurney fit, where V_{bi} is the applied voltage (V) corrected for the built-in voltage, are given in Figure 5.8c with the Mott-Gurney law fitting.

$$J_{SCLC} = (\frac{9}{8})(\frac{V^2}{L^3})\varepsilon_r\varepsilon_0\mu_0 exp(\Upsilon\sqrt{\frac{V_{bi}}{L}}) \tag{5.2.3}$$

where ε_r and ε_o are the dielectric constant of the active layer (=3) and the permittivity of free-space (=8.85 $\times 10^{-12}$ F/m), respectively, while γ and L represent the strength of the field-dependence and the thickness of the device, respectively. The charge mobility (μ_o) of the two

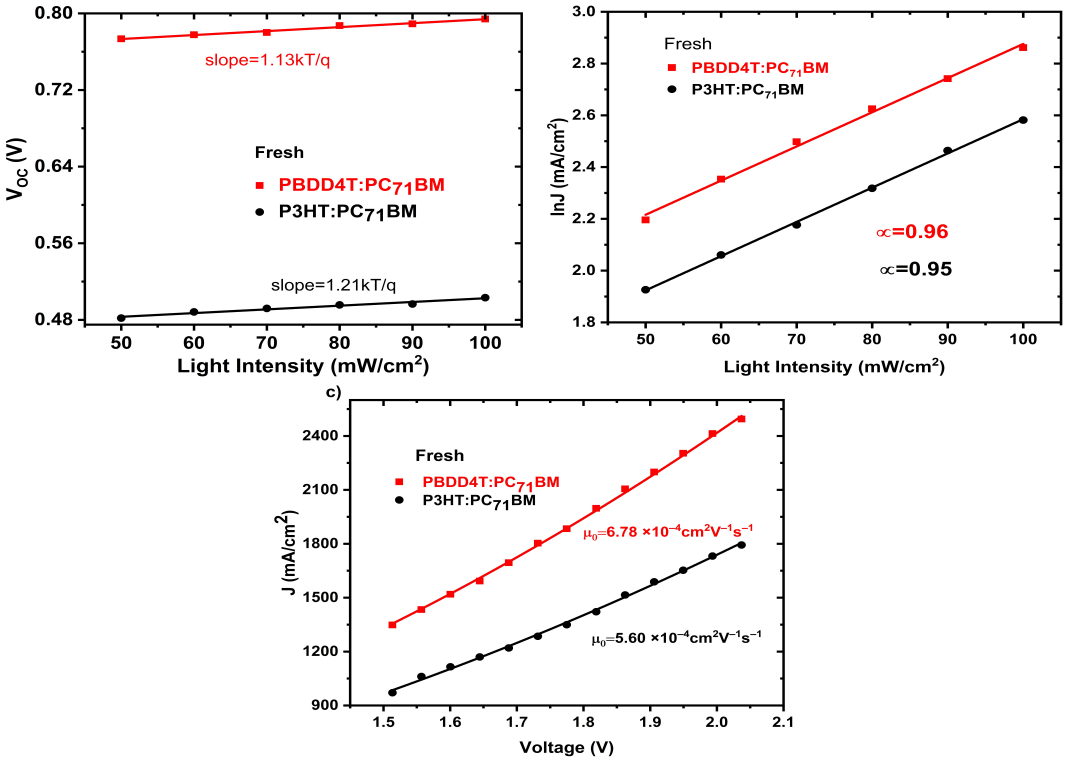


Figure 5.8: Light intensity dependence of (a) V_{OC} (b)J_{sc} in PBDD4T and P3HT based OSCs with their corresponding light fitting Equations (1) and (2), respectively and (c)charge mobility of PBDD4T and P3HT based OSCs fitted with Equation 5.2.3

devices was extracted from the fit of the J versus Voltage graph provided in Figure 5.8c, and was found to be 6.78 $\times 10^{-4}$ cm^2 V^{-1} s^{-1} for the PBDD4T device and 5.60 $\times 10^{-4}$ cm^2 V^{-1} s^{-1} for the P3HT-based device, consistent with the suppressed recombination that improved J_{sc} and FF in the BDD-copolymerized polymer. In summary, BDD-copolymerization suppressed trap-assisted recombination and improved charge mobility, resulting in higher J_{sc} and FF compared to the homopolymer, P3HT.

5.2.5 Device degradation

The evolution of the photovoltaic parameters due to photoinduced degradation was carefully studied for nearly 7 hours, as shown in Figure 5.9. The PBDD4T-based OSC retained more than 86% of its initial PCE, while the P3HT devices retained only 52% of their initial PCE after 7 hours of photoaging. This confirms that BDD-copolymerization could benefit the photostability of thiophene-based OSCs. In order to further elucidate the causes for these differences in the photostability of the devices, the evolution of J_{sc} and FF of the devices during aging are plotted,

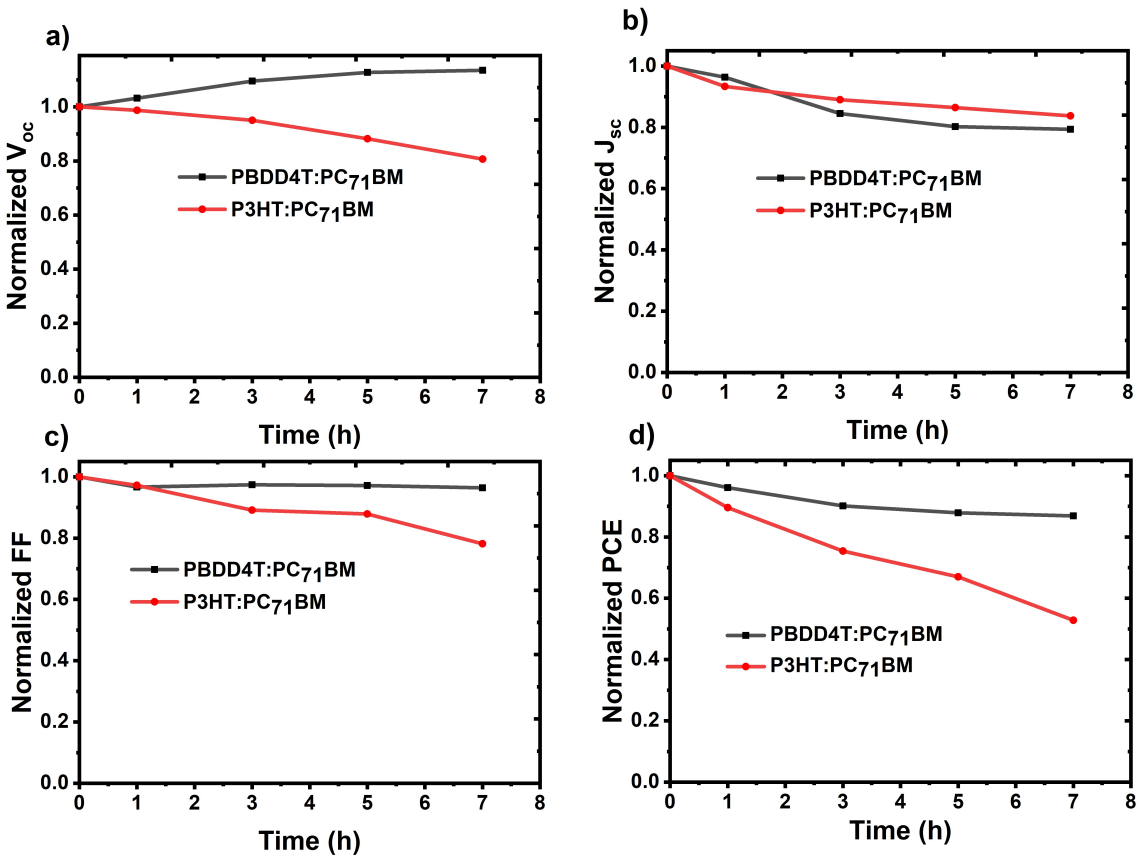


Figure 5.9: Time evolution of (a) Normalized V_{OC}, (b) Normalized J_{sc}, (c) Normalized FF, and (d) Normalized PCE with photo aging in PBDD4T:PC_{71}BM and P3HT:PC_{71}BM devices.

as shown in Figure 5.9.

The open circuit voltage, V_{OC} , of PBDD4T increased by 14% during photo-degradation. In contrast V_{OC} the in P3HT device decreased by more than 19% after aging. Comparing the decrease in V_{OC}, it can be concluded that photo-oxidation in PBDD4T is suppressed. This could be due to its deeper HOMO level (-5.30 eV) compared to the oxidation potential of oxygen (-5.20 eV), whereas the HOMO level of P3HT is at the same level as the oxidation potential of oxygen. [188, 196] On the other hand, the PCE of PBDD4T was reduced during aging mainly due to the loss in J_{sc}, while in P3HT devices, all the PV parameters, namely, V_{OC}, J_{sc}, and FF, decreased during aging, finally losing approximately 50% of its initial PCE. This shows that different degradation mechanisms are responsible for the two devices. The loss in J_{sc} of a device can be due to multiple processes that include loss of absorption and/or charge recombination, which can be caused by deteriorating morphology and lower charge mobility. The latter can also contribute to a lower FF.

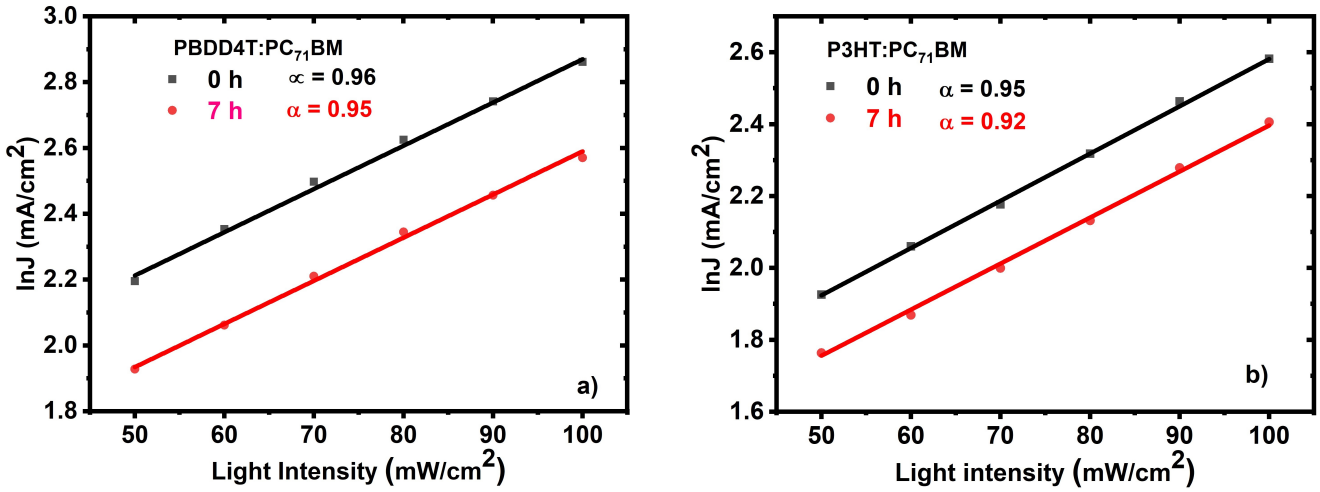


Figure 5.10: Light intensity dependence of lnJ_{sc} a) PBDD4T:PC_{71}BM b) P3HT:PC_{71}BM films

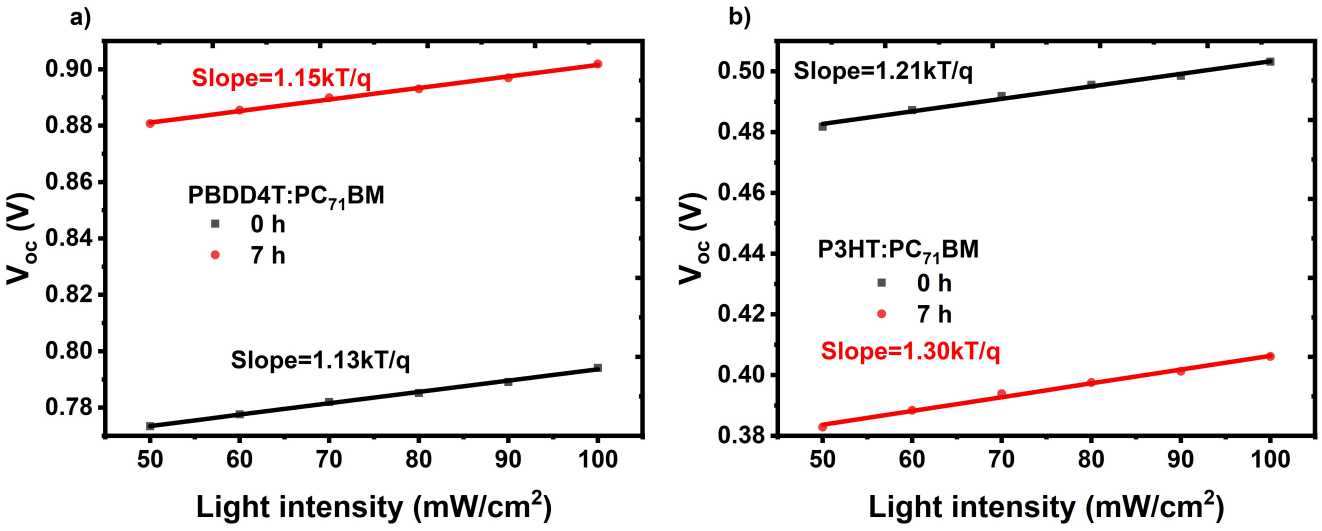


Figure 5.11: Light intensity dependence of a) PBDD4T:PC_{71}BM and b)P3HT:PC_{71}BM films

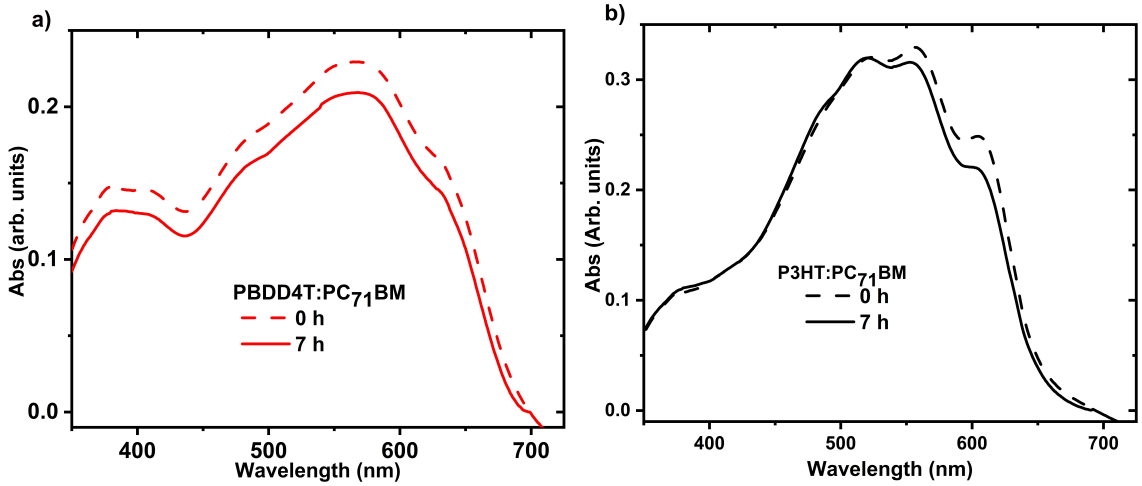


Figure 5.12: The absorption loss due to photodegradation in a) PBDD4T:PC_{71}BM b) P3HT:PC_{71}BM films

We determined the evolution of the recombination dynamics in the devices from the slope of J_{sc} versus intensity and V_{OC} versus intensity curves, as depicted in Figure 5.10a-b and 5.11a-b respectively. The values of α for PBDD4T and P3HT-based devices reduced from 0.96 to 0.95 and 0.95 to 0.92, respectively, after photoaging. The evolution of bimolecular recombination in PBDD4T is insignificant, which consequently contributed to its stable FF. On the contrary, the increased bimolecular recombination in P3HT-based devices could lead to the reduction of both J_{sc} and FF [197].

Moreover, from light intensity curves, slope values of $1.13kT/q$ and $1.15kT/q$ before and after 7 hours of photo-aging for PBDD4T-based devices, and $1.21kT/q$ and $1.30kT/q$ for P3HT-based devices, confirmed that degradation slightly impacts trap-assisted recombination in P3HT-based devices. Hence, recombination in PBDD4T was suppressed due to BDD-copolymerization, while P3HT showed an increase in bimolecular recombination that led to the approximately 50% loss of its initial PCE. However, the reduced J_{sc} in PBDD4T device cannot be attributed to the increase in recombination, as the intensity-dependent measurements confirmed. Thus, we further looked into the mobility evolution in the devices and found that the total mobility (μ_0) of the fresh and degraded PBDD4T and P3HT to be 6.78 and 5.80, 5.60 and 4.10 ($\times 10^{-4} cm^2 V^{-1} s^{-1}$), respectively. Hence, reduced charge mobility in both devices contributed to their loss of J_{sc}.

It's worth noting that the absorption of photons in the active layer significantly contributes to the J_{sc} of the device. The absorption of PBDD4T and P3HT thin films were recorded during photodegradation, as illustrated in Figure 5.12 a-b. A decrease in absorbance due to photobleaching was observed in PBDD4T, as evidenced by its similar profile after photoaging.

Conversely, in the P3HT film, an increase in absorbance at its 0-0 and 0-1 transitions was noted, often associated with improved intermolecular interaction [198]. This could potentially lead to self-assembly of P3HT, resulting in phase segregation [199] and deterioration of the active layer morphology[200]. The AFM images of the active layers of both devices were taken before and after degradation, as depicted in Figure 5.13 to investigate the contribution of morphology evolution on the degrdation of the devices.

The initial roughness of the active layer in fresh devices were found to be 1.1 nm and 2.1 nm for PBDD4T and P3HT-based devices, respectively. After 7 hours of photoaging, these values

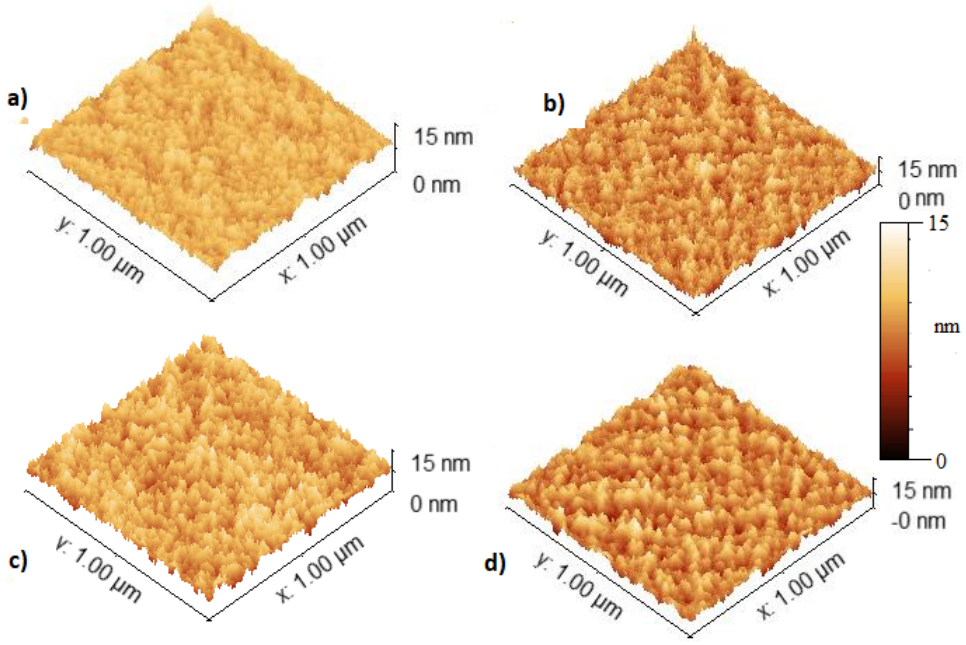


Figure 5.13: Surface topography images of BDD4T:$PC_{71}BM$ (a, c) and P3HT:$PC_{71}BM$ (b, d) where a and c for 0 h and b and d for 7h.

increased to 1.90 nm and 3.15 nm, respectively. Evidently, the rise in surface roughness observed in both devices contributed to the decrease in their J_{sc}.

Conclusion

The photo-stability of a copolymer incorporating a BDD co-polymerized thiophene unit (PBDD4T) and P3HT was investigated to understand the impact of non-electron withdrawing unit copolymerization on the stability of thiophene-based copolymers. The copolymer exhibited a deeper HOMO level due to its higher electron-donating properties, as indicated by higher ESP values in its backbone. This led to broader absorption and consequently higher J_{sc} in the PBDD4T-$PC_{71}BM$-based device compared to the P3HT-based device. After aging for 7 hours under AM 1.5 illumination, the PBDD4T and P3HT devices lost 14% and 48% of their initial PCE, respectively. The deeper HOMO level of PBDD4T reduced photo-oxidation in the polymer, maintaining its energy levels and resulting in a stable V_{OC} , whereas P3HT experienced an approximately 20 % loss in after aging. Charge dynamics studies confirmed that neither device exhibited the evolution of trap-mediated recombination after photo-degradation. The stable FF in PBDD4T was attributed to the suppression of trap-assisted and bimolecular recombination evolution. In contrast, the P3HT-based device showed an increase in bimolecular recombination, explaining its loss in FF. Additionally, both devices experienced a deterioration in charge mobility and surface roughness due to photo-aging causing a loss in J_{sc} in both devices.

Chapter 6

Summary and Outlook

6.1 Summary

This thesis investigates the thermal and photo stability of various donor and acceptor materials, specifically P3HT and PBDD4T as donors, and $PC_{60}BM$, $PC_{71}BM$, and ITIC as acceptors, in accordance with standardized testing protocols.

The role of acceptor materials in the thermal stability of P3HT-based inverted OSCs was experimentally studied using three acceptors: $PC_{60}BM$, $PC_{70}BM$, and ITIC. Evidence of thermal degradation was observed through changes in the optical and morphological properties of the polymer films. Characterization data revealed that the degradation behavior strongly depends on the specific acceptor molecules used in the polymer matrix. Among the materials studied, $PC_{60}BM$-based blends demonstrated greater thermal stability compared to ITIC-based blends. This was evident from device performance parameters such as short-circuit current density (J_{sc}) and open-circuit voltage (V_{oc}), which showed significant reductions in P3HT:ITIC-based devices. Notably, ITIC-based solar cells exhibited a 50 % drop in (V_{oc}) within just one hour of thermal degradation. The FTIR analysis indicated the formation of -OH groups due to oxidation, leading to trap states that hinder conductivity and reduce J_{sc}.

Furthermore, the photostability of a copolymer, PBDD4T, incorporating a BDD co-polymerized thiophene unit, was studied in comparison with P3HT. Optical and electrochemical characterization revealed that BDD copolymerization in PBDD4T results in a deeper HOMO level and

broader light absorption than P3HT. Consequently, PBDD4T-based devices achieved a higher power conversion efficiency (PCE) due to improved V_{oc} and J_{sc}. Photostability tests showed that PBDD4T-based devices retained 86 % of their initial PCE after 7 hours of irradiation, while P3HT-based devices suffered a 48 % reduction in PCE. Further investigation attributed the superior photostability of PBDD4T-based devices to reduced photooxidation and recombination processes, as the BDD copolymerization helps suppress these effects. In contrast, P3HT:$PC_{71}BM$-based devices exhibited bimolecular recombination caused by photoaging, leading to decreased stability. Both systems experienced a decline in photogenerated current, attributed to reduced charge mobility and increased surface roughness during degradation.

6.2 Future Outlook

The studies discussed in this thesis focused primarily on the thermal and photo stability of thiophene-based polymers and their blends under different degradation conditions. The findings underscore the need for further research into the selection and optimization of acceptor materials in OSCs. Understanding the mechanisms behind thermal degradation can guide the development of more stable and efficient organic solar cells, ultimately contributing to advancements in renewable energy technologies. We also recommend the importance of new design materials for organic solar cells. By utilizing non-electron- withdrawing unit copolymerization strategies, researchers can develop polymers that not only enhance efficiency but also significantly improve the longevity and reliability of organic solar cells in practical applications. This approach aligns with the golden triangle principle in organic photovoltaics, which emphasizes the critical balance among efficiency, stability, and processability. Achieving this balance is essential for translating lab-scale performance into commercially viable and scalable solar technologies.

Bibliography

[1] Jung S. Seo J. Jeong G. Choi Y. Lee J. ... Park H. Koo, D. Flexible organic solar cells over 15% efficiency with polyimide-integrated graphene electrodes. *Joule*, 4(5):1021–1034, 2020.

[2] Xu M. Li Z. Gao Y. Yang L. Zhang D. Shao M. Wang, Z. Intrinsically stretchable organic solar cells beyond 10% power conversion efficiency enabled by transfer printing method. *Advanced Functional Materials*, 31(35):2103534, 2021.

[3] Yao H. Hu B. Zhang G. Arunagiri L. Ma L. K. ... Yan H. Chen, S. A nonfullerene semitransparent tandem organic solar cell with 10.5% power conversion efficiency. *Advanced Energy Materials*, 8(31):1800529, 2018.

[4] Wang F. Yang G. Ding X. Lv J. Sun Y. ... Hu H Sun, X. From 20% single-junction organic photovoltaics to 26% perovskite/organic tandem solar cells: self-assembled hole transport molecules matter. *Energy & Environmental Science*, 2025.

[5] You J. Yang Y. Meng, L. Addressing the stability issue of perovskite solar cells for commercial applications. *Nature communications*, 9(1):1–4, 2018.

[6] Popkirov G. Gergova R. Grancharov G. Gancheva V. Sendova-Vassileva, M. Study of impedance spectra parameters of pcdtbt: Pc70bm solar cells as a function of the deposition solution concentration. In *Journal of Physics: Conference Series*, volume 992, page 012045. IOP Publishing, 2018.

[7] Lingxian Meng, Yamin Zhang, Xiangjian Wan, Chenxi Li, Xin Zhang, Yanbo Wang, Xin Ke, Zuo Xiao, Liming Ding, Ruoxi Xia, et al. Organic and solution-processed tandem solar cells with 17.3% efficiency. *Science*, 361(6407):1094–1098, 2018.

[8] Lijian Zuo, Shuhua Zhang, Hanying Li, and Hongzheng Chen. Toward highly efficient large-area ito-free organic solar cells with a conductance-gradient transparent electrode. *Advanced Materials (Deerfield Beach, Fla.)*, 27(43):6983–6989, 2015.

[9] İlhan Volkan Öner, Efe Çetin Yilmaz, Muhammet Kaan Yesilyurt, Gökhan Ömeroglu, and Ahmet Numan Özakin. Operational stability and degradation of organic solar cells. *Periodicals of Engineering and Natural Sciences (PEN)*, 5(2), 2017.

[10] Yong Cui, Huifeng Yao, Jianqi Zhang, Tao Zhang, Yuming Wang, Ling Hong, Kaihu Xian, Bowei Xu, Shaoqing Zhang, Jing Peng, et al. Over 16% efficiency organic photovoltaic cells enabled by a chlorinated acceptor with increased open-circuit voltages. *Nature communications*, 10(1):2515, 2019.

[11] Qishi Liu, Yufan Jiang, Ke Jin, Jianqiang Qin, Jingui Xu, Wenting Li, Ji Xiong, Jinfeng Liu, Zuo Xiao, Kuan Sun, et al. 18% efficiency organic solar cells. *Science Bulletin*, 65(4):272–275, 2020.

[12] Julia Schafferhans, Andreas Baumann, Alexander Wagenpfahl, Carsten Deibel, and Vladimir Dyakonov. Oxygen doping of p3ht: Pcbm blends: Influence on trap states, charge carrier mobility and solar cell performance. *Organic Electronics*, 11(10):1693–1700, 2010.

[13] Andrea Seemann, Tobias Sauermann, Christoph Lungenschmied, Oskar Armbruster, Siegfried Bauer, H-J Egelhaaf, and Jens Hauch. Reversible and irreversible degradation of organic solar cell performance by oxygen. *Solar Energy*, 85(6):1238–1249, 2011.

[14] Newayemedhin A Tegegne, Hailemariam Wendimu, Zelalem Abdissa, Wendimagegn Mammo, Mats R Andersson, Fekadu Gashaw Hone, Dinsefa M Andoshee, Olufemi Olaoye, and Gurthwin Bosman. Light-induced degradation of a push–pull copolymer for ito-free

organic solar cell application. *Journal of Materials Science: Materials in Electronics*, 31:21303–21315, 2020.

[15] Craig H Peters, IT Sachs-Quintana, William R Mateker, Thomas Heumueller, Jonathan Rivnay, Rodigo Noriega, Zach M Beiley, Eric T Hoke, Alberto Salleo, and Michael D McGehee. The mechanism of burn-in loss in a high efficiency polymer solar cell. *Advanced Materials*, 24(5):663–668, 2012.

[16] Tracey M Clarke, Christoph Lungenschmied, Jeff Peet, Nicolas Drolet, Kenji Sunahara, Akihiro Furube, and Attila J Mozer. Photodegradation in encapsulated silole-based polymer: Pcbm solar cells investigated using transient absorption spectroscopy and charge extraction measurements. *Advanced Energy Materials*, 3(11):1473–1483, 2013.

[17] Camilla Lindqvist, Anke Sanz-Velasco, Ergang Wang, Olof Bäcke, Stefan Gustafsson, Eva Olsson, Mats R Andersson, and Christian Müller. Nucleation-limited fullerene crystallisation in a polymer–fullerene bulk-heterojunction blend. *Journal of Materials Chemistry A*, 1(24):7174–7180, 2013.

[18] IT Sachs-Quintana, Thomas Heumüller, William R Mateker, Darian E Orozco, Rongrong Cheacharoen, Sean Sweetnam, Christoph J Brabec, and Michael D McGehee. Electron barrier formation at the organic-back contact interface is the first step in thermal degradation of polymer solar cells. *Advanced Functional Materials*, 24(25):3978–3985, 2014.

[19] Anirudh Sharma, Gunther Andersson, and David A Lewis. Role of humidity on indium and tin migration in organic photovoltaic devices. *Physical Chemistry Chemical Physics*, 13(10):4381–4387, 2011.

[20] Matthieu Manceau, Eva Bundgaard, Jon E Carlé, Ole Hagemann, Martin Helgesen, Roar Søndergaard, Mikkel Jørgensen, and Frederik C Krebs. Photochemical stability of π-conjugated polymers for polymer solar cells: a rule of thumb. *Journal of Materials Chemistry*, 21(12):4132–4141, 2011.

[21] Jon E Carlé, Martin Helgesen, Morten V Madsen, Eva Bundgaard, and Frederik C Krebs. Upscaling from single cells to modules–fabrication of vacuum-and ito-free polymer solar

cells on flexible substrates with long lifetime. *Journal of Materials Chemistry C*, 2(7):1290–1297, 2014.

[22] Thomas Heumueller, William R Mateker, IT Sachs-Quintana, Koen Vandewal, Jonathan A Bartelt, Timothy M Burke, Tayebeh Ameri, Christoph J Brabec, and Michael D McGehee. Reducing burn-in voltage loss in polymer solar cells by increasing the polymer crystallinity. *Energy & Environmental Science*, 7(9):2974–2980, 2014.

[23] Jaemin Kong, Suhee Song, Minji Yoo, Ga Young Lee, Obum Kwon, Jin Kuen Park, Hyungcheol Back, Geunjin Kim, Seoung Ho Lee, Hongsuk Suh, et al. Long-term stable polymer solar cells with significantly reduced burn-in loss. *Nature communications*, 5(1):5688, 2014.

[24] P Papadopoulos, G Floudas, C Chi, and Gerhard Wegner. Molecular dynamics of oligofluorenes: A dielectric spectroscopy investigation. *The Journal of chemical physics*, 120(5):2368–2374, 2004.

[25] Jiri George Drobny. *Polymers for electricity and electronics: materials, properties, and applications*. John Wiley & Sons, 2012.

[26] SK Manirul Haque, Jorge Alfredo Ardila-Rey, Yunusa Umar, Abdullahi Abubakar Mas' ud, Firdaus Muhammad-Sukki, Binta Hadi Jume, Habibur Rahman, and Nurul Aini Bani. Application and suitability of polymeric materials as insulators in electrical equipment. *Energies*, 14(10):2758, 2021.

[27] Hideki Shirakawa, Edwin J Louis, Alan G MacDiarmid, Chwan K Chiang, and Alan J Heeger. Synthesis of electrically conducting organic polymers: halogen derivatives of polyacetylene,(ch) x. *Journal of the Chemical Society, Chemical Communications*, (16):578–580, 1977.

[28] Shengqiang Xiao, Huaxing Zhou, and Wei You. Conjugated polymers of fused bithiophenes with enhanced π-electron delocalization for photovoltaic applications. *Macromolecules*, 41(15):5688–5696, 2008.

[29] Mansoor Ani Najeeb, Zubair Ahmad, and Rana A Shakoor. Organic thin-film capacitive and resistive humidity sensors: a focus review. *Advanced Materials Interfaces*, 5(21):1800969, 2018.

[30] Fred W Billmeyer. *Textbook of polymer science*. John Wiley & Sons, 1984.

[31] Wolfgang Brütting. Physics of organic semiconductors. *physica status solidi (a)*, 201(6):1031–1031, 2004.

[32] Dargie Hailu Deribew. *Structure, morphology and performance relationships of organic photovoltaic devices: the block copolymer approach*. PhD thesis, Bordeaux 1, 2013.

[33] Aurélien Tournebize. *Electronic structure and stability of materials for organic photovoltaic*. PhD thesis, Université Blaise Pascal-Clermont-Ferrand II; Eberhard-Karls-Universität ..., 2015.

[34] Krebs F. C. Spanggaard, H. A brief history of the development of organic and polymeric photovoltaics. *Solar Energy Materials and Solar Cells*, 83(2-3):125–146, 2004.

[35] A Pochettino. The development of organic conductors, including semiconductors, metals and superconductors cont. *Academy Lincei Rendus*, 15:355, 1906.

[36] Akhtar M. Gau S. C. Weinberger, B. R. Polyacetylene photovoltaic devices. *Synthetic Metals*, 4(3):187–197, 1982.

[37] Tourillon G. Garnier F. Glenis, S. Influence of the doping on the photovoltaic properties of thin films of poly-3-methylthiophene. *Thin Solid Films*, 139(3):221–231, 1986.

[38] C. W. Tang. Two-layer organic photovoltaic cell. *Applied physics letters*, 48(2):183–185, 1986.

[39] Xin Song, Le Mei, Xinjie Zhou, Hongxiang Li, Hao Xu, Xingting Liu, Shenzheng Gao, Shanlei Xu, Yahui Yang, Weiguo Zhu, et al. Frenkel and charge-transfer excitonic couplings strengthened by thiophene-type solvent enables binary organic solar cells with 19.8% efficiency. *Angewandte Chemie International Edition*, 63(44):e202411512, 2024.

[40] Topinka M. A. McGehee, M. D. Pictures from the blended zone. *Nature materials*, 5(9):675–676, 2006.

[41] Venkataraman D Benanti, T. L. Organic solar cells: An overview focusing on active layer morphology. *Photosynthesis research*, 87:73–81, 2006.

[42] Meng W. Peng Y. Wang R. Li R. Xie H. ... Ye Z Ma, C. Numerical study on short-circuit current of single layer organic solar cells with schottkey contacts. *Science China Technological Sciences*, 53:1023–1027, 2010.

[43] J. Nelson. Organic photovoltaic films. *Current Opinion in Solid State and Materials Science*, 6(1):87–95, 2002.

[44] Sariciftci N. S. Scharber, M. C. Efficiency of bulk-heterojunction organic solar cells. *Progress in polymer science*, 38(12):1929–1940, 2013.

[45] T. Kietzke. Recent advances in organic solar cells. *Advances in OptoElectronics*, 2007(1):040285, 2007.

[46] Schwenn P. E. Smith A. R. Cavaye H. Shaw P. E. Krueger K. B. ... Gentle I. R. Lee, K. H. Morphology of all-solution-processed "bilayer" organic solar cells. *Advanced Materials*, 6(23):766–770, 2011.

[47] Qiao Q. Xu, T. Organic photovoltaics: basic concepts and device physics. *Encyclopedia of Nanotechnology; Bhushan, B., Ed.; Springer: Dordrecht, The Netherlands*, pages 2022–2031, 2012.

[48] Sariciftci N. S Hoppe, H. Morphology of polymer/fullerene bulk heterojunction solar cells. *Journal of Materials Chemistry*, 16(1):45–61, 2006.

[49] Leiping Duan, Bram Hoex, and Ashraf Uddin. Progress in semitransparent organic solar cells. *Solar RRL*, 5(5):2100041, 2021.

[50] Belcher W. J. Fell C. J. Dastoor P. C. Feron, K. Organic solar cells: understanding the role of förster resonance energy transfer. *International journal of molecular sciences*, 13(12):17019–17047, 2012.

[51] Azimi H. Scharber M. Morana M. Blom P. W. Loi M. A. Mikhnenko, O. V. Exciton diffusion length in narrow bandgap polymers. *Energy & Environmental Science*, 5(5):6960–6965, 2012.

[52] Richard R Lunt, Noel C Giebink, Anna A Belak, Jay B Benziger, and Stephen R Forrest. Exciton diffusion lengths of organic semiconductor thin films measured by spectrally resolved photoluminescence quenching. *Journal of Applied Physics*, 105(5), 2009.

[53] McGehee M. D. Scully, S. R. Effects of optical interference and energy transfer on exciton diffusion length measurements in organic semiconductors. *Journal of applied physics*, 100(3), 2006.

[54] Yexiao Huang, Abdul Azeez, Jingjing Zhao, Zhenmin Zhao, Muneendra Dasannagari, Frédéric Laquai, Zhipeng Kan, and Safakath Karuthedath. Enhanced device performance through optimization of acceptor layer thickness relative to exciton diffusion length and ionization energy offset in bilayer organic solar cells. *Journal of Materials Chemistry C*, 2025.

[55] Muhammad T Sajjad, Arvydas Ruseckas, Lethy Krishnan Jagadamma, Yiwei Zhang, and Ifor DW Samuel. Long-range exciton diffusion in non-fullerene acceptors and coarse bulk heterojunctions enable highly efficient organic photovoltaics. *Journal of Materials Chemistry A*, 8(31):15687–15694, 2020.

[56] Jung Y. K. Lee D. Y. Jang J. W. Cho S. Son S. ... Park S. H. Lee, J. Enhanced efficiency of bilayer polymer solar cells by the solvent treatment method. *Synthetic Metals*, 199:408–412, 2015.

[57] Nurlan Tokmoldin, Seyed Mehrdad Hosseini, Meysam Raoufi, Le Quang Phuong, Oskar J Sandberg, Huilan Guan, Yingping Zou, Dieter Neher, and Safa Shoaee. Extraordinarily long diffusion length in pm6: Y6 organic solar cells. *Journal of materials chemistry A*, 8(16):7854–7860, 2020.

[58] Zhu L. Zhou G. Hao T. Qiu C. Zhao Z. ... Liu F. Zhang, M. Single-layered organic photovoltaics with double cascading charge transport pathways: 18% efficiencies. *Nature Communications*, 12(1):309, 2021.

[59] Yambem S. D. Haldar A. Alley N. J. Curran S. A. Liao, K. S. Designs and architectures for the next generation of organic solar cells. *Energies*, 3(6):1212–1250, 2010.

[60] Katz E. A. Tromholt T. Hirsch B. Krebs F. C. Manor, A. Origin of size effect on efficiency of organic photovoltaics. *Journal of Applied Physics*, 109(7), 2011.

[61] Neher D. Blakesley, J. C. Relationship between energetic disorder and open-circuit voltage in bulk heterojunction organic solar cells. *Physical Review B—Condensed Matter and Materials Physics*, 84(7):075210, 2011.

[62] Leong W. L. Banerji N. Dennler G. Heeger A. J. Cowan, S. R. Identifying a threshold impurity level for organic solar cells: Enhanced first-order recombination via well-defined pc84bm traps in organic bulk heterojunction solar cells. *Advanced Functional Materials*, 21(16):3083–3092, 2011.

[63] Hu X. Zhong C. Huang M. Wang K. Zhang Z. ... Heeger A. J. Liu, C. The influence of binary processing additives on the performance of polymer solar cells. *Nanoscale*, 6(23):14297–14304, 2014.

[64] Dingding Qiu, Muhammad Abdullah Adil, Kun Lu, and Zhixiang Wei. The crystallinity control of polymer donor materials for high-performance organic solar cells. *Frontiers in Chemistry*, 8:603134, 2020.

[65] Agostinelli T. Pires E. Hampton M. Nelson J. Macdonald J. E. Lilliu, S. Dynamics of crystallization and disorder during annealing of p3ht/pcbm bulk heterojunctions. *Macromolecules*, 44(8):2725–2734, 2011.

[66] James D. T. Kim J. S. Nicholson P. G. Murphy C. E. Bradley D. D. ... Kim J. S. Tsoi, W. C. The nature of in-plane skeleton raman modes of p3ht and their correlation to

the degree of molecular order in p3ht: Pcbm blend thin films. *Journal of the American Chemical Society*, 133(25):9834–9843, 2011.

[67] Lilliu S. Labram J. G. Campoy-Quiles M. Hampton M. Pires E. ... Macdonald J. E. Agostinelli, T. Real-time investigation of crystallization and phase-segregation dynamics in p3ht: Pcbm solar cells during thermal annealing. *Advanced Functional Materials*, 21(9):1701–1708, 2011.

[68] Kroon J. M. Andriessen R. Blom P. W. Grossiord, N. Degradation mechanisms in organic photovoltaic devices. *Organic Electronics*, 13(3):432–456, 2012.

[69] Jamieson F. C. Maurano A. Nelson J. Durrant J. R. Dibb, G. F. Limits on the fill factor in organic photovoltaics: distinguishing nongeminate and geminate recombination mechanisms. *The journal of physical chemistry letters*, 4(5):803–808, 2013.

[70] Myers D. Emery K. Gueymard, C. A. Proposed reference irradiance spectra for solar energy systems testing. *Solar energy*, 73(6):443–467, 2002.

[71] F. Schauer. Space-charge-limited currents for organic solar cells optimisation. *Solar energy materials and solar cells*, 87(1-4):235–250, 2005.

[72] Ahmed M. M. Karimov K. S. Rehman F. Lee J. H. Moiz, S. A. Space charge limited current–voltage characteristics of organic semiconductor diode fabricated at various gravity conditions. *Synthetic Metals*, 159(13):1336–1339, 2009.

[73] Iraqi A. Aziz S. B. N. Abdullah S. Brza M. A. R. Murad, A. Conducting polymers for optoelectronic devices and organic solar cells: A review. *Polymers*, 12(11):2627, 2020.

[74] Riede M. Gombert A. Leo K. Niggemann, M. Light trapping in organic solar cells. *physica status solidi (a)*, 205(12):2862–2874, 2008.

[75] Noel C Giebink and Stephen R Forrest. Excitonic shockley-read-hall recombination in organic semiconductors. *Physical Review Applied*, 21(6):064019, 2024.

[76] He C. Li Y. Chen T. Xia X. Fu W. ... Chen H Chen, S. Improving the device performance of organic solar cells with immiscible solid additives. *Journal of Materials Chemistry C*, 10(7):2749–2756, 2022.

[77] Wu Z. Hu J. Song Q. Wu B. Lam Tam H. ... Zhu F. Liu, H. Efficient and ultraviolet durable inverted organic solar cells based on an aluminum-doped zinc oxide transparent cathode. *Applied Physics Letters*, 103(4), 2013.

[78] Choi M. Yoon T. S. Lee H. H. Kim Y. S. Baek, W. H. Use of fluorine-doped tin oxide instead of indium tin oxide in highly efficient air-fabricated inverted polymer solar cells. *Applied Physics Letters*, 96(13), 2010.

[79] Kwon S. N. Na S. I. Yoo Y. Z. Seong T. Y. Kim, J. H. Inverted organic solar cells fabricated with room-temperature-deposited transparent multilayer electrodes. *Bulletin of the Korean Chemical Society*, 38(8):856–860, 2017.

[80] Liu B. Ma C. Q. Huang F. Feng G. Chen H. ... Bo Z. Liu, Y. Recent progress in organic solar cells (part ii device engineering). *Science China Chemistry*, 65(8):1457–1497, 2022.

[81] Zhan X. Cheng, P. Stability of organic solar cells: challenges and strategies. *Chemical Society Reviews*, 45(9):2544–2582, 2016.

[82] Kim J. K. Seo J. H. Park O. O. Park J. H. Wang, D. H. Stability comparison: A pcdtbt/pc71bm bulk-heterojunction versus a p3ht/pc71bm bulk-heterojunction. *Solar Energy Materials and Solar Cells*, 101:249–255, 2012.

[83] Strzalka J. Darling S. B. Nikiforov, M. P. Delineation of the effects of water and oxygen on the degradation of organic photovoltaic devices. *Solar energy materials and solar cells*, 110:36–42, 2013.

[84] Faber T. Von Hauff E. Brown T. M. Lira-Cantu M. Hoppe H. Roesch, R. Procedures and practices for evaluating thin-film solar cell stability. *Advanced Energy Materials*, 5(20):1501407, 2015.

[85] Jung J. W. Jo J. W. Jo W. H. Lee, J. U. Degradation and stability of polymer-based solar cells. *Journal of Materials Chemistry*, 22(46):24265–24283, 2012.

[86] Qin J. Qin Y. Zhao T. Cao Y. Cai Q. ... Zhang Y. Hu, X. Effects of photo-oxidation and transition metals on the formation of reactive oxygen species from aromatic compounds using spectroscopic method. *Journal of Environmental Sciences*, 151:1–11, 2025.

[87] D. Feldman. Polymer weathering: photo-oxidation. *Journal of Polymers and the Environment*, 10:163–173, 2002.

[88] Yue Wang, Yan Lin, Shanying He, Shaohua Wu, and Chunping Yang. Singlet oxygen: Properties, generation, detection, and environmental applications. *Journal of hazardous materials*, 461:132538, 2024.

[89] Mikhail V Motyakin, John L Gerlock, and Shulamith Schlick. Electron spin resonance imaging (esri) of degradation and stabilization processes in polymers: Poly (acrylonitrile-butadiene-styrene)(abs) polymers. *Ageing Studies and Lifetime Extension of Materials*, pages 353–357, 2001.

[90] Caubergh S. Larsson P. O. Tian Y. Scheblykin I. G. Louis, B. Light and oxygen induce chain scission of conjugated polymers in solution. *Physical Chemistry Chemical Physics*, 20(3):1829–1837, 2018.

[91] Barnes P. W. Bornman J. F. Gouin T. Madronich S. White C. C. ... Jansen M. A. Andrady, A. L. Oxidation and fragmentation of plastics in a changing environment; from uv-radiation to biological degradation. *Science of The Total Environment*, 851:158022, 2022.

[92] Zhuang Yao, Hyeon Jeong Seong, and Yu-Sin Jang. Environmental toxicity and decomposition of polyethylene. *Ecotoxicology and Environmental Safety*, 242:113933, 2022.

[93] Agnès Rivaton, Sylvain Chambon, Matthieu Manceau, Jean-Luc Gardette, Noëlla Lemaître, and Stéphane Guillerez. Light-induced degradation of the active layer of polymer-based solar cells. *Polymer Degradation and Stability*, 95(3):278–284, 2010.

[94] Guillaume Tillet, Bernard Boutevin, and Bruno Ameduri. Chemical reactions of polymer crosslinking and post-crosslinking at room and medium temperature. *Progress in polymer science*, 36(2):191–217, 2011.

[95] Evan Trinh and Kevin Trinh. Investigating the presence of different catalysts [mno2, pbo2, fe2o3] and its effect on the rate of decomposition of hydrogen peroxide (h2o2) at various temperatures (30° c, 60° c, 90° c), analyzed through the change in oxygen volume in controlled laboratory conditions. 2024.

[96] Long Chen, Yu Huang, Yonggang Xue, Zhihui Jia, and Wenliang Wang. Oh-initiated atmospheric degradation of hydroxyalkyl hydroperoxides: mechanism, kinetics, and structure–activity relationship. *Atmospheric Chemistry and Physics*, 22(5):3693–3711, 2022.

[97] S Aslanzadeh and M Haghighat Kish. Photo-oxidation of polypropylene fibers exposed to short wavelength uv radiations. *Fibers and Polymers*, 11:710–718, 2010.

[98] Xiyu Zhang, Zhenxing Yin, Songbai Xiang, Huayu Yan, and Hailing Tian. Degradation of polymer materials in the environment and its impact on the health of experimental animals: a review. *Polymers*, 16(19):2807, 2024.

[99] Aekjira Kuyyakanont and Minoru Iwata. Study of different degradation effects in uv-sensitive polymers using xenon lamp and deuterium lamp to simulate uv irradiation in space environment. *Nuclear Instruments and Methods in Physics Research Section B: Beam Interactions with Materials and Atoms*, 549:165267, 2024.

[100] Yingjun An, Tomoko Kajiwara, Adchara Padermshoke, Thinh Van Nguyen, Sinan Feng, Hiroyasu Masunaga, Yutaka Kobayashi, Hiroshi Ito, Sono Sasaki, Atsuhiko Isobe, et al. Photooxidative degradation and fragmentation behaviors of oriented isotactic polypropylene. *Polymer Journal*, 56(4):379–389, 2024.

[101] Riccardo Rizzo, Nika Petelinšek, Angela Bonato, and Marcy Zenobi-Wong. From free-radical to radical-free: A paradigm shift in light-mediated biofabrication. *Advanced Science*, 10(8):2205302, 2023.

[102] Adam R Tetreault, Itzel Lopez-Carreon, Marzieh Riahinezhad, Elnaz Esmizadeh, Peter Collins, Kamran Alasvand Zarasvand, Naren Vivekanandan, Ajinkya Mandlik, Michelle Fernandes, Kevin Golovin, et al. Assessing individual material degradation toward organic solar cells using accelerated nanolayer lifetime protocols: Implications for solar cell longevity. *ACS Applied Nano Materials*, 7(4):4182–4198, 2024.

[103] Roger L Clough, Norman C Billingham, and Kenneth T Gillen. *Polymer durability: degradation, stabilization, and lifetime prediction*. ACS Publications, 1996.

[104] Shin Maekawa. *Oxygen-free museum cases*. Getty Publications, 1999.

[105] Huanqi Cao, Weidong He, Yiwu Mao, Xiao Lin, Ken Ishikawa, James H Dickerson, and Wayne P Hess. Recent progress in degradation and stabilization of organic solar cells. *Journal of Power Sources*, 264:168–183, 2014.

[106] Y. Qin, N. Balar, Z. Peng, A. Gadisa, I. Angunawela, A. Bagui, S. Kashani, J. Hou, and H. Ade. The performance-stability conundrum of btp-based organic solar cells. *Joule*, 5(8):2129–2147, 2021.

[107] W. R Mateker and M. D McGehee. Progress in understanding degradation mechanisms and improving stability in organic photovoltaics. *Advanced materials*, 29(10):1603940, 2017.

[108] Bo Li, Yan-Ping Cao, Xi-Qiao Feng, and Huajian Gao. Mechanics of morphological instabilities and surface wrinkling in soft materials: a review. *Soft Matter*, 8(21):5728–5745, 2012.

[109] H Hintz, C Sessler, H Peisert, H-J Egelhaaf, and T Chassé. Wavelength-dependent pathways of poly-3-hexylthiophene photo-oxidation. *Chemistry of Materials*, 24(14):2739–2743, 2012.

[110] M. Manceau, J. Gaume, A. Rivaton, J. Gardette, G. Monier, and L. Bideux. Further insights into the photodegradation of poly (3-hexylthiophene) by means of x-ray photoelectron spectroscopy. *Thin Solid Films*, 518(23):7113–7118, 2010.

[111] M. Manceau, Agnès Rivaton, Jean-Luc Gardette, S. phane Guillerez, and journal=Polymer Degradation and Stability volume=94 number=6 pages=898–907 year=2009 publisher=Elsevier Lemaître, No. The mechanism of photo-and thermooxidation of poly (3-hexylthiophene)(p3ht) reconsidered.

[112] J. B Patel, P. Tiwana, N. Seidler, G. E Morse, O. R Lozman, M. B Johnston, and L. M Herz. Effect of ultraviolet radiation on organic photovoltaic materials and devices. *ACS applied materials & interfaces*, 11(24):21543–21551, 2019.

[113] S. Karuthedath. *Tracing degradation effects in organic solar cells*. PhD thesis, Universidad Autónoma de Madrid, 2015.

[114] Younts R. Lee W. Lee S. Gundogdu K. Kim B. J Kim, T. Impact of the photo-induced degradation of electron acceptors on the photophysics, charge transport and device performance of all-polymer and fullerene–polymer solar cells. *Journal of Materials Chemistry A*, 5(42):22170–22179, 2017.

[115] Andreas Distler, Tobias Sauermann, Hans-Joachim Egelhaaf, Sheila Rodman, Dave Waller, Kap-Soo Cheon, Mike Lee, and Dirk M Guldi. The effect of pcbm dimerization on the performance of bulk heterojunction solar cells. *Advanced Energy Materials*, 4(1):1300693, 2014.

[116] Y. Wang, N. Qian D. Zhang F. Ederth T. Moons E. Wang J. Inganäs O. Huang Wei Jafari, M. J. Wang, et al. Light-induced degradation of fullerenes in organic solar cells: a case study on tq1: Pc 71 bm. *Journal of Materials Chemistry A*, 6(25):11884–11889, 2018.

[117] Jung Yong Kim. Phase behavior of conjugated polymer solutions and blends: The flory–huggins lattice model. *The Journal of Physical Chemistry C*, 2025.

[118] Jung Yong Kim and C Daniel Frisbie. Correlation of phase behavior and charge transport in conjugated polymer/fullerene blends. *The Journal of Physical Chemistry C*, 112(45):17726–17736, 2008.

[119] Jianhua Han, Han Xu, Sri Harish Kumar Paleti, Anirudh Sharma, and Derya Baran. Understanding photochemical degradation mechanisms in photoactive layer materials for organic solar cells. *Chemical Society Reviews*, 2024.

[120] Qing Guo, Qiang Guo, Yanfang Geng, Ailing Tang, Maojie Zhang, Mengzhen Du, Xiangnan Sun, and Erjun Zhou. Recent advances in pm6: Y6-based organic solar cells. *Materials Chemistry Frontiers*, 5(8):3257–3280, 2021.

[121] Jarmila Müllerová, Michal Kaiser, Vojtech Nádaždy, Peter Šiffalovič, and Eva Majková. Optical absorption study of p3ht: Pcbm blend photo-oxidation for bulk heterojunction solar cells. *Solar Energy*, 134:294–301, 2016.

[122] EM Speller. The significance of fullerene electron acceptors in organic solar cell photo-oxidation. *Materials Science and Technology*, 33(8):924–933, 2017.

[123] Him Cheng Wong, Zhe Li, Ching Hong Tan, Hongliang Zhong, Zhenggang Huang, Hugo Bronstein, Iain McCulloch, Joao T Cabral, and James R Durrant. Morphological stability and performance of polymer–fullerene solar cells under thermal stress: The impact of photoinduced pc60bm oligomerization. *ACS nano*, 8(2):1297–1308, 2014.

[124] Jingming Xin, Chao Zhao, Ziqi Geng, Wenyue Xue, Zhenyu Chen, Chunpeng Song, Han Yan, Qiuju Liang, Zongcheng Miao, Wei Ma, et al. Elucidate the thermal degradation mechanism of y6-based organic solar cells by establishing structure-property correlation. *Advanced Energy Materials*, 14(30):2401433, 2024.

[125] Leiping Duan and Ashraf Uddin. Progress in stability of organic solar cells. *Advanced Science*, 7(11):1903259, 2020.

[126] Jiangfeng Wang, Zhixin Liu, Jianpeng Xu, Ying Zhang, Wenbo Peng, Peide Zhu, Yintai Xu, Jie Zeng, Deng Wang, Yong Zhang, et al. Achieving stable organic solar cells with 19.2% efficiency via fine interpenetrating network with fused-ring aromatic lactone donor. *Nano Energy*, 131:110246, 2024.

[127] Zijian Zhang, Junhui Miao, Zicheng Ding, Bin Kan, Baojun Lin, Xiangjian Wan, Wei Ma, Yongsheng Chen, Xiaojing Long, Chuandong Dou, et al. Efficient and thermally stable organic solar cells based on small molecule donor and polymer acceptor. *Nature communications*, 10(1):3271, 2019.

[128] Yilin Chang, Xiangwei Zhu, Yanan Shi, Yanan Liu, Ke Meng, Yanxun Li, Jingwei Xue, Lingyun Zhu, Jianqi Zhang, Huiqiong Zhou, et al. Regulating phase separation and molecular stacking by introducing siloxane to small-molecule donors enables high efficiency all-small-molecule organic solar cells. *Energy & Environmental Science*, 15(7):2937–2947, 2022.

[129] Haoyu Zhao, Nathaniel Prine, Soumya Kundu, Guorong Ma, and Xiaodan Gu. Effect of thermal stress on morphology in high-performance organic photovoltaic blends. *JACS Au*, 2024.

[130] Christopher Wöpke, Clemens Göhler, Maria Saladina, Xiaoyan Du, Li Nian, Christopher Greve, Chenhui Zhu, Kaila M Yallum, Yvonne J Hofstetter, David Becker-Koch, et al. Traps and transport resistance are the next frontiers for stable non-fullerene acceptor solar cells. *Nature communications*, 13(1):3786, 2022.

[131] Pierayeh Vahdani, Xianzhen Li, Chi Zhang, Steven Holdcroft, and Barbara J Frisken. Morphological characterization of a new low-bandgap thermocleavable polymer showing stable photovoltaic properties. *Journal of Materials Chemistry A*, 4(27):10650–10658, 2016.

[132] Xiaoli Zhou, Wenting Liang, Ruijie Ma, Cuifen Zhang, Zhengxing Peng, Top Archie Dela Peña, Jiaying Wu, Zaifei Ma, Yaozu Liao, Gang Li, et al. Synergistic control of multilength-scale morphology and vertical phase separation for high-efficiency organic solar cells. *Energy & Environmental Science*, 17(20):7762–7771, 2024.

[133] Keqiang He, Pankaj Kumar, Yi Yuan, and Yuning Li. Wide bandgap polymer donors for high efficiency non-fullerene acceptor based organic solar cells. *Materials Advances*, 2(1):115–145, 2021.

[134] Mohamed Shaban, Mohamed Benghanem, Abdullah Almohammedi, and Mohamed Rabia. Optimization of the active layer p3ht: Pcbm for organic solar cell. *Coatings*, 11(7):863, 2021.

[135] Mujib Ur Rahman, Yonghao Xi, Muhammad Khalid, Sameen Aslam, Mumtaz A Qaisrani, and Muhammad Punhal Sahto. Recent advances in stabilizing the organic solar cells. *MRS Energy & Sustainability*, pages 1–32, 2024.

[136] Zhipeng Yin, Huan Zhao, Lijun Chen, Yunjie Li, Xingyu Liu, Jianfei Fu, Hai-Qiao Wang, and Ning Li. Understanding the metal-electrode-correlated degradation of organic solar cells under illumination/thermal stress. *Chemical Engineering Journal*, 489:151255, 2024.

[137] Suchol Savagatrup, Adam D Printz, Timothy F O'Connor, Aliaksandr V Zaretski, Daniel Rodriquez, Eric J Sawyer, Kirtana M Rajan, Raziel I Acosta, Samuel E Root, and Darren J Lipomi. Mechanical degradation and stability of organic solar cells: molecular and microstructural determinants. *Energy & Environmental Science*, 8(1):55–80, 2015.

[138] Hansung Kim, Md Towfiq Tofail, and Ciby John. The effect of interface cracks on the electrical performance of solar cells. *JOM*, 70(4):473–478, 2018.

[139] Hyung Jin Son, Hong-Kwan Park, Ji Yeon Moon, Byeong-Kwon Ju, and Sung Hyun Kim. Thermal degradation related to the pedot: Pss hole transport layer and back electrode of the flexible inverted organic photovoltaic module. *Sustainable Energy & Fuels*, 4(4):1974–1983, 2020.

[140] Amaresh Mishra. Interfacial materials for organic solar cells. In *Solar Energy: Systems, Challenges, and Opportunities*, pages 373–423. Springer, 2019.

[141] Bright Walker, Hyosung Choi, and Jin Young Kim. Interfacial engineering for highly efficient organic solar cells. *Current Applied Physics*, 17(3):370–391, 2017.

[142] Jung Yong Kim. Phase diagrams of binary low bandgap conjugated polymer solutions and blends. *Macromolecules*, 52(11):4317–4328, 2019.

[143] Jong Hyun Kim, Gun Ho Lee, Jong Bin Kim, and Shin-Hyun Kim. Macroporous hydrogels for fast and reversible switching between transparent and structurally colored states. *Advanced Functional Materials*, 30(22):2001318, 2020.

[144] Roja Singh, Sudeshna Ghosh, Anand S Subbiah, Neha Mahuli, and Shaibal K Sarkar. Ald al2o3 on hybrid perovskite solar cells: Unveiling the growth mechanism and long-term stability. *Solar Energy Materials and Solar Cells*, 205:110289, 2020.

[145] Sashivinay Kumar Gaddam, Ramyakrishna Pothu, and Rajender Boddula. Advanced polymer encapsulates for photovoltaic devices- a review. *Journal of Materiomics*, 7(5):920–928, 2021.

[146] Vida Turkovic, Sebastian Engmann, Nikos Tsierkezos, Harald Hoppe, Morten Madsen, Horst-Günter Rubahn, Uwe Ritter, and Gerhard Gobsch. Long-term stabilization of organic solar cells using uv absorbers. *Journal of Physics D: Applied Physics*, 49(12):125604, 2016.

[147] Yongjie Cui, Zeng Chen, Peipei Zhu, Wei Ma, Haiming Zhu, Xunfan Liao, and Yiwang Chen. Enhancing photostability and power conversion efficiency of organic solar cells by a "sunscreen" ternary strategy. *Science China Chemistry*, 66(4):1179–1189, 2023.

[148] Long Fang, Yihu Song, Xiaonan Zhu, and Qiang Zheng. Influence of lanthanum stearate as a co-stabilizer on stabilization efficiency of calcium/zinc stabilizers to polyvinyl chloride. *Polymer degradation and stability*, 94(5):845–850, 2009.

[149] Yissa A Mohammed, Fekadu G Hone, Genene T Mola, and Newayemedhin A Tegegne. Non-electron withdrawing unit copolymerization to enhance photo-stability of thiophene-based organic solar cells. *Energy Technology*, 13(3):2401316, 2025.

[150] Huifeng Yao, Long Ye, Hao Zhang, Sunsun Li, Shaoqing Zhang, and Jianhui Hou. Molecular design of benzodithiophene-based organic photovoltaic materials. *Chemical reviews*, 116(12):7397–7457, 2016.

[151] Rocío Domínguez, Gisela L Schulz, Pilar de la Cruz, Peter Bäuerle, and Fernando Langa. Cyclopentadithiophene-based co-oligomers for solution-processed organic solar cells. *Dyes and Pigments*, 143:112–122, 2017.

[152] Erika MONTERO-GUZMAN, R GALINDO, and R FUENTES-RAMIREZ. Incorporation of zno nanoparticles in polymeric matrices as uv protector. *Journal of Technology and Innovation*, pages 7–20, 2020.

[153] Fatemeh Yousefi, Seyed Borhan Mousavi, Saeed Zeinali Heris, and Samin Naghash-Hamed. Uv-shielding properties of a cost-effective hybrid pmma-based thin film coatings using tio2 and zno nanoparticles: a comprehensive evaluation. *Scientific Reports*, 13(1):7116, 2023.

[154] Hiroki Saito, Takayuki Uchiyama, Yoshiko Okada-Shudo, Wedimagegn Mammo, Kruger Tjaart, Varun Vohra, and Newayemedhin Aberra Tegegne. Benzodithiophene unit copolymerization to improve the stability of thiophene-based organic solar cells. *Journal of Physics D: Applied Physics*, 2022.

[155] Yisak Tsegazab Gerase, Javier Garcia Lopez, Jose Prince Madalaimuthu, Anna Elmanova, Sarah Jasmin Finkelmeyer, Andrea Dellith, Daniel Blaschke, Heidemarie Schmidt, Kalina Peneva, Harald Hoppe, et al. Long-term stable organic solar cells through amphiphilic additives. *ACS Applied Electronic Materials*, 6(4):2258–2267, 2024.

[156] Myrsini Giannouli, Vasileios M Drakonakis, Achilleas Savva, Polyvios Eleftheriou, Georgios Florides, and Stelios A Choulis. Methods for improving the lifetime performance of organic photovoltaics with low-costing encapsulation. *ChemPhysChem*, 16(6):1134–1154, 2015.

[157] LRB Elton and Daphne F Jackson. X-ray diffraction and the bragg law. *American Journal of Physics*, 34(11):1036–1038, 1966.

[158] Yanfeng Liu, Aymen Yangui, Rui Zhang, Alexander Kiligaridis, Ellen Moons, Feng Gao, Olle Inganäs, Ivan G Scheblykin, and Fengling Zhang. In situ optical studies on morphology formation in organic photovoltaic blends. *Small Methods*, 5(10):2100585, 2021.

[159] Iqtiar Md Siddique. Exploring functional groups and molecular structures: A comprehensive analysis using ftir spectroscopy. *development*, 1:2, 2024.

[160] Newayemedhin A Tegegne. Aggregation and thermally induced photo-physics and structural ordering of thiophene-quinoxaline copolymer. *Materials Research Express*, 8(9):095307, 2021.

[161] E Hleli, M Mbarek, Z Gouid, C Ulbricsht, S Romdhane, R Ben Said, M Guesmi, DAM Egbe, and H Bouchriha. Dft study of optical and electronic properties of anthracene containing ppe-ppvs. *Journal of Physics and Chemistry of Solids*, 136:109157, 2020.

[162] International standard astm e 1171 requires thermal stability testing of solar cells at a temperature of 85 °c. 2015.

[163] Nutifafa Y Doumon, Mikhail V Dryzhov, Felix V Houard, Vincent M Le Corre, Azadeh Rahimi Chatri, Panagiotis Christodoulis, and L Jan Anton Koster. Photostability of fullerene and non-fullerene polymer solar cells: the role of the acceptor. *ACS applied materials & interfaces*, 11(8):8310–8318, 2019.

[164] Yunpeng Qin, Mohammad Afsar Uddin, Yu Chen, Bomee Jang, Kang Zhao, Zhong Zheng, Runnan Yu, Tae Joo Shin, Han Young Woo, and Jianhui Hou. Highly efficient fullerene-free polymer solar cells fabricated with polythiophene derivative. *Advanced Materials*, 28(42):9416–9422, 2016.

[165] Erkin Zakhidov, Mukhib Imomov, Vakhob Quvondikov, Sherzod Nematov, Ilkhom Tajibaev, Aziz Saparbaev, Irfan Ismail, Bilal Shahid, and Renqiang Yang. Comparative study of absorption and photoluminescent properties of organic solar cells based on p3ht: Pcbm and p3ht: Itic blends. *Applied Physics A*, 125(11):1–7, 2019.

[166] Liangang Xiao, Bo He, Qin Hu, Lorenzo Maserati, Yun Zhao, Bin Yang, Matthew A Kolaczkowski, Christopher L Anderson, Nicholas J Borys, Liana M Klivansky, et al. Multiple roles of a non-fullerene acceptor contribute synergistically for high-efficiency ternary organic photovoltaics. *Joule*, 2(10):2154–2166, 2018.

[167] Leiping Duan, Cheng Xu, Haimang Yi, Mushfika Baishakhi Upama, Md Arafat Mahmud, Dian Wang, Faiazul Haque, and Ashraf Uddin. Non-fullerene-derivative-dependent dielectric properties in high-performance ternary organic solar cells. *IEEE Journal of Photovoltaics*, 9(4):1031–1039, 2019.

[168] Zhenye Li, Baobing Fan, Baitian He, Lei Ying, Wenkai Zhong, Feng Liu, Fei Huang, and Yong Cao. Side-chain modification of polyethylene glycol on conjugated polymers for ternary blend all-polymer solar cells with efficiency up to 9.27%. *Science China Chemistry*, 61(4):427–436, 2018.

[169] Chao Hu, Jingjing Xu, Songming Cai, Peihao Huang, Jiyeon Oh, Changduk Yang, Shanshan Chen, Kuan Sun, Ke Yang, and Shirong Lu. Efficiency improvement of all-small-molecule organic solar cells through fused-aromatic-ring side-chained donors. *Solar RRL*, 5(12):2100705, 2021.

[170] Zaifei Ma, Wenjun Sun, Scott Himmelberger, Koen Vandewal, Zheng Tang, Jonas Bergqvist, Alberto Salleo, Jens Wenzel Andreasen, Olle Inganäs, Mats R Andersson, et al. Structure–property relationships of oligothiophene–isoindigo polymers for efficient bulk-heterojunction solar cells. *Energy & Environmental Science*, 7(1):361–369, 2014.

[171] Genene Tessema Mola and Newayemedhin Abera. Correlation between lumo offset of donor/acceptor molecules to an open circuit voltage in bulk heterojunction solar cell. *Physica B: Condensed Matter*, 445:56–59, 2014.

[172] Zhengrong Shang, Thomas Heumueller, Rohit Prasanna, George F Burkhard, Benjamin D Naab, Zhenan Bao, Michael D McGehee, and Alberto Salleo. Trade-off between trap filling, trap creation, and charge recombination results in performance increase at ultralow doping levels in bulk heterojunction solar cells. *Advanced Energy Materials*, 6(25):1601149, 2016.

[173] Tsegaye Endale, Enrico Sovernigo, Andrea Radivo, Simone Dal Zilio, Alessandro Pozzato, Teketel Yohannes, Lisa Vaccari, and Massimo Tormen. Investigation of photodegradation in polymer solar cells blended with different fullerenes derivatives. *Solar energy materials and solar cells*, 123:150–158, 2014.

[174] Obadiah G Reid, Keiko Munechika, and David S Ginger. Space charge limited current measurements on conjugated polymer films using conductive atomic force microscopy. *Nano letters*, 8(6):1602–1609, 2008.

[175] Clarke A. J. Aristidou N. Wyatt M. F. Francàs L. Fish G. ... Li Z. Speller, E. M. Toward improved environmental stability of polymer: fullerene and polymer: nonfullerene organic solar cells: a common energetic origin of light-and oxygen-induced degradation. *ACS energy letters*, 4(4):846–852, 2019.

[176] Yiwen Wang, Jinho Lee, Xueyan Hou, Chiara Labanti, Jun Yan, Eva Mazzolini, Amber Parhar, Jenny Nelson, Ji-Seon Kim, and Zhe Li. Recent progress and challenges toward highly stable nonfullerene acceptor-based organic solar cells. *Advanced Energy Materials*, 11(5):2003002, 2021.

[177] Artem Levitsky, Sebastian Alexander Schneider, Eugen Rabkin, Michael F Toney, and Gitti L Frey. Bridging the thermodynamics and kinetics of temperature-induced morphology evolution in polymer/fullerene organic solar cell bulk heterojunction. *Materials Horizons*, 8(4):1272–1285, 2021.

[178] Behayilu S Desalegn, Nika Bekri, Fekadu G Hone, Dinsefa M Andoshe, Wendimagegn Mammo, Zelalem Abdissa, Gurthwin Bosman, and Newayemedhin A Tegegne. One-pot synthesis and thermal stability of thiophene-bridged thieno [3, 2-b] thiophene donor-based copolymers. *Materials Today Communications*, 29:102803, 2021.

[179] Alexandre Rodrigues, M Cidália R Castro, Andreia SF Farinha, Manuel Oliveira, João PC Tomé, Ana V Machado, M Manuela M Raposo, Loic Hilliou, and Gabriel Bernardo. Thermal stability of p3ht and p3ht: Pcbm blends in the molten state. *Polymer testing*, 32(7):1192–1201, 2013.

[180] R Ramani, J Srivastava, and S Alam. Application of model-free kinetics to the thermal and thermo-oxidative degradation of poly (3-hexyl thiophene). *Thermochimica Acta*, 499(1-2):34–39, 2010.

[181] Biplab K Kuila and Arun K Nandi. Structural hierarchy in melt-processed poly (3-hexyl thiophene)- montmorillonite clay nanocomposites: novel physical, mechanical, optical, and conductivity properties. *The Journal of Physical Chemistry B*, 110(4):1621–1631, 2006.

[182] Qingling Nie, Ailing Tang, Peiqing Cong, Lie Chen, Qianqian Zhang, Hongru Ji, Gongqiang Li, Qiang Guo, and Erjun Zhou. Wide band gap photovoltaic polymer based on pyrrolo [3, 4-f] benzotriazole-5, 7-dione (tzbi) with ultrahigh v oc beyond 1.25 v. *The Journal of Physical Chemistry C*, 124(36):19492–19498, 2020.

[183] Sarah Holliday, Raja Shahid Ashraf, Andrew Wadsworth, Derya Baran, Syeda Amber Yousaf, Christian B Nielsen, Ching-Hong Tan, Stoichko D Dimitrov, Zhengrong Shang, Nicola Gasparini, et al. High-efficiency and air-stable p3ht-based polymer solar cells with a new non-fullerene acceptor. *Nature communications*, 7(1):1–11, 2016.

[184] Jon E Carlé, Mikkel Jørgensen, Matthieu Manceau, Martin Helgesen, Ole Hagemann, Roar Søndergaard, and Frederik C Krebs. Fused thiophene/quinoxaline low band gap polymers for photovoltaic's with increased photochemical stability. *Solar energy materials and solar cells*, 95(12):3222–3226, 2011.

[185] Holger Hintz, H-J Egelhaaf, Larry Luer, Jens Hauch, Heiko Peisert, and Thomas Chassé. Photodegradation of p3ht- a systematic study of environmental factors. *Chemistry of Materials*, 23(2):145–154, 2011.

[186] Matthieu Manceau, Sylvain Chambon, Agnès Rivaton, Jean-Luc Gardette, Stephane Guillerez, and Noëlla Lemaître. Effects of long-term uv-visible light irradiation in the absence of oxygen on p3ht and p3ht: Pcbm blend. *Solar Energy Materials and Solar Cells*, 94(10):1572–1577, 2010.

[187] Ilya V Martynov, Liana N Inasaridze, and Pavel A Troshin. Resist or oxidize: Identifying molecular structure–photostability relationships for conjugated polymers used in organic solar cells. *ChemSusChem*, 15(3):e202101336, 2022.

[188] Vinila N Viswanathan, Arun D Rao, Upendra K Pandey, Arul Varman Kesavan, and Praveen C Ramamurthy. Molecular-level architectural design using benzothiadiazole-based

polymers for photovoltaic applications. *Beilstein Journal of Organic Chemistry*, 13(1):863–873, 2017.

[189] Deping Qian, Wei Ma, Zhaojun Li, Xia Guo, Shaoqing Zhang, Long Ye, Harald Ade, Zhan'ao Tan, and Jianhui Hou. Molecular design toward efficient polymer solar cells with high polymer content. *Journal of the American Chemical Society*, 135(23):8464–8467, 2013.

[190] Shaoqing Zhang, Yunpeng Qin, Mohammad Afsar Uddin, Bomee Jang, Wenchao Zhao, Delong Liu, Han Young Woo, and Jianhui Hou. A fluorinated polythiophene derivative with stabilized backbone conformation for highly efficient fullerene and non-fullerene polymer solar cells. *Macromolecules*, 49(8):2993–3000, 2016.

[191] Nutifafa Y Doumon, Gongbao Wang, Xinkai Qiu, Adriaan J Minnaard, Ryan C Chiechi, and L Jan Anton Koster. 1, 8-diiodooctane acts as a photo-acid in organic solar cells. *Scientific reports*, 9(1):4350, 2019.

[192] HCF Martens, PWM Blom, and HFM Schoo. Comparative study of hole transport in poly (p-phenylene vinylene) derivatives. *Physical review B*, 61(11):7489, 2000.

[193] Huifeng Yao, Deping Qian, Hao Zhang, Yunpeng Qin, Bowei Xu, Yong Cui, Runnan Yu, Feng Gao, and Jianhui Hou. Critical role of molecular electrostatic potential on charge generation in organic solar cells. *Chinese Journal of Chemistry*, 36(6):491–494, 2018.

[194] Kyohei Nakano, Yumiko Kaji, and Keisuke Tajima. Origin of electric field-dependent charge generation in organic photovoltaics with planar and bulk heterojunctions. *Journal of Materials Chemistry A*, 11(48):26499–26507, 2023.

[195] Stefan Zeiske, Wei Li, Paul Meredith, Ardalan Armin, and Oskar J Sandberg. Light intensity dependence of the photocurrent in organic photovoltaic devices. *Cell Reports Physical Science*, 3(10), 2022.

[196] Kidan G Gebremariam, Fikadu G Hone, Jane Dai, Genene T Mola, Wendimagegn Mammo, and Newayemedhin A Tegegne. Effect of an ambient environment on light-induced degra-

dation of organic solar cells based on a benzodithiophene–quinoxaline copolymer in air. *New Journal of Chemistry*, 47(28):13331–13341, 2023.

[197] Seyed Mehrdad Hosseini, Steffen Roland, Jona Kurpiers, Zhiming Chen, Kai Zhang, Fei Huang, Ardalan Armin, Dieter Neher, and Safa Shoaee. Impact of bimolecular recombination on the fill factor of fullerene and nonfullerene-based solar cells: A comparative study of charge generation and extraction. *The Journal of Physical Chemistry C*, 123(11):6823–6830, 2019.

[198] Mincheol Chang, Jiho Lee, Nabil Kleinhenz, Boyi Fu, and Elsa Reichmanis. Photoinduced anisotropic supramolecular assembly and enhanced charge transport of poly (3-hexylthiophene) thin films. *Advanced Functional Materials*, 24(28):4457–4465, 2014.

[199] Gyounglyul Jo, Jaehan Jung, and Mincheol Chang. Controlled self-assembly of conjugated polymers via a solvent vapor pre-treatment for use in organic field-effect transistors. *Polymers*, 11(2):332, 2019.

[200] Yissa A Mohammed, Fikadu G Hone, Genene T Mola, and Newayemedhin A Tegegne. The roles of acceptors in the thermal-degradation of p3ht based organic solar cells. *Physica B: Condensed Matter*, 653:414666, 2023.

DECLARATION

I hereby declare that this PhD dissertation is my original work and has not been submitted for a degree at any other university. Furthermore, all sources of material used in this dissertation have been duly acknowledged.

Name: Yissa Abdie

Signature: _____

This PhD dissertation has been submitted for examination with my approval as University advisors.

Name: Dr.Newayemedhin Aberra (Associate Professor)

Signature: _____

Name: Prof. Genene Tessema

Signature: _____

Place and time of submission:

Addis Ababa University

June 12, 2025